Università degli studi di modena e reggio emilia

Dottorato di ricerca in Matematica
in convenzione con l'Università degli Studi di Ferrara e l'Università degli Studi di Parma

Ciclo XXXII

Numerical Simulations of a Suitable Set of Electrodynamics Equations in the Case of Biconic Antennas

Relatore:
Prof. Daniele Funaro

Candidato:
Dott. Lorenzo Diazzi

Correlatore:
Prof. Sergio Polidoro

Coordinatore del Corso di Dottorato:
Prof. Cristian Giardinà

Contents

Summary

By working with an extensions of the classical set of electromagnetic equations, we implemented some numerical techniques to study the near-field of a biconic antenna. Though the usual Maxwell's equations are included in the model, the generalization is necessary to handle the possible creation of regions displaying non-vanishing divergence in proximity of the boundaries, where perfect conductivity is not given for granted. Finite-difference schemes have been primarily used in a three-dimensional domain described by cylindrical coordinates. The numerical experiments include the simulation of solitary waves in vacuum and their behaviour when passing through media of different conductivity. In a successive development these waves are studied in conjunction with boundary constraints, due to the their interaction with the conductive guides. The goal of this analysis, only in part achieved, is a full understanding of the passage of the electromagnetic wave from the state of guided evolution to the one when the signal travels in free space.

In chapter 1, we introduce the equations of electromagnetism with a bit of historical background. To this end we will briefly refer to the work of James Clerk Maxwell (1831-1879). The original Maxwell's theory has been revised by other scientists, known as "the Maxwellians", and it has undergone through several changes according to the progress in both physics and mathematics. In the modern texts of physics and engineering, the set of equations known under the name of Maxwell's equations differs from the earliest version written by Maxwell himself at the end of the nineteenth century.
At the end of the first chapter, we will recall some features of the tensor formulation of the electromagnetic equations in the framework of the theory of relativity.

In chapter 2, we introduce the extension of the equations of electromagnetism proposed in [12]. The main idea is to postulate the existence of electromagnetic fields of divergence different from zero also in space regions where charges and currents sources are not present.

Thanks to this feature, in vacuum, the Ampère law contains a current terms due to the movement of the wave itself. The model is completed by introducing a new vector field $\boldsymbol{V}$ and a potential p. The presence of these fields, which are among the unknowns of the system, necessitates the adoption of further two equations borrowed from fluid dynamics. The extended model is analyzed throughout the chapter and special considerations are carried out in the case of the so called *free-waves*. Then, solitonic and spherical solutions of the extended model, which do not solve the Maxwell's equations, are considered. In the last part of the chapter a discussion on boundary conditions is introduced.

In chapter 3, we present the numerical schemes used to discretize the extended set of electrodynamics equations. For practical reasons we decided to work with low-order finite difference methods. The equation have been divided in sub-groups and different numerical schemes have been applied to each one. All the methods considered are defined on the same discrete grid, so that all the fields are approximated on these nodes. The group constituted by the equations involving the time derivatives of the electric and the magnetic fields has been discretized by the Lax-Wendroff scheme. Some considerations on the hyperbolicity of this group of equations have been made in order to investigate the stability of the method.
Another group of equations, recalling the inviscid Burger's equation, has been approximated using an upwind approach. Finally, the numerical treatment of the boundary conditions on the conductive guides is discussed, by taking in to account strategies that allow to model the mutual interaction between the dynamical sources on the guides and the fields between them. At the nodes of the external boundaries free outward flux conditions has been imposed. We mention the problem of imposing boundary conditions on the rotation axis in the case of cylindrical coordinates.

In chapter 4, we analyse some numerical experiments based on the methods developed in chapter 3. A first set of experiments is related to the test of the approximated equations on simple problems involving solitonic solutions. Comparisons are made with exact solutions. The simulation of guided waves is successively considered. A simple example constructed with parallel guides show that a suitable treatment of boundary conditions may act on the travelling wave by modifying its phase. To continue we consider the case of a soliton, in cylindrical coordinates, that is constrained in its movement by two conducting straight wave guides that cuts its support. Successively it is treated the case in which a soliton crosses a layer between two regions, of the computational domain, with

different electromagnetic properties. We then considered the problem of a biconic antenna in cylindrical coordinates, by placing a source of electromagnetic field at the entrance of the region delimited by a couple of conductive guides.

In chapter 5, some conclusive remarks about the results achieved and the problems encountered, are discussed. Some open questions remain, opening the way to further works. The thesis ends with a collection of appendices dedicated to collateral topics that have been removed from the main body for the sake of readability. Some appendices are related to theoretical considerations about the set of extended equations, whereas some others clarify some features of the numerical experiments.

Sommario

Dopo aver esteso il classico set di equazioni dell'elettromagnetismo, note in letteratura come equazioni di Maxwell, in modo da ampliare anche l'insieme delle loro soluzioni, sono stati applicati ad esse opportuni schemi numerici alle differenze finite al fine di costruire un set di loro approssimazioni implementabili su computer. Si è quindi proceduto alla simulazione numerica di onde elettromagnetiche solitoniche nel vuoto, attraverso mezzi lineari e infine inserendo guide conduttive. Unendo i risultati ottenuti in precedenza è stato costruito un modello di antenna biconica con l'intento di investigare il comportamento del campo elettromagnetico nel passaggio da un'espansione vincolata, dall'antenna stessa, ad una libera.

Nel capitolo 1, le equazioni dell'elettromagnetismo sono inquadrate in una cornice storica. In particolare, si accenna al lavoro del fisico James Clerk Maxwell (1831-1879). La teoria, originariamente sviluppata da Maxwell, fu rimaneggiata da altri scienziati, chiamati "i Maxwelliani", subendo numerose modifiche a seguito dei progressi che avvennero nei campi della fisica e della matematica. Non a caso nei moderni testi di fisica ed ingegneria, con il termine *equazioni di Maxwell* ci si riferisce ad un insieme di equazioni assai diverse da quelle scritte da Maxwell alla fine del diciannovesimo secolo.
Il capitolo termina con un richiamo alla teoria della relatività, in particolare vengono esposte le equazioni dell'elettromagnetismo in forma tensoriale.

Nel capitolo 2 si analizza un'estensione delle equazioni di Maxwell proposta in [12]. Il fulcro della versione estesa risiede nell'ipotizzare l'esistenza di campi elettromagnetici la cui divergenza possa essere diversa da zero anche in regioni dello spazio in cui non siano presenti sorgenti né di cariche né di correnti. Come conseguenza di questa assunzione, la legge di Ampère, nel caso di un onda elettromagnetica che si propaga nel vuoto, conta un termine di corrente dato dal propagarsi dell'onda stessa. Il modello si completa con

l'aggiunta di un campo vettoriale $\boldsymbol{V}$ e di un potenziale p, entrambi incognite del sistema di equazioni. A fronte dell'incremento del numero di funzioni incognite vengono incluse nel modello due ulteriori equazioni provenienti dal campo della fluidodinamica. Il set di equazioni così ottenuto viene analizzato in dettaglio, dedicando particolare attenzione a varie tipologie di sue soluzioni. Ad esempio, sono esaminate soluzioni solitoniche e sferiche che invece non risolvono le classiche equazioni di Maxwell. L'ultima parte è dedicata alle condizioni al bordo adatte a descrivere situazioni in cui elementi conduttori occupano regioni spaziali dove esistono dei campi elettromagnetici.

Nel capitolo 3 vengono presentati gli schemi numerici utilizzati per approssimare l'estensione delle equazioni dell'elettromagnetismo. Sono stati presi in considerazioni schemi alle differenze finite di basso ordine. Il set di equazioni è stato suddiviso in quattro sottoinsiemi, ciascuno dei quali è stato discretizzato mediante un diverso schema numerico. Tutti i metodi numerici considerati sono stati definiti sulla medesima griglia, cosicché tutti i campi venissero approssimati negli stessi nodi. Il primo sottoinsieme, che comprende le equazioni differenziali in cui compaiono le derivate temporali dei campi elettrico e magnetico, è stato discretizzato con il metodo di Lax-Wendroff. Al fine di chiarire delle questioni relative alla stabilità del suddetto metodo, è stato portato avanti uno studio sulla natura iperbolica di questo primo gruppo di equazioni.
Un altro sottoinsieme notevole è costituito da due equazioni che somigliano a quelle che definiscono il problema di Burger non viscoso. Per questo gruppo si è optato per una discretizzazione tramite un metodo di tipo upwind.
Infine, viene analizzato il trattamento numerico delle condizioni al contorno da imporre nel caso siano presenti delle guide d'onda conduttrici. In particolare, si cerca di modellizzare una situazione in cui sia permessa una reciproca interazione tra le sorgenti presenti sulle guide ed il campo elettromagnetici che si propaga tra esse. Nei nodi che fanno parte della frontiera esterna del dominio computazionale sono state imposte delle condizioni di flusso libero uscente, ed è accennato il problema della determinazione dei campi sull'asse di rotazione di un sistema di coordinate cilindriche.

Nel capitolo 4 sono presi in considerazione alcuni esperimenti numerici condotti applicando gli schemi descritti nel capitolo 3. Inizialmente sono stati considerati i casi relativamente semplici, di soluzioni solitoniche in coordinate cartesiane e cilindriche, con cui sono stati testati i metodi numerici. Tali test sono stati fondati sul confronto tra soluzioni approssimate ed esatte. Si passa quindi alla simulazione di onde guidate. Dapprima si è

considerato il caso di due guide parallele, in mezzo a cui un'onda subisce un'alterazione della propria fase a seguito dell'interazione con le guide stesse. È stato successivamente simulata l'evoluzione di un solitone in coordinate cilindriche costretto a muoversi tra due guide d'onda incidenti al suo supporto. Successivamente si è analizzato il caso di un solitone che attraversi una regione del dominio in cui si affacciano due mezzi contraddistinti da una diversa permittività. In ultimo, inserendo una sorgente di campi all'ingresso di una regione delimitata da una coppia di guide conduttrici, è stata condotta una simulazione del campo elettromagnetico emesso da un'antenna biconica.

Nel capitolo 5 sono stati riassunti i risultati ottenuti ed i problemi sorti durante questo lavoro. Alcune domande sono rimaste aperte, vi è quindi un ampia prospettiva per proseguire lo studio in questo campo.
La tesi termina con una serie di appendici in cui sono esposti alcuni argomenti rimossi dal corpo principale per non appesantirne la lettura. Qui sono esposte ulteriori considerazioni relative alle soluzioni del modello esteso delle equazioni dell'elettromagnetismo e dei chiarimenti in merito alla parte di esperimenti numerici.

On the equations of electromagnetism

1.1. Maxwell's equations

James Clerk Maxwell is acknowledged as the father of the mathematical theory of electromagnetism. He was born on 13 June 1831 in Edinburgh, the same city in which he has completed his studies before at the Academy and than at the University, where he had the possibility to apprehend electricity and magnetism from James Forbes. The empirical approach of the latter was in contrast with the more theoretical one, based on mathematical fluid theories, adopted by mainland European physicists. Maxwell studied Michael Faraday's works, from which he gained understanding on concepts such as force fields and force lines, he also read the books of Sir William Thomson, André-Marie Ampère, Gustav Kirchhoff, Franz Ernst Neumann and Heinrich Friedrich Weber.
From these readings he moved his first steps trying to give a mathematical expression to Faraday's field conception by using methods inspired from Thomson's field mathematics. In alternative to Thompson's approach based on electric and magnetic potentials, Maxwell made the lines of force the central concept of his theory. By considering a geometrical net of lines of force and orthogonal surfaces over Faraday's field, he was able to catch the mathematical field laws directly in terms of field quantities.

In the paper *On Physical Lines of Force*, Maxwell exhibited a mechanical model for the magnetic field based on the Thomson's idea of the vortical nature of magnetism. Furthermore, this model accounted for the mechanical forces of magnetic origin and electromagnetic induction. From this article came out the earliest evidence of his equations of electromagnetism, which also included the novel proposal of the displacement current that led Maxwell to conclude that light could be seen as a transverse electromagnetic wave.
Maxwell soon modified the model switching from the mechanical interpretation to a field

theory inspired by the work of Fararday. Thanks to that improvement he was able to include electrostatics and optics, providing the full set of electromagnetic field equations and the expression of the velocity of light in terms of electromagnetic quantities. These progresses bring to the paper *A Dynamical Theory of the Electromagnetic field* [28], where the vortex model is replaced by a dynamical justification of the field equations and the magnetic field is treated as a "hidden mechanism" whose motion is controlled by the electric current. Last but not least, a wave equation is obtained by combining field equations, reaching a truly electromagnetic optics in which light has the nature of a waving electromagnetic field. In [28] the equations of the electromagnetic field are carried out as the existing relations between fundamental electromagnetic quantities, whose writing where enforced by the thorough use of the mathematical notation, as here reported:

"[...] *In order to bring these results within the power of symbolical calculation, I then express them in the form of the General Equations of the Electromagnetic Field. These equations express -*

(A) The relation between electric displacement, true conduction, and the total current, compounded of both.

(B) The relation between the lines of magnetic force and the inductive coefficients of a circuit, as already deduced from the laws of induction.

(B) The relation between the lines of magnetic force and the inductive coefficients of a circuit, as already deduced from the laws of induction.

(C) The relation between the strength of a current and its magnetic effects, according to the electromagnetic system of measurement.

(D) The value of the electromotive force in a body, as arising from the motion of the body in the field, the alteration of the field itself, and the variation of electric potential from one part of the field to another.

(E) The relation between electric displacement, and the electromotive force which produces it.

(F) The relation between an electric current, and the electromotive force which produces it.

(G) The relation between the amount of free electricity at any point, and the electric displacements in the neighbourhood.

(H) The relation between the increase or diminution of free electricity and the electric currents in the neighbourhood.

There are twenty of these equations in all, involving twenty variable quantities.[...] "

$$\left.\begin{aligned} p' &= p + \tfrac{df}{dt} \\ r' &= r + \tfrac{dg}{dt} \\ q' &= q + \tfrac{dh}{dt} \end{aligned}\right\} \cdots\cdots\cdots\cdots\cdots (A) \qquad \left.\begin{aligned} \mu\alpha &= \tfrac{dH}{dy} - \tfrac{dG}{dz} \\ \mu\beta &= \tfrac{dF}{dz} - \tfrac{dH}{dx} \\ \mu\gamma &= \tfrac{dG}{dx} - \tfrac{dF}{dy} \end{aligned}\right\} \cdots\cdots\cdots\cdots\cdots\cdots (B)$$

$$\left.\begin{aligned} \tfrac{d\gamma}{dy} - \tfrac{d\beta}{dz} &= 4\pi p' \\ \tfrac{d\alpha}{dz} - \tfrac{d\gamma}{dx} &= 4\pi q' \\ \tfrac{d\beta}{dx} - \tfrac{d\alpha}{dy} &= 4\pi r' \end{aligned}\right\} \cdots\cdots\cdots\cdots (C) \qquad \left.\begin{aligned} P &= \mu\left(\gamma\tfrac{dy}{dt} - \beta\tfrac{dz}{dt}\right) - \tfrac{dF}{dt} - \tfrac{d\Psi}{dx} \\ Q &= \mu\left(\alpha\tfrac{dz}{dt} - \gamma\tfrac{dx}{dt}\right) - \tfrac{dG}{dt} - \tfrac{d\Psi}{dy} \\ R &= \mu\left(\beta\tfrac{dx}{dt} - \alpha\tfrac{dy}{dt}\right) - \tfrac{dH}{dt} - \tfrac{d\Psi}{dz} \end{aligned}\right\} \cdots (D)$$

$$\left.\begin{aligned} P &= kf \\ Q &= kg \\ R &= kh \end{aligned}\right\} \cdots\cdots\cdots\cdots\cdots\cdots (E) \qquad \left.\begin{aligned} P &= -\rho p \\ Q &= -\rho q \\ R &= -\rho r \end{aligned}\right\} \cdots\cdots\cdots\cdots\cdots\cdots\cdots\cdots (F)$$

$$e + \frac{df}{dx} + \frac{dg}{dy} + \frac{dh}{dz} = 0 \cdots\cdots (G) \qquad \frac{de}{dt} + \frac{dp}{dx} + \frac{dq}{dy} + \frac{dr}{dz} = 0 \cdots\cdots\cdots\cdots (H)$$

In these equations of the electromagnetic field we have assumed twenty variable quantities, namely,

For	*Electromagnetic Momentum*	F	G	H
"	*Magnetic Intensity*	α	β	γ
"	*Electromotive Force*	P	Q	R
"	*Current due to true conduction*	p	q	r
"	*Electric Displacement*	f	g	h
"	*Total Current (including variation of displacement)*	p'	q'	r'
"	*Quantity of free Electricity*	e		
"	*Electric Potential*	Ψ		

Between these twenty quantities we have found twenty equations, viz.

Three equations of	*Magnetic Force*	*(B)*
"	*Electric Currents*	*(C)*
"	*Electromotive Force*	*(D)*
"	*Electric Elasticity*	*(E)*
"	*Electric Resistance*	*(F)*
"	*Total Currents*	*(A)*
One equation of	*Free Electricity*	*(G)*
"	*Continuity*	*(H)*
[. . .]		

It is important to notice that electric and magnetic fields are given in terms of components, because the vector algebra was a novel mathematical tool at the time of Maxwell and he was used to the much more applied fluid-mechanics notation.
The new dynamical theory, that takes his final and exhaustive formulation in the book *A Treatise on Electricity and Magnetism* [29] written in 1873, mainly differs from the vortex model on the physical interpretation of the nature of charges and currents. In the vortex model, the electric current corresponded to the flow of particles between vortices and charges to their accumulation, while in the dynamical theory, Maxwell defined the electric current as a transfer of polarization, and charge as a discontinuity of polarization. Maxwell's concept of polarization is something totally different from the current meaning of polarization, for instance it does not distinguish between electric polarization and electric displacement, the first one existing in physical media while the second one occurring in free-space.
For what concerns the equations of electromagnetism, the main improvement done in [29] with respect to [28], was the introduction of a quaternion formulation. This kind of notation has been developed by William Rowan Hamilton and brought to the attention of Maxwell by his friend Peter Guthrie Tait, and let Maxwell to rewrite his equation in a compact differential form and also to introduce their integral formulation. The quaternion notation is clearly explained in [2], were it is presented as the fundamental step towards the reduction of the equation in a vector form, whereas for other authors this advance should be properly attributed to Oliver Heaviside, as we will see in the next section.

As Darrigol remarks[1], in Maxwell's theory all the basic concepts of field, charge and current have macroscopic meaning, matter and ether were treated as a single continuous

[1] See [7], Chapter 4.

medium without speculating on their microscopic models. Another brilliant Maxwell's intuition has been the rejection of the ideas of direct action at a distance and electric fluids, both very popular between physicists at the time; he could overtake them by combining the novel field theory approach, proposed by Faraday, with the geometrical interpretation of the fields themselves in terms of the line of force. It is known that Maxwell's major work [29] lacked of consistency under several aspects and it is a very hard reading, however it has been the guide for almost all further improvements in electrodynamics. Recent studies of his scientific production have established that Maxwell theory was far more consistent than has usually been admitted. Siegel[2] has shown the vortex model accounts for all electrodynamics and electrostatic phenomena known to Maxwell.

1.2. Modern formulation

The electromagnetic theory developed by Maxwell did not get attention until the publication of the book *A Treatise on Electricity and Magnetism* in 1873. In the following years the theory did not know a great diffusion as well. This initial indifference could be explained by taking in to account two main facts: on one hand Maxwell left his theory incomplete[3], on the other hand it encountered the disagreement of Sir William Thomson (Lord Kelvin) that was the highest authority in electricity at the time. Thomson, who was a great exponent of mechanical reductionism, did not believe in a purely electromagnetic theory of light able to reduce optics directly to electricity and magnetism. For this reason he completely disagreed with Maxwell's rejection of vortex model as a concrete mechanical basis of his theory.
Nevertheless, in the last decades of the 1800 a group of physicists approached Maxwell's theory and brought it to the limelight within national borders first, and further on the European continent. They were able to produce substantial modifications spreading it through the scientific community and preparing it to his great success. This group of scientists, usually referred as the Maxwellians, counts for example Horace Lamb, who eliminated the scalar potential from the equations showing that it was redundant, George Francis FitzGerald, who established that the displacement currents do not have to be the linear displacement of some substance, John Henry Poynting and Oliver Heaviside, who were able to relate the energy flux in an electromagnetic field with Maxwell's equations.

[2] See [33].
[3] Maxwell died in Cambridge in 1879, at the age of 48.

Another group of Maxwellians studied the magneto-optical properties of light, by modifying the Maxwell's Lagrangian and producing confirmation of Maxwell's theory of light.

One of the most debated Maxwellians is Heaviside, without any doubt an enthusiastic proponent of Maxwell's ideas. He has the merit to have clearly rewrite the theoretical apparatus, using the vector algebra formalism, cutting out the unpopular quaternion notation of the electromagnetic equations. Heaviside eliminated both of the potentials from Maxwell's equations and introduced the use of capital bold letter $\boldsymbol{E}$, $\boldsymbol{D}$, $\boldsymbol{B}$, $\boldsymbol{H}$ to indicate electric field strength, electric displacement, magnetic induction and magnetic field strength respectively. He also adopted the notation "curl" and "div" to indicate the rotor and the divergence of a field[4]. However, as it is pointed out in [37], while some authors refer to him as the father of the modern formulation of the Maxwell's equations, others authors such Waser argue that this claim is an overstatement, since the condensation from 20 to 4 equations was made by Maxwell himself with the quaternion formulation.

In Germany, Maxwell's theory was mainly handled by Heinrich Hertz and August Föppl. They both tried to achieve the clarity that was lacking in Maxwell's exposition and publicized in mainland Europe his work. However whereas while Hertz's did not adopt a modern mathematical structure, Föppl's did it, first following the vector analysis approach of Heaviside, then by publishing *Introduction to the Maxwellian Theory of Electricity*, a clear and well organized book about electrodynamics[5]. By the way, in [1] the equations of electromagnetism are listed separately in the second and third part of the book. Only in paragraph 60[6] two of the four equations of the modern set are coupled and referred to as the Heaviside-Hertz equations. Their expression is

$$\begin{cases} \dfrac{\varepsilon}{c}\dfrac{\partial \boldsymbol{E}}{\partial t} = \mathrm{curl}\boldsymbol{H} - \dfrac{4\pi\sigma}{c}\boldsymbol{E} \\ -\dfrac{\mu}{c}\dfrac{\partial \boldsymbol{H}}{\partial t} = \mathrm{curl}\{\boldsymbol{E} - \boldsymbol{E^e}\} \end{cases}$$

where c is the speed of light and capital bold letters are here used to replace the capital bold german characters of the original text.

[4]The notation will be finally turned in to the modern one with $\nabla\cdot$ and $\nabla\times$ by Josiah Willard Gibbs.
[5]Probably the first of this kind, since Heaviside books were only a collection of articles.
[6]The title of the paragraph could be translated as *Differential Equations of Electromagnetic Field for Bodies at Rest.*

As a last step in this brief exposition of the history of electromagnetic equations, we shall consider the formulation given by Hendrik Antoon Lorentz in [27], where he listed a full set of equations for the microscopic electromagnetic field in the framework of his own electron theory. Right at the end of the article, he provided five equations for the macroscopic fields, interpreted as some spatial average of the microscopic one. They read is more or less as follow:

$$\begin{cases} \mathrm{Div}\boldsymbol{D} = \rho \\ \mathrm{Div}\boldsymbol{S} = 0 \\ \mathrm{Rot}\boldsymbol{B} = 4\pi\boldsymbol{S} \\ \mathrm{Rot}\boldsymbol{E} = -\dot{\boldsymbol{B}} \\ \mathrm{Div}\boldsymbol{B} = 0 \end{cases}$$

Here again capital bold letter are used in place of german characters present in the Lorentz's article. Moreover, Lorentz uses the notation Rot and Div for rotor and divergence, as well as the dot to indicate the derivative with respect to time. The field $\boldsymbol{S}$, called *current field*, is defined as the sum of four contributes: the time variation of the electric displacement $\dot{\boldsymbol{D}}$, the conduction current $\boldsymbol{I}$, the convection current $\boldsymbol{C}$ and the Röntgen current $\boldsymbol{R}$.

The modern formulation of Maxwell's equations, that can be found in common texts of physics and engineering, is the following[7]

$$\begin{cases} \nabla \cdot \boldsymbol{D} \;=\; 4\pi\rho \\ \nabla \times \boldsymbol{H} - \dfrac{1}{c}\dfrac{\partial \boldsymbol{D}}{\partial t} \;=\; \dfrac{4\pi}{c}\boldsymbol{J} \\ \nabla \times \boldsymbol{E} + \dfrac{\partial \boldsymbol{B}}{\partial t} \;=\; 0 \\ \nabla \cdot \boldsymbol{B} \;=\; 0 \end{cases} \tag{1.1}$$

where ρ, $\boldsymbol{J}$ are the charge and current source in the medium respectively. In addition, these equations are coupled with some constitutive relations: one expresses the electric displacement $\boldsymbol{D}$ in terms of the electric polarization $\boldsymbol{P}$ of the medium and the electric

[7] This formulation is taken from [23].

field $\boldsymbol{E}$, the other one expresses the magnetic field $\boldsymbol{H}$ in terms of the magnetization $\boldsymbol{M}$ of the medium and the magnetic induction $\boldsymbol{B}$. The corresponding formulas are reported below

$$\boldsymbol{D} = \varepsilon_0 \boldsymbol{E} + \boldsymbol{P}$$

$$\boldsymbol{H} = \mu_0 \boldsymbol{B} - \boldsymbol{M}.$$

Finally, to complete the set of equations, it is usually also added the Lorentz's force equation, expressing the electromagnetic force acting on a point charge q that travels through an electromagnetic field with velocity $\boldsymbol{v}$, i.e.

$$\boldsymbol{F} = q(\boldsymbol{E} + \boldsymbol{v} \times \boldsymbol{B}).$$

In vacuum and in absence of field sources, the equations in (1.1) reduce to

$$\begin{cases} \dfrac{\partial \boldsymbol{E}}{\partial t} = c^2 \nabla \times \boldsymbol{B} \\ \dfrac{\partial \boldsymbol{B}}{\partial t} = -\nabla \times \boldsymbol{E} \\ \nabla \cdot \boldsymbol{B} = 0 \\ \nabla \cdot \boldsymbol{E} = 0 \end{cases} \tag{1.2}$$

Although (1.1) and (1.2) are nowadays the most common formulations, advanced frameworks allow to express the electromagnetic equations in alternative way. As an example[8], we mention the tensor version of the Einstein's relativity theory, or the one based on differential forms developed by Elie Cartan. Furthermore, as pointed out in [37], a certain number of scientist have tried to extend the "classic" set of electromagnetic equations inspired by different reasons; we could cite a first proposal that has been advanced by Hertz, in order to make Maxwell's equations invariant with respect to Galilei transformation, and another one done by Paul Dirac with the intent to symmetrize the four equations, by postulating the existence of magnetic monopoles.

[8] See [2].

To close this historical presentation, we report some phrases wrote by Darrigol[9] at the beginning of Chapter dedicated to Maxwell.
"*Glorification, however, tends to obscure the true nature of Maxwell's achievements. It was not a god who wrote these signs, but a man who had gone through two of the best British universities and had carefully studied Faraday and Thomson for himself. His electromagnetism and his style of physics, innovative though they were, owed much to Thomson, who had already transformed British physics in an even more significant manner and had defined basic concepts and new perspectives of electromagnetism. The heroic account also deforms Maxwell's results. His electrodynamics differed from today's 'Maxwell's theory' in several respects, as basic as the distinction between source and field. It was not a closed system, and it included suggestions for future electromagnetic research.*"

1.3. Tensor form

Following a very standard path[10], we briefly present here the tensor form of the electromagnetic equations in vacuum. This will help us later in order to make some comparisons with another theory developed to generalize the equations, as we will discuss in the next chapter.
Consider the two electromagnetic potentials $\boldsymbol{A}$ and Φ, that verify the following relations

$$\boldsymbol{B} = \frac{1}{c}\nabla \times \boldsymbol{A} \qquad\qquad \boldsymbol{E} = -\frac{1}{c}\frac{\partial \boldsymbol{A}}{\partial t} - \nabla\Phi. \tag{1.3}$$

To determinate uniquely the choice of the two potentials, we will assume the *Lorenz gauge* condition reported below

$$\nabla \cdot \boldsymbol{A} + \frac{1}{c}\frac{\partial \Phi}{\partial t} = 0.$$

Within the space-time cartesian coordinates framework $(x_0, x_1, x_2, x_3) = (ct, x, y, z)$ the electromagnetic field tensor is defined as

$$F_{\alpha\beta} = \partial_\alpha A_\beta - \partial_\beta A_\alpha,$$

[9] See [7], Chapter 4.
[10] See [23], chapters 6 and 11.

where ∂_α is the α-component of the differential operator $(\frac{\partial}{\partial x_0}, \nabla)$ and A_α is the generic entry of the tensor $(-\Phi, \boldsymbol{A})$.
Taking in to account the definition (1.3), the electromagnetic field tensor with two covariant indices is written as

$$F_{\alpha\beta} = \frac{\partial A_\beta}{\partial x_\alpha} - \frac{\partial A_\alpha}{\partial x_\beta} = \begin{pmatrix} 0 & E_x & E_y & E_z \\ -E_x & 0 & -cB_z & cB_y \\ -E_y & cB_z & 0 & -cB_x \\ -E_z & -cB_y & cB_x & 0 \end{pmatrix} \tag{1.4}$$

while its contravariant version is obtained through the application of the metric tensor $g^{\alpha\beta} = g_{\alpha\beta} = \text{diag}\{1, -1, -1, -1\}$, as show below

$$F^{\alpha\beta} = g^{\alpha\gamma} g^{\beta\delta} F_{\gamma\delta} = \begin{pmatrix} 0 & -E_x & -E_y & -E_z \\ E_x & 0 & -cB_z & cB_y \\ E_y & cB_z & 0 & -cB_x \\ E_z & -cB_y & cB_x & 0 \end{pmatrix}. \tag{1.5}$$

According to Einstein's notation, in (1.5) one has to sum up from 0 to 3 on repeated indices. From the expression

$$\partial_\alpha F^{\alpha\beta} = 0 \tag{1.6}$$

the first and the fourth equations of the system (1.2) are then obtained by choosing $\beta = 1, 2, 3$ and $\beta = 0$ respectively. Similarly, the second and the third equations immediately follow from

$$\partial_\alpha \mathscr{F}^{\alpha\beta} = 0, \tag{1.7}$$

where $\mathscr{F}^{\alpha\beta}$ is the dual field tensor[11], that in brief could be obtained from $F^{\alpha\beta}$ by exchanging $\boldsymbol{E}$ with $\boldsymbol{B}$ and $\boldsymbol{B}$ with $-\frac{1}{c^2}\boldsymbol{E}$, i.e.

$$\mathscr{F}^{\alpha\beta} = \begin{pmatrix} 0 & -B_x & -B_y & -B_z \\ B_x & 0 & \frac{1}{c}E_z & -\frac{1}{c}E_y \\ B_y & -\frac{1}{c}E_z & 0 & \frac{1}{c}E_x \\ B_z & \frac{1}{c}E_y & -\frac{1}{c}E_x & 0 \end{pmatrix}.$$

[11] As defined in [23], chapter 11.

Finally, the electromagnetic Lagrangian density assumes the form[12]

$$\mathscr{L} = -F_{\alpha\beta}F^{\alpha\beta} = 2(|\boldsymbol{E}|^2 - c^2|\boldsymbol{B}|^2). \tag{1.8}$$

Maxwell's equations are linked to the stationary points of this functional. As usual, it is possible to recover these equations by writing $\mathscr{L}$ in terms of the scalar and vector potentials Φ and A and successively differentiating with respect to the variations $\delta\Phi$ and δA[13].

[12]Hereafter $|\ .\ |$ is the standard Euclidean norm in three-dimensional space.
[13]For a detailed exposition of this procedure see [25] chapter 4 and [23] chapter 12.

An extended formulation for the electrodynamics

In this chapter we will present the extension of the electromagnetic equations (1.2) proposed by Daniele Funaro in a series of works[1], where substantially the free divergence equation $\nabla \cdot \boldsymbol{E} = 0$ is rejected, while it is postulated the possibility to have non-zero divergence for the electric field in vacuum and in absence of charge sources. This assumption will produce an extra current term in the Ampère's law. Two new variables and two new equations have been added to system (1.2) to built up the novel set of equations, as it will described in section 2.3.

One of the motivations that led to formulate the above extension is the need to expand the set of possible solutions of the electromagnetic equations. For instance, it is quite astonishing to observe that some elementary electromagnetic phenomena, such as solitary signal-packets, cannot be described by using (1.2). The extended set of equations has the advantage of fully incorporating "photons" within the framework of a differential model, even if in order to achieve this result it is necessary to abandon some aspects of the Maxwell's original model.
The remarkable unifying feature of this approach is that it does not make any actual difference between a photons and other electromagnetic phenomena as, for instance, waves emanating from an antenna.
With this interpretation, the photon is not the "carrier" of the electromagnetic field, but becomes a pure wave, carrying along electric and magnetic components. Due to the lack of time, before going on through the exposition, let us state that is far from our intentions to debate on fundamental physical topics, such as the quantum mechanics conception of photon. These issues are discussed in [13], [14] and in chapters 5 and 6 of [12] .

After giving an overview on the idea of solitonic solution, we will examine an exam-

[1] Some of those are [11], [12], [13] and [14].

ple to outline the reason why these kind of solutions are missing in the usual framework of equations (1.2). Finally we will formulate the extended version of the equations and give an insight of some of the features of the mentioned model.

2.1. Solitary waves

The first issue is to clarify the meaning hereafter attributed to the word *soliton*, since it does not exists a consensus general definition[2]. The term is commonly referred at any solution of a certain nonlinear equation which

i) represents a wave of permanent form,

ii) is localized, decaying or becoming constant at infinity,

iii) interacts with other solitons retaining its form[3].

According to this description, we will call *soliton* every smooth electromagnetic wave with compact support travelling along a straight trajectory at the speed of light. Taken at two different time values, the supports of such wave have to be similar.
From a mathematical point of view, we can restate the observation done at the beginning of the chapter by saying that Maxwell's equations (1.2) have a poor set of finite-energy solutions of the type above described. Indeed soliton are not admitted.

Despite the lack of a general definition of soliton, there are many specific cases in which solitary travelling waves belong to the set of solutions of nonlinear partial differential equations.
This is the case of the Korteweg-de Vries equation[4], introduced at the end of the 19^{th} century to describe wave motion in shallow canals, and then applied to the study of plasma physics by Norman J. Zabusky and Martin D. Kruskal. In 1965, they find for the first time a soliton[5] as result of some numerical simulations of the solutions of the Korteweg-de Vries equation.
Few years later, the spectral transform technique was developed by Clifford S. Gardner, John M. Greene, Martin D. Kruskal and Robert M. Miura, and the method was applied to

[2] See [9].
[3] When the principle of superposition holds.
[4] See [38].
[5] See [40].

Cauchy problems involving Korteweg-de Vries equations, nonlinear Schrödinger equation and others. For example, by considering stationary Schrödinger equation, a soliton turns out to be a solution corresponding to an initial datum whose spectral transform has a vanishing reflection coefficient and only a discrete eigenvalue in his whole spectrum[6]. The corresponding time evolution produces a wave of constant shape that moves at constant speed.

To conclude this dissertation about solitonic solutions we want to point out the problem of interaction between solitons. As we are going to discover, the extended formulation here proposed consist on a nonlinear set of partial differential equations, otherwise solitonic solution would not be allowed. The non-linearity can in many circumstances invalidate the *linear superposition principle*. For this reason, it is not guaranteed that solitons retain their original shape after collision.
Even if some other considerations relative to the linear superposition principle are going to be carried out in section 2.7, treating the case of spherical waves, the topic concerning the collision of soliton with both other solitons or matter will not be treated in this thesis.

2.2. Non-Maxwellian wave fronts

We will try to give an idea of the reason why the couple of conditions $\nabla \cdot \boldsymbol{B} = 0$ and $\nabla \cdot \boldsymbol{E} = 0$ cannot be both satisfied at the boundary of the compact support of an electromagnetic soliton. This issue, and all the other that will follow in this section, are discussed in detail in the chapter 1 of [12]. For shake of brevity, we have omitted a number of argumentation that will further clarify the concepts here exposed.

In the current framework becomes very important the concept of *wave-front*. This is the piece of a two-dimensional surface locally enveloped by the vectors $\boldsymbol{E}$ and $\boldsymbol{B}$. Those geometric entities cannot be defined for each electromagnetic wave, indeed in many cases it is impossible since the envelopes intersect each other. On the contrary, a case in which wave-fronts exist is the one of the *free-wave* that will be treated in section 2.4. For waves of this kind, in each point of the empty space, the vectors $\boldsymbol{E}$ and $\boldsymbol{B}$ are mutually orthog-

[6]The proposed characterization it is quite meaningless without the background given in first chapter of [6]. It has been reported just to give an idea of how a soilton could be defined in a rigorous way.

onal[7] and such that $|\boldsymbol{E}| = c|\boldsymbol{B}|$.
To follow the evolution of the wave-front let introduce the vector field $\boldsymbol{V}$. It is a velocity field and in the case of a free-wave it is locally orthogonal to the vectors $\boldsymbol{E}$ and $\boldsymbol{B}$ and normalized to c. At each instant, the light rays are determined by the field $\boldsymbol{V}$ according to the following fact: in its propagation, a light ray remains locally orthogonal to each wave-front. The energy is so carried away at the speed of light along the direction individuated by the Poynting vector $\boldsymbol{E} \times \boldsymbol{B}$, locally tangent to each ray. This means that for a free-wave $(\boldsymbol{V}, \boldsymbol{E}, \boldsymbol{B})$ is a right-hand oriented triple of orthogonal vectors.
The fronts of an electromagnetic wave, differing each other in intensity and polarization, are consecutively generated, producing a continuum along the propagation direction. Once generated by a source, wave-fronts develop without influencing each other, unless they find an obstacle, as for instance another group of wave-fronts.

Without loss of generality, by fixing a cartesian system of coordinates (x, y, z), we can describe a soliton that travels along the x-axis with the help of the following electric and magnetic vector fields

$$\boldsymbol{E} = \Big(e_x, e_y, e_z\Big)\ f\Big(t - \frac{x}{c}\Big), \qquad \boldsymbol{H} = \Big(h_x, h_y, h_z\Big)\ f\Big(t - \frac{x}{c}\Big). \tag{2.1}$$

Here f is a bounded function and all the components of $\boldsymbol{E}$ and $\boldsymbol{H}$ are zero outside a certain two-dimensional set Ω. Moreover, the electric and magnetic fields only depend on the coordinates y and z. In this way the vector field $\boldsymbol{V}$ is oriented as the x-axis, i.e. $\boldsymbol{V} = (V_x, 0, 0)$. As an immediate consequence of the $\boldsymbol{V}$ orientation, we have that the components E_x and B_x must be zero, otherwise the mutual orthogonality of $\boldsymbol{E}$, $\boldsymbol{H}$, $\boldsymbol{V}$ would be lost. By excluding trivial solutions, the only possibility is that $e_x = h_x = 0$.
We can now proceed by replacing the electric and magnetic fields in the system (1.2), i.e.

[7] See [25].

$$\frac{\partial \boldsymbol{E}}{\partial t} = \frac{1}{\varepsilon_0} \nabla \times \boldsymbol{H}$$

$$\frac{\partial \boldsymbol{H}}{\partial t} = -\frac{1}{\mu_0} \nabla \times \boldsymbol{E}$$

$$\nabla \cdot \boldsymbol{H} = 0$$

$$\nabla \cdot \boldsymbol{E} = 0.$$

Since we are in vacuum it follows that $\varepsilon = \varepsilon_0$, $\mu = \mu_0$ and $\boldsymbol{B} = \mu_0 \boldsymbol{H}$, where ε_0 and μ_0 are vacuum permittivity and permeability. In the simplified case we are examining, one gets

$$0 = \frac{1}{\varepsilon_0}\Big(\frac{\partial H_z}{\partial y} - \frac{\partial H_y}{\partial z}\Big) \tag{2.2}$$

$$\frac{\partial E_y}{\partial t} = -\frac{1}{\varepsilon_0}\frac{\partial H_z}{\partial x} \tag{2.3}$$

$$\frac{\partial E_z}{\partial t} = \frac{1}{\varepsilon_0}\frac{\partial H_y}{\partial x} \tag{2.4}$$

$$0 = -\frac{1}{\mu_0}\Big(\frac{\partial E_z}{\partial y} - \frac{\partial E_y}{\partial z}\Big) \tag{2.5}$$

$$\frac{\partial H_y}{\partial t} = +\frac{1}{\mu_0}\frac{\partial E_z}{\partial x} \tag{2.6}$$

$$\frac{\partial H_z}{\partial t} = -\frac{1}{\mu_0}\frac{\partial E_y}{\partial x} \tag{2.7}$$

from which it is possible to prove that e_y, e_z, h_y, h_z are harmonic functions, as we will check below only for $e_y(y, z)$. Let us start by taking the partial derivative of (2.3) with respect to y on both sides. Then by exchanging the order of derivation and using relation (2.2) we get

$$\frac{\partial}{\partial t}\frac{\partial E_y}{\partial y} = -\frac{1}{\varepsilon_0}\frac{\partial}{\partial x}\frac{\partial H_y}{\partial z}.$$

Switching the derivatives on the right-hand side and by using (2.4) we obtain

$$\frac{\partial}{\partial t}\frac{\partial E_y}{\partial y} = -\frac{1}{\varepsilon_0}\frac{\partial}{\partial z}\Big(\varepsilon_0 \frac{\partial E_z}{\partial t}\Big). \tag{2.8}$$

Taking a further derivative with respect to y, exchanging the order of derivation on both sides and applying relation (2.5) we can write

$$\frac{\partial}{\partial t}\frac{\partial^2 E_y}{\partial y^2} = -\frac{\partial}{\partial t}\frac{\partial^2 E_y}{\partial z^2}.$$

Finally, it is necessary to write down explicitly E_y and E_z and, unless f is constant in time, it is proved that e_y is an harmonic function since

$$\frac{\partial f}{\partial t}\Big(\frac{\partial^2 e_y}{\partial y^2}+\frac{\partial^2 e_y}{\partial z^2}\Big)=0.$$

Then it is well known that if e_y, e_z, h_y and h_z are harmonic functions in Ω and they are required to vanish at the boundary, than they must vanish on the entire set.
We have just shown that, if Ω is flat and bounded there is no possibility to get a solitonic solution of the electromagnetic equations (1.2) in vacuum, without introducing internal singularities or boundary discontinuities. Notice that, applying the same argument here used to prove $\Delta E_y = 0$, from equation (2.8) one can also deduce that $\nabla \cdot \boldsymbol{E} = 0$.

At this point, according to what is stated in first chapter of [12], we define *Maxwellian-waves* (in vacuum) those waves where the vector fields $\boldsymbol{E}$ and $\boldsymbol{H}$ are both divergence-free at any point. Forcing fields of (2.1) to be those waves one obtains the trivial null solution. An example of Maxwellian-wave is the transverse monochromatic plane wave. This is a travelling solution of of (1.2). By supposing that it travels along the x-direction of a cartesian reference frame (x, y, z), this wave is described by the following electric and magnetic fields

$$\boldsymbol{E}=\left(0,\ c\ \sin\Big(\omega t-\omega\frac{x}{c}\Big),\ 0\right),\qquad \boldsymbol{H}=\left(0,\ 0,\ \sin\Big(\omega t-\omega\frac{x}{c}\Big)\right),$$

where ω is the frequency having the dimension of the inverse of time. It is easy to see that wave-fronts are planes orthogonal to the x-direction. Unfortunately, this kind of wave does not exist in nature since it has associated an infinite energy. This is a consequence of the fact that it is not possible to constrict the fields $\boldsymbol{E}$ and $\boldsymbol{H}$ to be non-vanishing only in a bounded region of each wave-front. A detailed exposition of this fact can be found in chapter 1 of [12].

Otherwise a wave-front that has the shape of the surface of a sphere it is of Non-Maxwellain type: it is impossible to satisfy both the local orthogonality between $\boldsymbol{E}$ and $\boldsymbol{H}$ and the free-divergence conditions near the poles[8]. This topic will be further discuss in section 2.27.

[8] See [12] chapter 1, [14] and [16]

2.3. The extended set of equations

According to [12], by letting the divergence of the electric field be different from zero, even in some spatial regions that do not contain classical charges, we arrive at the following extended formulation of the electromagnetic equations

$$\begin{cases} \dfrac{\partial \boldsymbol{E}}{\partial t} \,=\, c^2\, \nabla \times \boldsymbol{B} \,-\, \rho\, \boldsymbol{V} \\ \\ \dfrac{\partial \boldsymbol{B}}{\partial t} \,=\, -\,\nabla \times \boldsymbol{E} \\ \\ \nabla \cdot \boldsymbol{B} \,=\, 0 \\ \\ \dfrac{\partial p}{\partial t} \,=\, \theta\, \rho\, \boldsymbol{E} \cdot \boldsymbol{V} \\ \\ \rho \left[\dfrac{D\boldsymbol{V}}{Dt} \,+\, \theta \left(\boldsymbol{E} \,+\, \boldsymbol{V} \,\times\, \boldsymbol{B} \right) \right] \,=\, -\nabla p \end{cases} \tag{2.9}$$

where $\rho = \nabla \cdot \boldsymbol{E}$. This nonlinear system counts ten unknowns, namely, the three components of the electric field $\boldsymbol{E}$, the three components of the magnetic induction $\boldsymbol{B}$, the three components of the velocity field $\boldsymbol{V}$ and the scalar function p. Hereafter, we will only consider the case of linear homogeneous media, corresponding to $\boldsymbol{D} = \varepsilon \boldsymbol{E}$ and $\boldsymbol{B} = \mu \boldsymbol{H}$. By comparing the extended version (2.9) with the usual Maxwell's equations (1.2), we can observe that only the *Faraday's Law* and the free-divergence equation for $\boldsymbol{B}$ are left untouched. Therefore, the other equations deserve some comments.

The first equation

$$\frac{\partial \boldsymbol{E}}{\partial t} \,=\, c^2\, \nabla \times \boldsymbol{B} \,-\, \rho\, \boldsymbol{V} \tag{2.10}$$

is the *Ampère's law* where, in absence of external sources of charge and current, the additional term $-\rho \boldsymbol{V}$ has to be interpreted as a free flow of immaterial current, with density ρ, associated with the movement of the electromagnetic wave.

The just mentioned term can be summed up to another one, due to the flow of current along a conductive medium that may interact with the wave. By taking in to account these additional contributions, it is possible to model the mutual interactions between wave and guides, as we will see in the last section of this chapter.
Going on, we find an equation that recalls the Euler's equation for inviscid fluids:

$$\rho \left[\frac{D\boldsymbol{V}}{Dt} + \theta \left(\boldsymbol{E} + \boldsymbol{V} \times \boldsymbol{B} \right) \right] = -\nabla p. \tag{2.11}$$

On the left-hand side we find ρ, i.e. the divergence of the electric field, multiplied by the sum of two terms: the first one is the total derivative[9] of $\boldsymbol{V}$ with respect to time and the second one is a forcing term of electromagnetic nature, based on the vector $\boldsymbol{E} + \boldsymbol{V} \times \boldsymbol{B}$. The constant θ appearing in (2.11) is a fundamental constant of the model, and has the dimension of a charge divided by a mass[10].
On the right-hand side appears the gradient of the scalar field p which, in analogy with the Euler's equation, plays the role of a *pressure*. We will actually treat the potential p as a pressure term, even though from a dimensional analysis turns out that p is measured in $\frac{V}{s^2}$.
An equation like (2.11) are usually coupled with Maxwell's equations in some plasma physics models, for instance the one related to magnetohydrodynamics[11]. Nevertheless, in such models a number of particles moves has a fluid and $\boldsymbol{V}$ has the meaning of the fluid flow velocity, p is a proper pressure and both mass density ρ_m and charge density ρ_q compares. On the contrary, in our model massive charge particles are not involved and $\boldsymbol{V}$, p and ρ has the meaning already explained above. Furthermore, as stated in [16], equation (2.11) combines the evolution of electromagnetic entities with that of a (non material) inviscid fluid.

Finally, an energy conservation argument leads to the equation

$$\frac{\partial p}{\partial t} = \theta \, \rho \, \boldsymbol{E} \cdot \boldsymbol{V}, \tag{2.12}$$

which reveal the possible arising of a pressure as a consequence of a lack of orthogonality between $\boldsymbol{E}$ and $\boldsymbol{V}$.

[9] The total derivative operator has the following expansion $\frac{D\square}{Dt} := \frac{\partial \square}{\partial t} + (\square \cdot \nabla)\square$.
[10] It has been estimated $\theta \approx 2.85 \times 10^{11}$ Culomb/Kg. See [13] appendix G and [15].
[11] See [20] and [31].

As for the Maxwell's equations, by multiplying the first two equation by $\boldsymbol{E}$ and $\boldsymbol{B}$ respectively and summing up, we get an energy balance equation

$$\frac{1}{2}\frac{\partial}{\partial t}\big(|\boldsymbol{E}|^2 + c^2|\boldsymbol{B}|^2 + \frac{2}{\theta}p\big) = -c^2\nabla\cdot\big(\boldsymbol{E}\times\boldsymbol{B}\big).$$

This equation differs from its classical counterpart as it counts an extra term due to the time variation of p. Nevertheless, in the case that we are going to consider in the following section the standard Poynting equation will be recovered as a consequence of the orthogonality between the fields $\boldsymbol{E}$ and $\boldsymbol{V}$.

Hence considering again equation (2.10) and by taking its divergence one find the following continuity equation for the current term $\rho\boldsymbol{V}$

$$\frac{\partial\rho}{\partial t} = -\nabla\cdot\big(\rho\boldsymbol{V}\big). \tag{2.13}$$

This last equation could be used to further expand the time derivative of (2.10) to get

$$\frac{\partial^2\boldsymbol{E}}{\partial t^2} = c^2\nabla\times\Big(\frac{\partial\boldsymbol{B}}{\partial t}\Big) - \Big[-\nabla\cdot\big(\rho\boldsymbol{V}\big)\Big]\boldsymbol{V} - \rho\frac{\partial\boldsymbol{V}}{\partial t}.$$

Then, using Faraday's law and applying the vector formula $\nabla\times(\nabla\times\boldsymbol{E}) = \nabla(\nabla\cdot\boldsymbol{E}) - \Delta\boldsymbol{E}$, we can rewrite it as

$$\frac{\partial^2\boldsymbol{E}}{\partial t^2} = c^2\nabla\times\Big(-\nabla\times\boldsymbol{E}\Big) + \Big[\big(\nabla\rho\cdot\boldsymbol{V}\big) + \rho\,\nabla\cdot\boldsymbol{V}\Big]\boldsymbol{V} - \rho\frac{\partial\boldsymbol{V}}{\partial t},$$

$$\frac{\partial^2\boldsymbol{E}}{\partial t^2} = c^2\Delta\boldsymbol{E} - c^2\nabla\rho + \big(\nabla\rho\cdot\boldsymbol{V}\big)\boldsymbol{V} + \rho\boldsymbol{V}\,\nabla\cdot\boldsymbol{V} - \rho\frac{\partial\boldsymbol{V}}{\partial t}. \tag{2.14}$$

It is clear from the context that here $\Delta\boldsymbol{E}$ has the meaning of vector Laplacian. We can further note that last equation for $\rho = 0$ reduces to classical vector wave equation.

2.4. The case of free-wave

We will distinguish between free-waves and constrained waves by meaning, on one side of waves such that the triplet $(\boldsymbol{V}, \boldsymbol{E}, \boldsymbol{B})$ is a local right-handed cartesian reference system

and $|\boldsymbol{E}| = c|\boldsymbol{B}|$, while on the other side of waves for which the mutual orthogonality of the fields does not hold in general.

Of course when ρ, $\frac{D\boldsymbol{V}}{Dt}$ and p are identically zero, Maxwell's equations (1.2) are directly recovered. Another interesting subcase is obtained by setting $p = 0$ and $\frac{D\boldsymbol{V}}{Dt} = 0$. With this last choice (2.9) reduces to

$$\begin{cases} \dfrac{\partial \boldsymbol{E}}{\partial t} = c^2 \nabla \times \boldsymbol{B} - \rho \boldsymbol{V} \\ \dfrac{\partial \boldsymbol{B}}{\partial t} = -\nabla \times \boldsymbol{E} \\ \nabla \cdot \boldsymbol{B} = 0 \\ \rho\big(\boldsymbol{E} + \boldsymbol{V} \times \boldsymbol{B}\big) = 0. \end{cases} \tag{2.15}$$

From the fourth equation, i.e.

$$\rho\big(\boldsymbol{E} + \boldsymbol{V} \times \boldsymbol{B}\big) = 0 \tag{2.16}$$

one could easily deduce the orthogonality of the couple of $\boldsymbol{E}$ and $\boldsymbol{B}$, and of the couple $\boldsymbol{E}$ and $\boldsymbol{V}$. Indeed, multiplying (2.16) by $\boldsymbol{B}$ gives $\boldsymbol{E} \cdot \boldsymbol{B} = 0$, while multiplying (2.16) by $\boldsymbol{V}$ produces $\boldsymbol{E} \cdot \boldsymbol{V} = 0$. So we can state that free-waves are solutions of (2.15).
Further on, we can notice that it comes natural to require $|V| = c$ for a free-wave that propagates in vacuum. As it is pointed out in first chapter of [12], this relation holds in many circumstances[12], for instance an interesting case occurs when $\boldsymbol{V}$ is compatible with the following expression

$$\boldsymbol{V} = c\, \frac{\boldsymbol{E} \times \boldsymbol{B}}{|\boldsymbol{E} \times \boldsymbol{B}|}$$

which also ensure the orthogonality of the whole triplet $(\boldsymbol{V}, \boldsymbol{E}, \boldsymbol{B})$, thus via relation (2.16) also $|\boldsymbol{E}| = c|\boldsymbol{B}|$ is recovered.

Another interesting feature is given by taking (2.14) in the case of (2.16) holds, and by assuming that $\boldsymbol{V}$ is a stationary field, orthogonal to $\boldsymbol{B}$ and such that $\nabla \cdot \boldsymbol{V} = 0$.

[12] It is also the case of the solitonic wave considered in section 2.6

Under these hypotesis the considered equation is simplified to

$$\frac{\partial^2 \boldsymbol{E}}{\partial t^2} = c^2 \Delta \boldsymbol{E} - c^2 \nabla \rho + \big(\nabla \rho \cdot \boldsymbol{V}\big)\boldsymbol{V}. \tag{2.17}$$

The operator at the right-hand side contains only second partial derivatives in the direction of $\boldsymbol{V}$ and this may explain why solitons may be generated with this model. This last statement could be clarified by further explanations which, to avoid weigh down this section, are provided in the appendix I.

In addition, as it is shown in chapter 2 of [12], the new system of equations is invariant under Lorentz transformations.
To conclude this section, we analyse the tensor version of (2.15) and compare it to the one relative to (1.2) shown in section 1.3. To this end, it is necessary to introduce the tensor $V_\alpha = (V_0, -\boldsymbol{V})$ and its contravariant version $V^\beta = g^{\beta\delta} V_\delta = (V^0, \boldsymbol{V})$. The same potential $\boldsymbol{A}$ and Φ defined in (1.3) and the same electromagnetic field tensors (1.4) and (1.5) are here used to rewrite equations (1.6) in the new way.
We obtain first vector equation of (2.15), that is

$$\partial F^{\alpha\beta} = \frac{\rho}{c} V^\beta, \tag{2.18}$$

when $\beta = 1, 2, 3$. Note that for $\beta = 0$ tensor equation (2.18) produces $\rho = \nabla \cdot \boldsymbol{E}$. This last is not actually an equation, but confirms the definition we have given to ρ.
The second and the third equations in (2.15) are the same as in system (1.2). They indeed correspond to the same dual tensors and relations (1.7) shall hold.
Another tensor relation must now be added, i.e.

$$F^{\alpha\beta} V_\beta = 0,$$

that retrieves equation (2.16) for $\beta = 1, 2, 3$, while for $\beta = 0$ states the orthogonality between $\boldsymbol{E}$ and $\boldsymbol{V}$.

The Lagrangian for the extended formulation is the same as the Maxwellian case. This is given by (1.8), nevertheless it is necessary to add a constraint on the potentials[13] to enforce that $\boldsymbol{A}$ and $\boldsymbol{V}$ are lined up. Thus we must find the stationary points of

[13] See [16].

$$\mathscr{L} = 2\big(|\boldsymbol{E}|^2 - c^2|\boldsymbol{B}|^2\big)$$

under the condition

$$c\boldsymbol{A} = \Phi\boldsymbol{V}.$$

It is remarkable that the Lagrangian proposed in [16] is identical as the classical one. Usually the attempts to generalize Maxwell's equation in a nonlinear way relay on the modification of the Lagrangian. For instance one may consider the Born-Infeld theory[14], in which the idea behind the modification of the Lagrangian is the so called *principle of finiteness* of physical quantities, that led Max Born and Leopold Infeld to assume the existence of an upper limit for the electromagnetic field strength. Soliton-like solution, later called "BIons", are admitted by this model.
Although the Born-Infeld theory, as the great part of nonlinear electrodynamics theories, have quite nothing in common with the extension here considered, they reveal the effort of a part of the scientific community to move towards new theories that can embrace a larger number of electromagnetic phenomena.

[14] See [4].

2.5. The equations in various systems of coordinates

By using the linearity relation $\boldsymbol{B} = \mu \boldsymbol{H}$ we rewrite the system of extended equations (2.9) as follow

$$\begin{cases} \dfrac{\partial \boldsymbol{E}}{\partial t} = \dfrac{1}{\varepsilon} \nabla \times \boldsymbol{H} - \rho \boldsymbol{V} \\ \dfrac{\partial \boldsymbol{H}}{\partial t} = -\dfrac{1}{\mu} \nabla \times \boldsymbol{E} \\ \nabla \cdot \boldsymbol{H} = 0 \\ \dfrac{\partial p}{\partial t} = \theta \rho \boldsymbol{E} \cdot \boldsymbol{V} \\ \rho \left[\dfrac{D\boldsymbol{V}}{Dt} + \theta \left(\boldsymbol{E} + \mu V \times \boldsymbol{H} \right) \right] = -\nabla p. \end{cases} \tag{2.19}$$

We have already seen that this 3-dimensional electromagnetic problem has 10 unknowns. This number may decrease in special symmetric configurations. Some examples in cartesian coordinates and cylindrical coordinates are going to be proposed here. Both the frameworks here considered, allow to reduce a 3-dimensional problem in terms of a collection of equivalent 2-dimensional problems.
Since hereafter we will frequently recall these special configurations, let us call *cartesian framework* the one relative to cartesian coordinates and *cylindrical framework* the other one relative to cylindrical coordinates.

Cartesian Framework

For what concerns the so called *cartesian framework* let us start by fixing a cartesian coordinate frame (x, y, z) and assume that all the fields do not depend on the z-coordinate. Thus, we now solve the equations in the plane (x, y), by observing that derivatives with respect to z are zero.
In such a framework the divergence of the electric field takes the form

$$\rho := \frac{\partial E_x}{\partial x} + \frac{\partial E_y}{\partial y}$$

and the equations of the system (2.19) are rewritten as

$$\frac{\partial E_x}{\partial t} = \frac{1}{\varepsilon}\frac{\partial H_z}{\partial y} - \rho V_x \qquad \frac{\partial H_x}{\partial t} = -\frac{1}{\mu}\frac{\partial E_z}{\partial y}$$

$$\frac{\partial E_y}{\partial t} = -\frac{1}{\varepsilon}\frac{\partial H_z}{\partial x} - \rho V_y \qquad \frac{\partial H_y}{\partial t} = \frac{1}{\mu}\frac{\partial E_z}{\partial x}$$

$$\frac{\partial E_z}{\partial t} = \frac{1}{\varepsilon}\left(\frac{\partial H_y}{\partial x} - \frac{\partial H_x}{\partial y}\right) - \rho V_z \qquad \frac{\partial H_z}{\partial t} = -\frac{1}{\mu}\left(\frac{\partial E_y}{\partial x} - \frac{\partial E_x}{\partial y}\right)$$

$$\frac{\partial H_z}{\partial x} + \frac{\partial H_z}{\partial y} = 0 \qquad \frac{\partial p}{\partial t} = \theta\,\rho\left(E_x V_x + E_y V_y + E_z V_z\right)$$

$$\rho\left[\frac{\partial V_x}{\partial t} + V_x\frac{\partial V_x}{\partial x} + V_y\frac{\partial V_x}{\partial y} + \theta\left(E_x + \mu\left(V_y H_z - V_z H_y\right)\right)\right] = -\frac{\partial p}{\partial x}$$

$$\rho\left[\frac{\partial V_y}{\partial t} + V_x\frac{\partial V_y}{\partial x} + V_y\frac{\partial V_y}{\partial y} + \theta\left(E_y + \mu\left(V_z H_x - V_x H_z\right)\right)\right] = -\frac{\partial p}{\partial y}$$

$$\rho\left[\frac{\partial V_z}{\partial t} + V_x\frac{\partial V_z}{\partial x} + V_y\frac{\partial V_z}{\partial y} + \theta\left(E_z + \mu\left(V_x H_y - V_y H_x\right)\right)\right] = 0.$$

By further requiring that electric and velocity fields have to be orthogonal to the magnetic one, which is lined up with the z-direction, we come out with a *transverse electric mode wave*. This solves the following system, that only has six unknowns depending on two spatial coordinates and time

$$
\begin{cases}
\dfrac{\partial E_x}{\partial t} \;=\; \dfrac{1}{\varepsilon}\,\dfrac{\partial H_z}{\partial y} \;-\; \rho\, V_x \\[2ex]
\dfrac{\partial E_y}{\partial t} \;=\; -\dfrac{1}{\varepsilon}\,\dfrac{\partial H_z}{\partial x} \;-\; \rho\, V_y \\[2ex]
\dfrac{\partial H_z}{\partial t} \;=\; -\dfrac{1}{\mu}\left(\dfrac{\partial E_y}{\partial x} \;-\; \dfrac{\partial E_x}{\partial y}\right) \\[2ex]
\dfrac{\partial p}{\partial t} \;=\; \theta\,\rho\left(E_x\, V_x + E_y\, V_y\right) \\[2ex]
\rho\left[\dfrac{\partial V_x}{\partial t} + V_x\dfrac{\partial V_x}{\partial x} + V_y\dfrac{\partial V_x}{\partial y} \;+\; \theta\left(E_x \;+\; \mu\, V_y\, H_z\right)\right] \;=\; -\dfrac{\partial p}{\partial x} \\[2ex]
\rho\left[\dfrac{\partial V_y}{\partial t} + V_x\dfrac{\partial V_y}{\partial x} + V_y\dfrac{\partial V_y}{\partial y} \;+\; \theta\left(E_y \;-\; \mu\, V_x\, H_z\right)\right] \;=\; -\dfrac{\partial p}{\partial y}.
\end{cases}
\tag{2.20}
$$

Cylindrical framework

Since we will deal with problems displaying radial symmetry, it is advantageous to opt for cylindrical coordinates[15] (r, φ, y). In such a case, the 3-dimensional space is split in a collection of half-planes whose intersection is the rotation axis, here taken as the y-axis. The unknowns in this situation are not supposed to depend on the variable φ. We are now going to write the equations in the *cylindrical framework*. This will be useful later to study a biconic antenna.

By applying the divergence operator in cylindrical coordinates to the electric field one obtains

$$
\rho := \frac{1}{r}\frac{\partial (r E_r)}{\partial r} + \frac{\partial E_y}{\partial y}.
$$

Therefore, the system (2.19) takes the following form[16]

[15] Here (r, φ) are polar coordinates in each plane of the 3-dimensional space obtained by fixing y.

[16] By taking in to account that in cylindrical coordinates (r, φ, y) the rotor operator is written as $\nabla \times \boldsymbol{F} = \left(\frac{1}{r}\frac{\partial F_y}{\partial \varphi} - \frac{\partial F_\varphi}{\partial y} \;,\; \frac{\partial F_r}{\partial y} - \frac{\partial F_y}{\partial r} \;,\; \frac{1}{r}\frac{\partial (r F_\varphi)}{\partial r} - \frac{1}{r}\frac{\partial F_r}{\partial \varphi} \right)$.

$$\frac{\partial E_r}{\partial t} = -\frac{1}{\varepsilon}\frac{\partial H_\varphi}{\partial y} - \rho V_r \qquad \frac{\partial H_r}{\partial t} = \frac{1}{\mu}\frac{\partial E_\varphi}{\partial y}$$

$$\frac{\partial E_\varphi}{\partial t} = \frac{1}{\varepsilon}\left(\frac{\partial H_r}{\partial y} - \frac{\partial H_y}{\partial r}\right) - \rho V_\varphi \qquad \frac{\partial H_\varphi}{\partial t} = -\frac{1}{\mu}\left(\frac{\partial E_r}{\partial y} - \frac{\partial E_y}{\partial r}\right)$$

$$\frac{\partial E_y}{\partial t} = \frac{1}{r\varepsilon}\frac{\partial (rH_\varphi)}{\partial r} - \rho V_y \qquad \frac{\partial H_y}{\partial t} = -\frac{1}{r\mu}\frac{\partial (rE_\varphi)}{\partial r}$$

$$\frac{1}{r}\frac{\partial (rH_r)}{\partial r} + \frac{\partial H_y}{\partial y} = 0 \qquad \frac{\partial p}{\partial t} = \theta\,\rho\left(E_r V_r + E_\varphi V_\varphi + E_y V_y\right)$$

$$\rho\left[\frac{\partial V_r}{\partial t} + V_r\frac{\partial V_r}{\partial r} - \frac{V_r V_\varphi}{r} + V_y\frac{\partial V_r}{\partial y} + \theta\left(E_r + \mu\left(V_\varphi H_y - V_y H_\varphi\right)\right)\right] = -\frac{\partial p}{\partial r}$$

$$\rho\left[\frac{\partial V_\varphi}{\partial t} + V_r\frac{\partial V_\varphi}{\partial r} + \frac{V_r V_\varphi}{r} + V_y\frac{\partial V_\varphi}{\partial y} + \theta\left(E_\varphi + \mu\left(V_y H_r - V_r H_y\right)\right)\right] = 0$$

$$\rho\left[\frac{\partial V_y}{\partial t} + V_r\frac{\partial V_y}{\partial r} + V_y\frac{\partial V_y}{\partial y} + \theta\left(E_y + \mu\left(V_r H_\varphi - V_\varphi H_r\right)\right)\right] = -\frac{\partial p}{\partial y}.$$

Similarly to what has been done before, we restrict ourselves to consider the case in which the electric field and the velocity field have only components only along the r-direction and the y-direction, while the the magnetic field is oriented along φ. Reminding that the dependence on φ disappears, we obtain the following system in six variables

$$
\begin{cases}
\dfrac{\partial E_r}{\partial t} \;=\; -\dfrac{1}{\varepsilon}\,\dfrac{\partial H_\varphi}{\partial y} \;-\; \rho\, V_r \\[2ex]
\dfrac{\partial E_y}{\partial t} \;=\; \dfrac{1}{r\varepsilon}\,\dfrac{\partial (r H_\varphi)}{\partial r} \;-\; \rho\, V_y \\[2ex]
\dfrac{\partial H_\varphi}{\partial t} \;=\; -\dfrac{1}{\mu}\left(\dfrac{\partial E_r}{\partial y} \;-\; \dfrac{\partial E_y}{\partial r}\right) \\[2ex]
\dfrac{\partial p}{\partial t} \;=\; \theta\,\rho\left(E_r\, V_r + E_y\, V_y\right) \\[2ex]
\rho\left[\dfrac{\partial V_r}{\partial t} + V_r\dfrac{\partial V_r}{\partial r} + V_y\dfrac{\partial V_r}{\partial y} \;+\; \theta\left(E_r \;-\; \mu\, V_y\, H_\varphi\right)\right] \;=\; -\dfrac{\partial p}{\partial r} \\[2ex]
\rho\left[\dfrac{\partial V_y}{\partial t} + V_r\dfrac{\partial V_y}{\partial r} + V_y\dfrac{\partial V_y}{\partial y} \;+\; \theta\left(E_y \;+\; \mu\, V_r\, H_\varphi\right)\right] \;=\; -\dfrac{\partial p}{\partial y}.
\end{cases}
\tag{2.21}
$$

2.6. Exact solutions: solitons

By assuming the extended system of electromagnetic equations (2.19) rather than the classic one (1.2), the set of admissible solution is enlarged, as anticipated at the beginning of this chapter. Some of these brand-new solutions are going to be presented here. In particular, we will consider two solitons, one relative to the *cartesian framework* and another one related to the *cylindrical framework*.

Cartesian framework

In the cartesian coordinate system (x, y, z), we fix a positive real number τ and a point $C \equiv (x_C, y_C)$ of the plane $z = 0$. We can then define the functions

$$\phi_x(x) := \begin{cases} \dfrac{1}{2}\left[1+\cos\left((x-x_C)\,\dfrac{\pi}{\tau}\right)\right] & \text{if} \quad |x-x_C| \le \tau \\ \\ 0 & \text{elsewhere} \end{cases}$$

$$\phi_y(y) := \begin{cases} \dfrac{1}{2}\left[1+\cos\left((y-y_C)\,\dfrac{\pi}{\tau}\right)\right] & \text{if} \quad |y-y_C| \le \tau \\ \\ 0 & \text{elsewhere} \end{cases}$$

$\phi(x,y) := \phi_x(x)\phi_y(y)$.

The function[17] $\phi(x,y)$, assumes values in the interval $[0,1]$ and has as compact support the set $\left\{(x,y) \in \mathbf{R}^2 \;\middle|\; |x-x_C| \le \tau,\ |y-y_C| \le \tau\right\}$, centered in C. Here, τ is half of the side of the squared support.
Successively we consider $\phi(x-ct,y)$ which correspond to the function $\phi(x,y)$ shifting along x (positive direction) with velocity c as time increases. The constant c is the speed of light. A direct computation[18] shows that the following choice of fields $\boldsymbol{E}$, $\boldsymbol{H}$ and $\boldsymbol{V}$ is an analytical solution of (2.20)

$$\begin{aligned} \boldsymbol{E} &= \left(\ 0\ ,\ c\ \phi(x-ct,y)\ ,\ 0\ \right) \\ \boldsymbol{H} &= \left(\ 0\ ,\ 0\ ,\ \frac{1}{\mu}\ \phi(x-ct,y)\ \right) \\ \boldsymbol{V} &= \left(\ c\ ,\ 0\ ,\ 0\ \right). \end{aligned} \tag{2.22}$$

Since the fourth equation of (2.20) is satisfied when $\nabla p = 0$, the field p is determined up to a constant. We suggest to choose p identically zero in the whole space-time domain.

[17] See figure 2.1.
[18] See Appendix II.

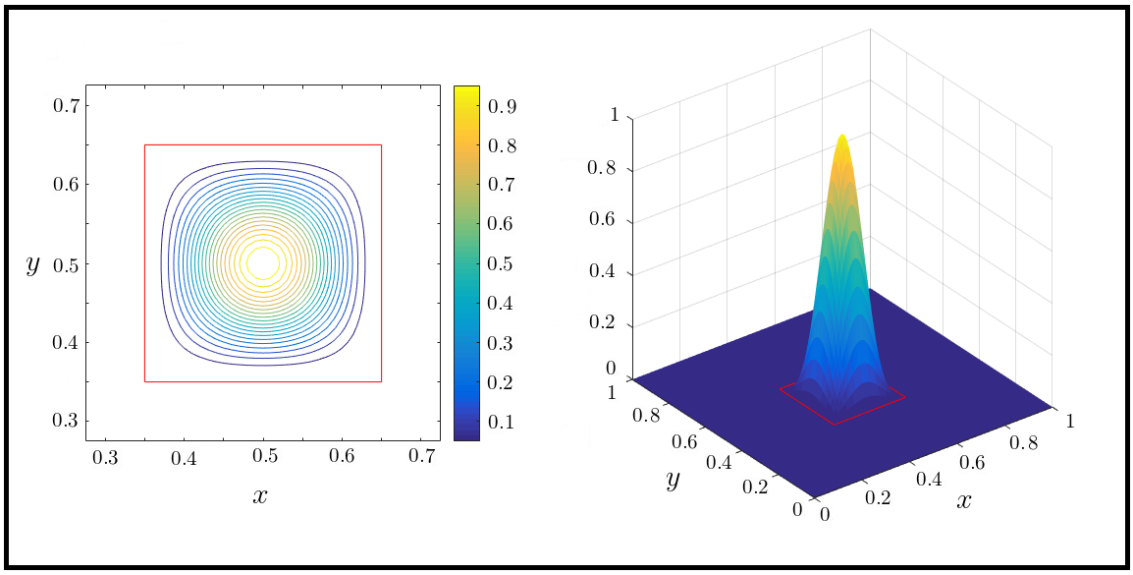

Figure 2.1: Contour lines and surface representation of the function $\phi(x, y)$ for $C = (0.5, 0.5)$ and $\tau = 1.5$. The red segments denote the bounds of the squared support.

Other solutions can be found by changing the shape of the soliton. An example is obtained by substituting ϕ with ϕ^2 as follow

$$\begin{aligned} \boldsymbol{E} &= \Big(\ 0 \ , \ c \ \phi^2(x - ct, y) \ , \ 0 \ \Big) \\ \boldsymbol{H} &= \Big(\ 0 \ , \ 0 \ , \ \frac{1}{\mu} \ \phi^2(x - ct, y) \ \Big) \\ \boldsymbol{V} &= \Big(\ c \ , \ 0 \ , \ 0 \ \Big). \end{aligned} \tag{2.23}$$

Cylindrical framework

To discuss the next exact solution it is necessary to fix a three dimensional cylindrical coordinate system (r, φ, y). We then choose two positive real numbers τ, K_τ and two points $C \equiv (r_C, y_C)$, $P_0 \equiv (0, y_0)$ of the half-plane defined by $\varphi = 0$. Successively, we have to introduce the following coordinates transformation

$$T: \begin{array}{ccc} \mathbb{R}^2 & \longrightarrow & \mathbb{R}^2 \\ (r', y') & \longmapsto & (r, y) \end{array} \quad \text{with} \quad \begin{cases} r = r' \ \cos\Big(K_\tau \ (y' - y_0)\Big) \\ \\ y = y_0 + r' \ \sin\Big(K_\tau \ (y' - y_0)\Big) \end{cases}$$

and its inverse one

$$T^{-1}: \begin{array}{ccc} \mathbb{R}^2 & \longrightarrow & \mathbb{R}^2 \\ (r, y) & \longmapsto & (r', y') \end{array} \quad \text{with} \quad \begin{cases} r' = \sqrt{r^2 + (y - y_0)^2} \\ \\ y' = y_0 + \dfrac{1}{K_\tau} \ \arctan\left(\dfrac{y - y_0}{r}\right). \end{cases}$$

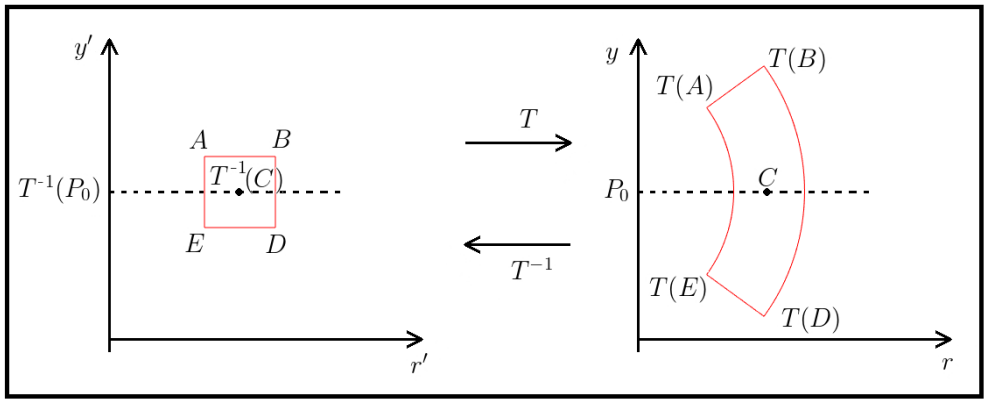

Figure 2.2: Schematic representation of the transformations T and T^{-1}.

The (r', y')-plane could be interpreted as the (x, y)-plane, so that the transformation T^{-1} brings the function ϕ into its cylindrical version. This last statement and figure 2.2 could clarify the following construction. Note that P_0 it is a fixed point of both transformations T and T^{-1}. The point $T^{-1}(C)$ plays the role of the center of a square of side 2τ. This is the support of the soliton described in cartesian coordinates (r', y') through the function $\phi(r', y')$. This last function is the same of $\phi(x, y)$ as it was defined in the *cartesian framework*, one has just to write r' and y' instead of x and y respectively. Is is clear that the same variable renaming it can be naturally extended to the functions $\phi_x(x, y)$ and $\phi_y(x, y)$, which becomes $\phi_{r'}(r', y')$ and $\phi_{y'}(r', y')$. Furthermore, choosing $y_C = y_0$, we have that C it is fixed point too of T and T^{-1}. This means that, the squared

support in the (r', y')-plane, that in general is defined as

$$\Big\{(r', y') \;\Big|\; |r' - T^{-1}((r_C, y_C)) \cdot (1, 0)| \leq \tau \;,\; |y' - T^{-1}((r_C, y_C)) \cdot (0, 1)| \leq \tau \Big\}$$

it simplifies to

$$\Big\{(r', y') \;\Big|\; |r' - r_C| \leq \tau \;,\; |y' - y_C| \leq \tau \Big\}.$$

Now it is possible to construct three new functions. Two of those are defined on the (r, y)-plane by going from each point (r, y) to its correspondent (r', y') through the transformation T, then its coordinates are used to evaluate $\phi_{r'}(r', y')$ and $\phi_{y'}(r', y')$. The third one it is given by the their product. At the end we obtain

$$\phi_{r'}(r'(r, y)) := \begin{cases} \dfrac{1}{2}\left[1 + \cos\Big((r'(r, y) - r_C)\ \dfrac{\pi}{\tau}\Big)\right] & \text{if} \quad |r'(r, y) - r_C| \leq \tau \\ \\ 0 & \text{elsewhere} \end{cases}$$

$$\phi_{y'}(y'(r, y)) := \begin{cases} \dfrac{1}{2}\left[1 + \cos\Big((y'(r, y) - y_C)\ \dfrac{\pi}{\tau}\Big)\right] & \text{if} \quad |y'(r, y) - y_C| \leq \tau \\ \\ 0 & \text{elsewhere} \end{cases}$$

which allow to define

$$\zeta(r'(r, y), y'(r, y)) := \ \phi_{r'}(r'(r, y))\ \phi_{y'}(y'(r, y)).$$

The positive constant τ is related to the shape of the function ζ, but in the (r, y)-plane it does not play the role of the half of the side of the domain as it was in the (r', y')-plane. The support of ζ it is not squared. A picture of ζ it is shown in figure 2.3. The positive constant K_τ produces an elongation or a compression[19] along the angular direction of the support of ζ. The action of K_τ is symmetric with respect to the straight line passing from P_0 and C.

[19]The elongation occurs when K_τ is greater than 1, on the contrary the compression is given by values of K_τ lower than 1.

It is worthwhile to notice that with this setting the function ζ is not separable with respect to the variables r and y.

The time dependent function $\zeta(r'-ct,y')$ describes the shift of $\zeta(r',y')$ along the radial directions outgoing from P_0, as time passes. With the following choice, the fields solve[20] the system (2.21)

$$\begin{aligned}
\boldsymbol{E} &= \Big(-\ \frac{c}{r}\ \zeta(r'-ct,y')\ U_y\ ,\ 0\ ,\ \frac{c}{r}\ \zeta(r'-ct,y')\ U_r\ \Big) \\
\boldsymbol{H} &= \Big(\ 0\ ,\ -\frac{1}{\mu r}\ \zeta(r'-ct,y')\ ,\ 0\ \Big) \\
\boldsymbol{V} &= \Big(\ c\ U_r\ ,\ 0\ ,\ c\ U_y\ \Big).
\end{aligned} \tag{2.24}$$

where

$$U_r(r,y) := \frac{r}{\sqrt{r^2+(y-y_0)^2}}, \qquad\qquad U_y(r,y) := \frac{y-y_0}{\sqrt{r^2+(y-y_0)^2}}.$$

Since the last three equations of (2.21) are satisfied when p is constant in space and time, this field is determined up to a constant, so that we suggest to choose p identically zero in the whole domain.

Another possible exact solution is easily recovered from (2.24) by substituting ζ with ζ^2, obtaining

$$\begin{aligned}
\boldsymbol{E} &= \Big(-\ \frac{c}{r}\ \zeta^2(r'-ct,y')\ U_y\ ,\ 0\ ,\ \frac{c}{r}\ \zeta^2(r'-ct,y')\ U_r\ \Big) \\
\boldsymbol{H} &= \Big(\ 0\ ,\ -\frac{1}{\mu r}\ \zeta^2(r'-ct,y')\ ,\ 0\ \Big) \\
\boldsymbol{V} &= \Big(\ c\ U_r\ ,\ 0\ ,\ c\ U_y\ \Big).
\end{aligned} \tag{2.25}$$

[20] See Appendix *II*

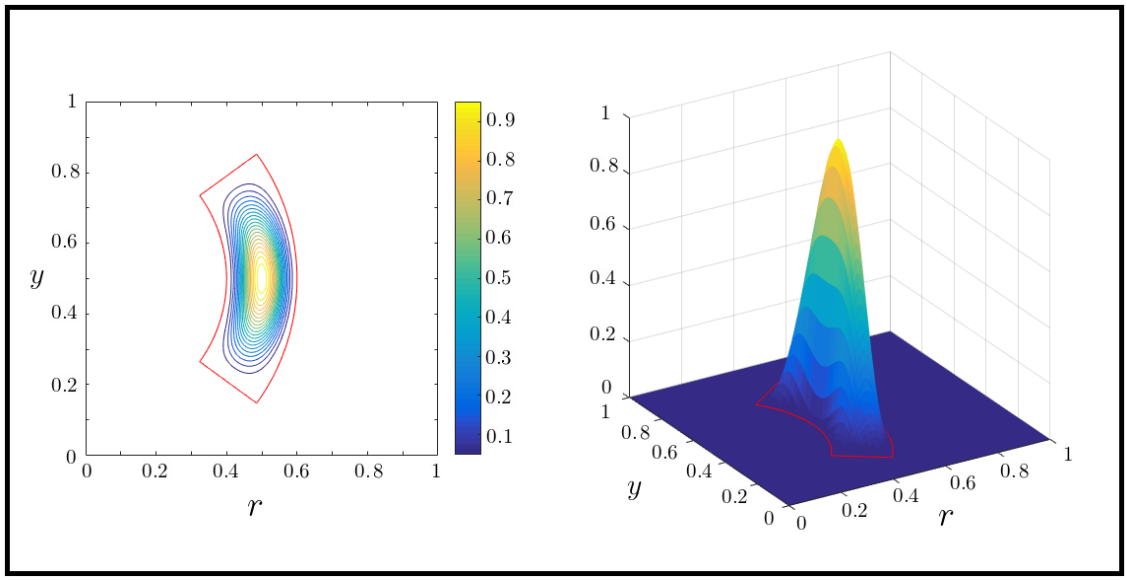

Figure 2.3: Contour lines and surface representation of the function $\zeta(r, y)$ for $C = (0.5, 0.5)$, $P_0 = (0, 0.5)$, $\tau = 0.1$, $K_\tau = 2\pi$. The bounds of the support correspond to the red lines.

To conclude, we would like to observe that the velocity field $\boldsymbol{V}$ taken in (2.24) and (2.25) has non vanishing divergence in each point of the (r, y)-plane, as show below

$$\begin{aligned}\nabla \cdot \boldsymbol{V} = \frac{1}{r}\frac{\partial}{\partial r}(rV_r) + \frac{\partial V_y}{\partial y} &= \frac{c}{r}U_r + \frac{\partial U_r}{\partial r} + \frac{\partial U_y}{\partial y} \\ &= c\Big(\frac{1}{\sqrt{r^2 + (y - y_0)^2}} + \frac{(y - y_0)^2}{(r^2 + (y - y_0)^2)^{3/2}} + \frac{r^2}{(r^2 + (y - y_0)^2)^{3/2}}\Big) \qquad (2.26) \\ &= \frac{2c}{\sqrt{r^2 + (y - y_0)^2}}.\end{aligned}$$

2.7. Exact solutions: spherical waves

We want to review the definition of "spherical" wave in both the Maxwellian and the Non-Maxwellian framework, by comparing the behavior of wave-fronts generated by an infinitesimal dipole. In this circumstance, it is convenient to work with a spherical system of coordinates (R, ϑ, φ).

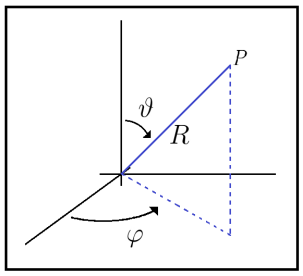

Figure 2.4: Spherical system of coordinates. $R \geq 0$, $\vartheta \in [0, \pi]$, $\varphi \in [0, 2\pi[$.

An electromagnetic wave displaying perfect spherical fronts is given, in appendix D of [13], by the following triplet of fields

$$\begin{aligned} \boldsymbol{E} &= \Big(0,\ \frac{c}{R}\ g_1(\vartheta,\varphi) f(ct-R),\ \frac{c}{R}\ g_2(\vartheta,\varphi) f(ct-R)\ \Big) \\ \boldsymbol{H} &= \Big(0,\ -\frac{1}{\mu R}\ g_2(\vartheta,\varphi) f(ct-R),\ \frac{1}{\mu R}\ g_1(\vartheta,\varphi) f(ct-R)\ \Big) \\ \boldsymbol{V} &= \Big(\ c,\ 0\ ,\ 0\ \Big), \end{aligned} \tag{2.27}$$

where f, g_1 and g_2 are arbitrary smooth functions. In order to have $\nabla \cdot \boldsymbol{B} = 0$, the following relation must be satisfied[21]

$$\frac{\partial\big(g_2 \sin\vartheta\big)}{\partial\theta} = \frac{\partial g_1}{\partial\varphi}. \tag{2.28}$$

Note that the electric and magnetic fields have no component along the radial direction and $\boldsymbol{E} \cdot \boldsymbol{H} = 0$. These fields shift along the radial direction with velocity c modulated by the function $f(ct - R)$. The wave-fronts turn out to be the skin of spheres centered in the

[21] We recall the form of the divergence operator in spherical coordinates (R, ϑ, φ):
$\nabla \cdot \boldsymbol{u} = \dfrac{1}{R^2}\dfrac{\partial}{\partial R}(R^2\ u_R) + \dfrac{1}{R\sin\vartheta}\dfrac{\partial}{\partial\vartheta}(\sin\vartheta\ u_\vartheta) + \dfrac{1}{R\sin\vartheta}\dfrac{\partial u_\varphi}{\partial\varphi}.$

origin, where an infinitesimal oscillating dipole is placed.
By explicitly computing the divergence of the electric field

$$\nabla \cdot \boldsymbol{E} = \frac{c}{R^2 \sin\vartheta} f(ct-R)\left(\frac{\partial\big(g_1 \sin\vartheta\big)}{\partial\theta} \; + \; \frac{\partial g_2}{\partial\varphi} \right)$$

it turns out[22] that there are no possibilities to impose the free divergence condition required from equations (1.2), unless one chooses the trivial null solution. On the contrary the above triplet (2.27) verifies the extended set of equations[23].
Let us observe that the field $\boldsymbol{V}$ has a non vanishing divergence, i.e. $\nabla \boldsymbol{V} = 2cR^{-1}$. We can further observe that, for R tending to infinity, $\nabla \cdot \boldsymbol{E}$ decreases faster than $\boldsymbol{E}$. This shows that the non-linearity of the equations becomes weaker and weaker as the fields are evaluated far from the source. From this observation it follows that the superposition principle, that as a consequence of the non-linearity of the equation does not hold, it may be recovered for sufficiently large values of R, since the term $\rho\boldsymbol{V}$ decays faster as R increases. This agrees with the fact that the superposition principle is true in many applications involving wave propagation, as for instance the constructive and destructive interference.

In the framework of the standard electrodynamics equations, the Hertz's solution[24] for the infinitesimal dipole is usually taken as an example of spherical wave that solves (1.2). Up to a multiplicative constant the electric and magnetic fields associated to the Hertzian solution take the form given here below

$$\begin{aligned} \boldsymbol{E} &= \left(\frac{2\cos\vartheta}{R^2}\Big(\frac{1}{R}f_1 + k f_2\Big),\; \frac{\sin\vartheta}{R}\Big(\frac{k}{R}f_2 + \frac{1}{R^2}f_1 - k^2 f_1\Big),\; 0 \right), \\ \boldsymbol{H} &= \left(0,\; 0,\; -\frac{k\sin\vartheta}{R}\sqrt{\frac{\varepsilon}{\mu}}\Big(k f_1 - \frac{1}{R}f_2\Big) \right). \end{aligned} \tag{2.29}$$

Where $f_1 = \sin(ckt - kR)$ and $f_2 = \cos(ckt - kR)$. The constant k has the dimension of the inverse of a length.

In this case, the divergence of both electric and magnetic fields is identically zero and

[22] The complex function $g_1 - i\, g_2 \;\sin(\vartheta)$ is holomorphic on the Riemann sphere, so it has to vanish. See [16].
[23] The proof of this statement is given in appendix I.
[24] See [22].

it is trivial to observe that $\boldsymbol{E} \cdot \boldsymbol{B} = 0$. Nevertheless, the relation between electric and magnetic fields intensity $|\boldsymbol{E}| = c|\boldsymbol{B}|$ does not hold. As discussed in appendix D of [13], the behavior of the wave-fronts of the Hertz's solution is hard to understand, especially in the near field zone. The envelope of the electric and magnetic fields does not correspond to sphere, wave fronts have toroid shape and do not move according to geometrical optics[25] The Hertz's dipole wave propagates according to geometrical optics rules, following the radial direction outgoing from the dipole, only on the plane orthogonal to the dipole and passing through its center. At great distance from the source it can be show that the behaviour of the electromagnetic fields is more or less closer to the one of a spherical wave[26], on the contrary close to the dipole this is no more true. For instance, the Poynting vector is not everywhere radial and sometimes it is directed toward the source[27] (See figure 2.5).

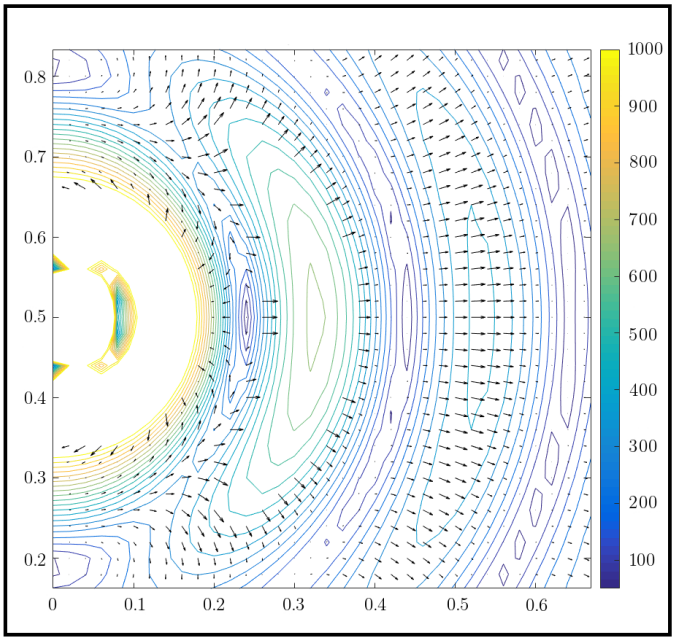

Figure 2.5: Contour lines of the norm of the electric field and Poynting vector (black) relative to the Hertzian solution 2.29. The exact solution is evaluated on a squared grid with 50×50 nodes. The contour lines relative to values greater than 1000 are not displayed. Note that in proximity of the source (placed at $(0, 1/2)$) the Poynting vector it is not radial.

[25] To find an in-depth exposition of those facts see [13] appendix D and [12], chapter 1.
[26] See [23] chapter 9.
[27] See [30].

2.8. Boundary conditions

Since later we will be interested in the study of the electromagnetic fields generated by a biconic antenna, (and, more in general, with guided propagation of electromagnetic waves) it is necessary to investigate how fields interact with conductive boundaries. The matter is not simple and there exists a lot of literature about the topic of boundary conditions both from the physical and the engineering point of view.

As pointed out by John David Jackson in [24] there is bit of confusion around the behaviour of electromagnetic energy radiated by an antenna.
This process could be divided in three parts: first the energy emerges from a localized source, then is guided by the antenna conductor and ultimately becomes free to form the radiation described by the asymptotic Poynting vector.
Jackson identifies in the second part of the process a possible source of misunderstanding in the treatment of the antenna problem. Indeed many researchers believe that the current of each volume element along the guides is the real source of the radiated energy.
This approach induces to think that a suitable *a priori* choice of source field on the body of the antenna is the right way to solve correctly the problem. On the other hand, a radiating antenna may be seen as an electromagnetic boundary value problem, in which the current distributed on the guides emerges as a part of the solution, not as an input.
It is commonly accepted that the antenna structure does not itself radiate, but rather guides the energy from the input source and launches it into its final radiation pattern.
For instance if one considers the case of an antenna composed by thin straight conducting elements, which could be approximated with elements of infinitesimal section, it can be shown that an oscillating sinusoidal current is distributed on them. Nevertheless, this is only an ideal case in which it is possible to predetermine electric and magnetic field on the conducting elements[28] that match quite well experimental results. Even though in such cases specifying plausible fields source on the guide elements may be appropriate, it does not mean that this strategy also works for the treatment of a realistic antenna.

It is standard to approach at the boundary condition problem relative to an electromagnetic wave in presence of a conductive guide, by considering the general problem of the boundary conditions at interface between different media, as we are going to recover for the extended framework.

[28] It is the case of centered linear antenna in which the length of its arms is smaller with respect to the wavelength. See [23], chapter 9.

Let $\mathcal{U}$ be a finite volume of the three dimensional space, denote with

- dv a volume element,
- $\partial\mathcal{U}$ the closed surface bounding $\mathcal{U}$,
- du an element of area on $\partial\mathcal{U}$,
- $\boldsymbol{n}$ the outward normal, defined on $\partial\mathcal{U}$, to the enclosed volume.

Let S be an open surface of the three dimensional space, denote with

- ds a surface element,
- ∂S the contour of S,
- $d\boldsymbol{l}$ an oriented line element on ∂S,
- $\boldsymbol{n}'$ a normal, defined on S by applying the right-hand side rule according to the orientation of $d\boldsymbol{l}$.

It is possible to give an integral formulation of first three equations of system (2.9) plus the definition of divergence, obtaining

$$\begin{cases} \displaystyle\int_S \frac{\partial(\varepsilon \boldsymbol{E})}{\partial t}\, ds = \int_S \nabla \times \boldsymbol{H}\, ds - \int_S (\varepsilon \rho_{free} \boldsymbol{V} + \boldsymbol{J}_s)\, ds \\ \displaystyle\int_S \frac{\partial(\mu \boldsymbol{H})}{\partial t}\, ds = -\int_S \nabla \times \boldsymbol{E}\, ds \\ \displaystyle\int_{\mathcal{U}} \nabla \cdot (\mu \boldsymbol{H})\, dv = 0 \\ \displaystyle\int_{\mathcal{U}} \nabla \cdot (\varepsilon \boldsymbol{E})\, dv = \int_{\mathcal{U}} (\rho_{free} + \rho_s)\, dv. \end{cases}$$

Here the hypothesis of linear homogeneous media, i.e. $\boldsymbol{D} = \epsilon \boldsymbol{E}$ and $\boldsymbol{B} = \mu \boldsymbol{H}$, is assumed. The term $\boldsymbol{J}_s$ is the contribution of the current source across the surface S, ρ_s is the contribution of the charge sources present in the volume $\mathcal{U}$, while ρ_{free} counts the contribution due to electric fields that has non-zero divergence also in absence of sources. At this point we have all the elements necessary to use the divergence theorem[29] and

[29] $\displaystyle\int_{\mathcal{U}} \nabla \cdot \boldsymbol{F}\, dv = \oint_{\partial\mathcal{U}} \boldsymbol{F} \cdot \boldsymbol{n}\, du$, where field and domain of integration satisfies certain regularity property. See [23] and [19].

Stokes's theorem[30], to rewrite the previous system of integral equations in the following form

$$\begin{cases} \displaystyle\int_S \left[\frac{\partial(\varepsilon \boldsymbol{E})}{\partial t}\right] \cdot \boldsymbol{n}' \; ds = \oint_{\partial S} \boldsymbol{H} \cdot d\boldsymbol{l} - \int_S (\varepsilon \rho_{free} \boldsymbol{V} + \boldsymbol{J}_s) \; ds \\ \displaystyle\int_S \frac{\partial(\mu \boldsymbol{H})}{\partial t} \; ds = -\oint_{\partial S} \boldsymbol{E} \cdot d\boldsymbol{l} \\ \displaystyle\oint_{\partial \mathcal{U}} (\mu \boldsymbol{H}) \cdot \boldsymbol{n} \; du = 0 \\ \displaystyle\oint_{\partial \mathcal{U}} (\varepsilon \boldsymbol{E}) \cdot \boldsymbol{n} \; du = \int_{\mathcal{U}} (\rho_{free} + \rho_s) \; dv. \end{cases} \tag{2.30}$$

The system (2.30) has the same form as its analogue relative to classical Maxwell's equations. This means that by taking two different linear homogeneous media separated by a surface where the normal $\mathbf{n}$ has been uniquely defined, and by indexing with 1 the fields relative to the half-space from which the normal is outward and with 2 the fields relative to the half space from which the normal is in-going respectively, it is possible to invoke appropriate geometrical arguments[31] (See figure 2.6) to carry out the following *continuity equations* for the electric and magnetic fields at the boundary

$$\begin{aligned} &\boldsymbol{n} \times (\boldsymbol{E}_2 - \boldsymbol{E}_1) = 0 \\ &\boldsymbol{n} \times (\boldsymbol{H}_2 - \boldsymbol{H}_1) = \boldsymbol{J}_{surf} \\ &(\mu_2 \boldsymbol{H}_2 - \mu_1 \boldsymbol{H}_1) \cdot \boldsymbol{n} = 0 \\ &(\varepsilon_2 \boldsymbol{E}_2 - \varepsilon_1 \boldsymbol{E}_1) \cdot \boldsymbol{n} = \sigma_{surf} \end{aligned} \tag{2.31}$$

Here J_{surf} and σ_{surf} indicates the current and the surface charge density on the separation surface between media 1 and media 2. These last two quantities, which in general are function of the point considered on the surface, are related to the ρ_{free}, ρ_s and $\boldsymbol{J}_s$ previously defined.

[30] $\displaystyle\int_{\mathcal{S}} (\nabla \times \boldsymbol{F}) \cdot \boldsymbol{n} \; ds = \oint_{\partial \mathcal{S}} \boldsymbol{F} \cdot d\boldsymbol{l}$, where field and the domain of integration satisfies certain regularity property. See [23] and [19].

[31] The detailed procedure here omitted can be found in [23], chapter 1.

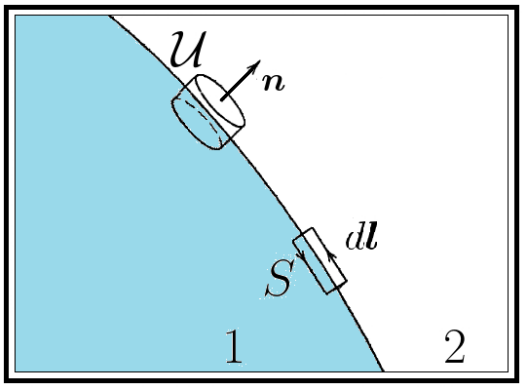

Figure 2.6: Schematic diagram of the surface between different media. The volume $\mathcal{U}$ is a small pillbox, half in one medium and half in the other one. The rectangular contour S is partly in one medium and partly in the other one, and is oriented with its plane perpendicular to the surface.

The equations presented above are used to theoretically investigate the interaction between a *perfect electric conductor* (PEC) and an electromagnetic wave, from which it is possible to deduce the characterization of null tangential electric field component at the interface.

A PEC it is an idealized medium that does not allow the propagation of electromagnetic waves in its interior. On the boundary surface between a PEC and another medium could exist a density of charge or current when an electromagnetic field interacts with the conductor.

Consider the case of an empty domain that is partially filled with a PEC. Suppose that the boundary between them is a straight line. If the normal to the the boundary is directed from the empty space into the perfect conductor, then, according to the notation of (2.31) the PEC is indexed as 2, while the empty space is indexed as 1.

It is known that the PEC does not allow the propagation of electromagnetic fields in its interior, so it turns out that $\boldsymbol{E}_2 = 0$ and $\boldsymbol{H}_2 = 0$. One can finally recover from (2.31) the equations that describe the behavior of an electromagnetic wave on the boundary between the empty space and the PEC, i.e.

$$\boldsymbol{n} \times \boldsymbol{E}_1 = 0$$

$$\boldsymbol{n} \times \boldsymbol{H}_1 = -\boldsymbol{J}_{surf}$$

$$\boldsymbol{H}_1 \cdot \boldsymbol{n} = 0$$

$$\boldsymbol{E}_1 \cdot \boldsymbol{n} = -\frac{\sigma_{surf}}{\varepsilon_1}.$$

Thus, the tangential component (with respect to the boundary), of the electric field has to vanish on the separation surface. The same holds for the normal component of the magnetic field.
Charges and currents on the boundary change in order to produce suitable discontinuities of the normal component of the electric field and the tangential component of the magnetic field, necessary to the preservation of a null electromagnetic field inside the conductor.
It is important to remark that, only in the static case, there is no electric field inside a conductor. Of course, since a PEC is a conceptual media, one could assume that the charge inside it instantly moves in response to field variations, in order to produce the correct surface density ensuring the absence of the electric field in its interior.
Nevertheless, under specific hypothesis related to the frequency of the electromagnetic radiation, a real conductor can be approximated by a PEC media, and this is the case of the skin effect[32].
This is the reason why to impose that the tangential component of the electric field and the normal component of the magnetic field both vanish is a way to express boundary conditions for a conductive wave guide.

To conclude this section, we want to introduce an additional contribute to the computation of the electric field at the boundaries, that enforces the dependence on the behaviour of the field at the interior of conductive wave guides. Once the normal component at the guide has been determined according to the above conditions, it is further subjected to the following transport equation

$$\frac{\partial E_n}{\partial t} = (c - v_g)\ \boldsymbol{n} \times \nabla E_n. \tag{2.32}$$

[32]It occurs when the *skin depth* is much smaller than the section of a conductor. The *skin depth* is the distance in which the electric fields exponentially decays to zero inside a conductor.

Here, the constant v_g is a positive real number lower than c. The imposition of this condition produces a transport of the normal component of the electric field along the boundary trasversal direction. In the case $v_g = c$ the right-hand side of (2.32) vanishes and the classic PEC conditions are recovered since no transport occours. The numerical treatment of (2.32) is exhibited in section 3.5, while its application and the produced effect on simulated electromagnetic fields can be found in section 4.2.

Numerical methods

In this chapter we describe the numerical methods used to approximate both systems (2.20) and (2.21).
Due to the originality of formulation (2.19), examples of numerical treatment of the whole system of equations are not available in literature[1].
However, regarding each equation one can find plenty of suitable numerical methods.
We decided to focus our choice on low-order finite difference schemes. It was our intention to deal with easy-implementable discrete equations, through this may have a negative impact on computational costs.
One of our purposes was to quickly reach a working model, able to catch the behaviour we were interested in and leave to future developments the research of higher accurate methods.

Since we were oriented to finite difference schemes, our first choice has been the popular *Yee scheme*[2]. By the way, soon it turned out that this was not a suitable method[3]. Basically, the main problem with the Yee scheme arises in the treatment of fields with divergence different from zero changing with time. The structured grid, used in the Yee scheme forces instead the conservation of such a quantity.

We finally decided to split each one of systems (2.20) and (2.21) in three parts as show below.

[1] Numerical simulations related to problems involving a simplified version of the extended equations (2.19) have been carried out in [11], [17], [18] and [36].
[2] See [39] and [35].
[3] See appendix IV.

Subdivision of system (2.20)**, relative to cartesian framework**

$$\begin{cases} \dfrac{\partial E_x}{\partial t} \;=\; \dfrac{1}{\varepsilon}\,\dfrac{\partial H_z}{\partial y} \;-\; \rho\, V_x \\ \\ \dfrac{\partial E_y}{\partial t} \;=\; -\dfrac{1}{\varepsilon}\,\dfrac{\partial H_z}{\partial x} \;-\; \rho\, V_y \\ \\ \dfrac{\partial H_z}{\partial t} \;=\; -\dfrac{1}{\mu}\left(\dfrac{\partial E_y}{\partial x} \;-\; \dfrac{\partial E_x}{\partial y}\right) \end{cases} \tag{3.1}$$

$$\begin{cases} \rho\left[\dfrac{\partial V_x}{\partial t} + V_x\dfrac{\partial V_x}{\partial x} + V_y\dfrac{\partial V_x}{\partial y} \;+\; \theta\left(E_x \;+\; \mu\, V_y\, H_z\right)\right] \;=\; -\dfrac{\partial p}{\partial x} \\ \\ \rho\left[\dfrac{\partial V_y}{\partial t} + V_x\dfrac{\partial V_y}{\partial x} + V_y\dfrac{\partial V_y}{\partial y} \;+\; \theta\left(E_y \;-\; \mu\, V_x\, H_z\right)\right] \;=\; -\dfrac{\partial p}{\partial y}. \end{cases} \tag{3.2}$$

$$\frac{\partial p}{\partial t} \;=\; \theta\,\rho\left(E_x\, V_x + E_y\, V_y\right) \tag{3.3}$$

Subdivision of system (2.21)**, relative to cylindrical framework**

$$\begin{cases} \dfrac{\partial E_r}{\partial t} \;=\; -\dfrac{1}{\varepsilon}\,\dfrac{\partial H_\varphi}{\partial y} \;-\; \rho\, V_r \\ \\ \dfrac{\partial E_y}{\partial t} \;=\; \dfrac{1}{r\varepsilon}\,\dfrac{\partial (r H_\varphi)}{\partial r} \;-\; \rho\, V_y \\ \\ \dfrac{\partial H_\varphi}{\partial t} \;=\; -\dfrac{1}{\mu}\left(\dfrac{\partial E_r}{\partial y} \;-\; \dfrac{\partial E_y}{\partial r}\right) \end{cases} \tag{3.4}$$

$$\begin{cases} \rho\left[\dfrac{\partial V_r}{\partial t} + V_r\dfrac{\partial V_r}{\partial r} + V_y\dfrac{\partial V_r}{\partial y} \;+\; \theta\left(E_r \;-\; \mu\, V_y\, H_\varphi\right)\right] \;=\; -\dfrac{\partial p}{\partial r} \\ \\ \rho\left[\dfrac{\partial V_y}{\partial t} + V_r\dfrac{\partial V_y}{\partial r} + V_y\dfrac{\partial V_y}{\partial y} \;+\; \theta\left(E_y \;+\; \mu\, V_r\, H_\varphi\right)\right] \;=\; -\dfrac{\partial p}{\partial y}. \end{cases} \tag{3.5}$$

$$\frac{\partial p}{\partial t} = \theta\,\rho\left(E_r\,V_r + E_y\,V_y\right) \tag{3.6}$$

In both cases the first part is strictly related to the classic Maxwell's equations. This three equations can be seen as a sub-problem in which only the components of the electric and magnetic fields play the role of unknown. The additional term $-\rho\boldsymbol{V}$, that compares in the Ampère's law, introduces the components of the vector $\boldsymbol{V}$ as variable coefficients of both partial differential equation systems (3.1) and (3.4). This feature will be clarified by looking to the reformulations of (3.1) and (3.4) in to (3.11) and (3.13) respectively.
The second group, i.e. (3.2) for the cartesian framework and (3.5) for the cylindrical framework, is constituted by the couple of equations involving velocity derivative with respect to time, in which also compares the nonlinear term $(\boldsymbol{V}\cdot\nabla)\boldsymbol{V}$. That term, together with the presence of ρ at the denominator of a fraction, will be the source of many difficulties for the numerical approximation, as we will see in section 3.3.
Finally, the third part, i.e. (3.3) for the cartesian framework and (3.6) for the cylindrical framework, consist on the single equation describing the time variation of p.
Thanks to the presented subdivision, each block can be attached with a suitable numerical method, as it is show in the following sections.

3.1. Lax-Wendroff scheme

Both groups of three equations (3.1) and (3.4) constitute an hyperbolic system of partial differential equations, as we are going to show later on in this section. We decided to approximate it by the Lax-Wendroff scheme[4]. Such a numerical method is one-step explicit in time and provides second-order accuracy, at least in the case of scalar partial differential equations with constant coefficients. Concerning with the simulation of solitary electromagnetic waves the scheme has already been applied in [36] and [11].
Since we have to deal with a system of equations in two spatial dimension and non constant coefficients, we will mainly work with the vector version of the Lax-Wendroff[5].

To begin with, it is useful to recall the definition[6] of a hyperbolic system of first or-

[4] See [26].
[5] See [36], [34] and [21].
[6] See [21].

der partial differential equations with constant coefficients in d dimensions.
Given n scalar equations written in the following form

$$\frac{\partial \boldsymbol{F}}{\partial t} = \sum_{\nu=1}^{d} M_{x_\nu} \frac{\partial \boldsymbol{F}}{\partial x_\nu} \tag{3.7}$$

with $\quad \boldsymbol{F} : \mathbb{R}^d \times [0,T] \longrightarrow \mathbb{R}^n \quad$ and $\quad M_{x_\nu} \in \mathcal{M}_{n\times n}(\mathbb{R}) \quad \forall \nu = 1, \ldots, d.$

one can consider a Cauchy problem by adding an initial condition $\boldsymbol{F}(\boldsymbol{x}, 0)$, $x \in \mathbb{R}^d$. Hereafter we consider the initial data, for $t = 0$, assigned when needed together with some boundary conditions at the inflow boundary.

Definition. 3.1 *Given the system* (3.7)*, consider the matrix P to be the linear combination of the matrices M_{x_ν} defined in the following way,*

$$P(\boldsymbol{\omega}) = \sum_{\nu=1}^{d} \omega_\nu M_{x_\nu}, \qquad \boldsymbol{\omega} := (\omega_1, \ldots, \omega_d) \in \mathbb{R}^d, \quad \textit{with} \quad \sum_{\nu=1}^{d} \omega_\nu^2 = 1.$$

System (3.7) *then is called*

- ***strictly hyperbolic*** *if, for every vector $\boldsymbol{\omega}$, the eigenvalues of $P(\boldsymbol{\omega})$ are real and distinct,*
- ***symmetric hyperbolic*** *if all matrices M_{x_ν} are symmetric*[7]*,*
- ***strongly hyperbolic*** *if there is a constant $K > 0$ and, for every $\boldsymbol{\omega}$, a non-singular transformation $T(\boldsymbol{\omega})$ exists with,*

  $$\sup_{\boldsymbol{\omega}} \Big(\max_{|\boldsymbol{x}|=1} \mid T^{-1}(\boldsymbol{\omega})\ \boldsymbol{x} \mid \ + \ \max_{|\boldsymbol{x}|=1} \mid T(\boldsymbol{\omega})\ \boldsymbol{x} \mid \Big) \leq K$$

  such that $T^{-1}(\boldsymbol{\omega})P(\boldsymbol{\omega})T(\boldsymbol{\omega})$ is a diagonal matrix with real eigenvalues,
- ***weakly hyperbolic*** *if the eigenvalues of $P(\boldsymbol{\omega})$ are real.*

To extend the above definitions, to the case of non-constant coefficients, i.e. when the matrices M_{x_ν} are functions of the coordinates x_ν and t, it is necessary to require that those properties hold pointwise, i.e. for each $(x_1, x_2, \ldots, x_d, t)$ in the domain of definition

[7] This condition ensures that the matrix $P(\boldsymbol{\omega})$ is symmetric too. A consequence of the so called *spectral theorem* is that each symmetric real matrix can be diagonalized through an orthogonal matrix. If $P(\boldsymbol{\omega})$ is symmetric, then have real eigenvalues and admits an horthonormal basis of eigrnvectors.

of the problem (3.7).

From the definition it is clear that strictly, symmetric and strongly hyperbolic systems are also weakly hyperbolic systems. It is also true that strictly and symmetric hyperbolic systems are strongly hyperbolic systems[8].

Some authors[9] name *hyperbolic systems* those systems of partial differential equations (3.7), such that the matrix $P(\boldsymbol{\omega})$ is similar to a diagonal matrix with real eigenvalues and the matrices T and T^{-1} have are uniformly bounded with respect to a certain norm. These properties are strictly related to the notion of *well-posed* problem[10], where it is required the existence of a unique regular solution that cannot indiscriminately grow during its time evolution. In the case of non-dissipative hyperbolic problems with constant coefficient and initial datum $\boldsymbol{F}(\boldsymbol{x}, 0) = \boldsymbol{F}_0(\boldsymbol{x})$, except for weakly hyperbolic systems, inequalities like the following one hold

$$||\boldsymbol{F}(\boldsymbol{x}, t)||_{L^2} \leq Ke^{\alpha(t)}||\boldsymbol{F}_0(\boldsymbol{x})||_{L^2}.$$

Here α and K are two given real constants independent on the choice of $\boldsymbol{F}_0(\boldsymbol{x})$. By the way, in some particular cases the exponential term at the right-hand side can be eliminated.

In chapter 6 in [21], three theorems are given, where well-posedness is ensured for strongly hyperbolic systems with constant coefficients and for symmetric and strictly hyperbolic systems with variable coefficients.
The results of well-posedness for both the constant and variable coefficients cases, follow from the fact that it is possible to build a *symmetrizer*, as stated by the following theorems[11].

[8] The non trivial proof of this last implication can be found in chapter 6 of [21].

[9] For example see [34] and [32]. In the chapter 1 of [34] and in the chapter 7 of [32] the definition of hyperbolic system of partial differential equations is given for the one-dimensional case. This is the case of the system 3.1 in which one fix $d = 1$, thus the matrix P reduces to the only M_{x_1}. Both definition requires that M_{x_1} is diagonalisable with real eigenvalues. The higher dimensional case is treated only in chapter 9 of [34]. Here the definition of hyperbolic system recalls the one of strongly hyperbolic systems given in definition 3.1 of this thesis.

[10] A consensus definition of well-posed problem do not exist, for instance one can refer to the one given in chapter 4 of [21].

[11] See [21], chapter 6

Theorem. 3.1 *Let M be a matrix with real eigenvalues and a complete set of eigenvectors that are the columns of a matrix T. Then, given a real positive diagonal matrix D, the matrix $S := (T^{-1})^t D T^{-1}$ is positive defined and SM is a symmetric matrix.*

The matrix S is called symmetrizer of M and plays an important role in the determination of the well-posedness of an hyperbolic problem, as stated in the following theorem.

Theorem. 3.2 *Assume that a symmetrizer can be chosen as a smooth function of all variables on which the matrix $P(\omega)$ depends. Then the initial value problem* (3.7) *is well posed. If the system is strictly hyperbolic, then there is a smooth symmetrizer.*

Note that in the case of constant coefficients $P(\omega)$ depends only on the components of ω, while in the case of variable coefficients $P(\omega)$ depends on the components of ω, on the spatial coordinates x_ν and on the time t.

Our purpose is to work with equations (3.1) and (3.4), so that we shall consider $d = 2$, furthermore, in order to use discrete schemes it is necessary to consider a bounded domain. These considerations allow to rewrite the systems of partial differential equations in the following form

$$\frac{\partial \boldsymbol{F}}{\partial t} = M_{x_1} \frac{\partial \boldsymbol{F}}{\partial x_1} + M_{x_2} \frac{\partial \boldsymbol{F}}{\partial x_2}, \tag{3.8}$$

where $\boldsymbol{F} : [a_1, b_1] \times [a_2, b_2] \times [0, T] \longrightarrow \mathbb{R}^n$ and $M_{x_1}, M_{x_2} \in \mathcal{M}_{n\times n}(\mathbb{R})$.

The general coordinates notation (x_1, x_2, t) used here takes the meaning of (x, y, t) when it is referred to equations (3.1), and of (r, y, t) when it is referred to equations (3.4). Similarly, the hyper-rectangle $[a_1, b_1] \times [a_2, b_2] \times [0, T]$ and the vector function $\boldsymbol{F} = (F_1, F_2, F_3)$ indicate $[a_x, b_x] \times [a_y, b_y] \times [0, T]$ and (E_x, E_y, H_z), or $[a_r, b_r] \times [a_y, b_y] \times [0, T]$ and (E_r, H_φ, E_y), depending on whether one considers cartesian or cylindrical frameworks.

Definition. 3.2 *Given the vector function $\boldsymbol{F}$, depending on two space variables x_1, x_2 and on a time variable t, defined on the finite set $[a_1, b_1] \times [a_2, b_2] \times [0, T]$ and given three positive integer N_1, N_2, N_t it is possible to construct the discretization parameters*

$$\Delta x_1 = \frac{b_1 - a_1}{N_1}, \quad \Delta x_2 = \frac{b_2 - a_2}{N_2}, \quad \Delta t = \frac{T}{N_t}.$$

*Our **discrete grid** will be the following collection of points of the three dimensional space*

$$\mathcal{G}_{x_1,x_2,t} = \Big\{ \; (\, a_1 + i\Delta x_1 \, , \, a_2 + j\Delta x_2 \, , \, k\Delta t \,) \;\Big|\; i \in [0, N_1], \;\; j \in [0, N_2], \;\; k \in [0, N_t] \; \Big\}.$$

*Furthermore, with **spatial sub-grid** we will refer to the set containing only the spatial nodes*

$$\mathcal{G}^{sub}_{x_1,x_2} = \Big\{ \; (\, a_1 + i\Delta x_1 \, , \, a_2 + j\Delta x_2 \,) \;\Big|\; i \in [0, N_1], \;\; j \in [0, N_2] \; \Big\}.$$

For shake of simplicity, we avoid the use of different step length for the two spatial directions, thus hereafter we can consider only the case $\Delta x_1 = \Delta x_2 = h$.
By denoting with $\boldsymbol{f}^k_{i,j}$ the numerical approximation of $\boldsymbol{F}$ at the grid point $(\, a_1 + ih \, , \, a_2 + jh \, , \, k\Delta t \,)$, i.e.

$$\boldsymbol{f}^k_{i,j} \sim \boldsymbol{F}(\, a_1 + ih \, , \, a_2 + jh \, , \, k\Delta t \,),$$

the Lax-Wendroff scheme allows to compute the approximated solution at time $(k+1)\Delta t$ knowing it at time $k\Delta t$ via the following formula

$$\begin{aligned}
\boldsymbol{f}^{k+1}_{i,j} = & \Big[I_n - \lambda^2 \big(M^2_{x_1} + M^2_{x_2} \big) \Big] \, \boldsymbol{f}^k_{i,j} + \\
& \frac{\lambda}{2} \, M_{x_1} \big(I_n + \lambda M_{x_1} \big) \, \boldsymbol{f}^k_{i+1,j} \; + \; \frac{\lambda}{2} \, M_{x_2} \big(I_n + \lambda M_{x_2} \big) \, \boldsymbol{f}^k_{i,j+1} - \\
& \frac{\lambda}{2} \, M_{x_1} \big(I_n - \lambda M_{x_1} \big) \, \boldsymbol{f}^k_{i-1,j} \; - \; \frac{\lambda}{2} \, M_{x_2} \big(I_n - \lambda M_{x_2} \big) \, \boldsymbol{f}^k_{i,j-1} + \\
& \frac{\lambda^2}{8} \, \big(M_{x_1} M_{x_2} + M_{x_2} M_{x_1} \big) \, \big(\boldsymbol{f}^k_{i+1,j+1} + \boldsymbol{f}^k_{i-1,j-1} - \boldsymbol{f}^k_{i-1,j+1} - \boldsymbol{f}^k_{i+1,j-1} \big).
\end{aligned} \tag{3.9}$$

Here $\lambda = h/\Delta t$, and I_n denotes the identity squared matrix of dimension n.

The system of discrete equations (3.9) refers to the case of constant coefficients, nevertheless, it may be used in the case of variable coefficients by freezing the variables x_1, x_2 and t in the expression of the matrices M_{x_1} and M_{x_2}.

The stencil related to the discrete equation (3.9) is shown in figure 3.1.
The discussion about domain boundary conditions it is postponed at section 3.6.

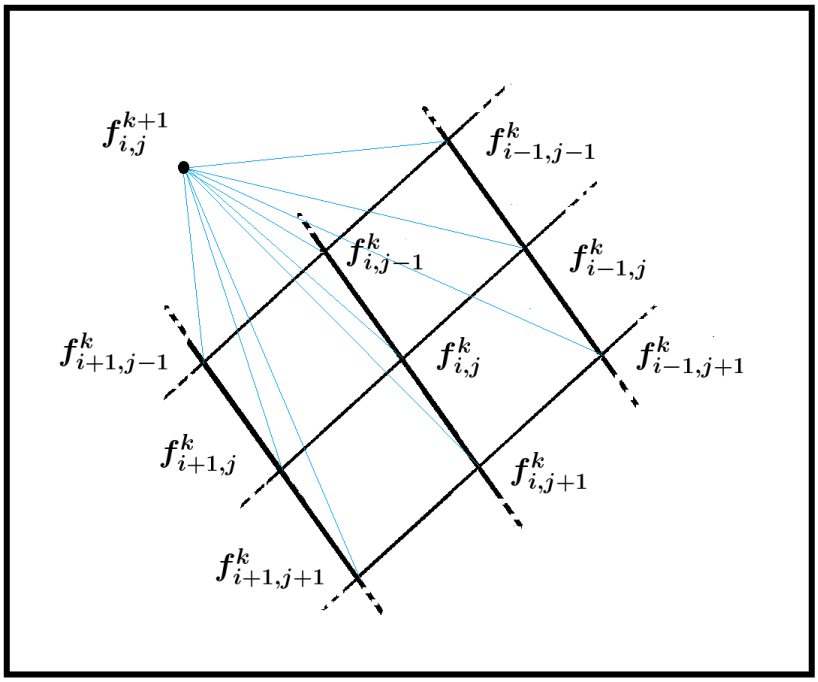

Figure 3.1: The stencil of the Lax-Wendroff scheme in the case of two spacial and one temporal dimensions.

To ensure stability of (3.9) the following condition should be satisfied

$$\lambda \left(\max_i \ |\sigma_i^{x_1}| \right) \ \leq \frac{1}{2\sqrt{2}}, \qquad \lambda \left(\max_i \ |\sigma_i^{x_2}| \right) \ \leq \frac{1}{2\sqrt{2}} \tag{3.10}$$

where $\{\sigma_i^{x_1}\}_{i=1,2,3}$ and $\{\sigma_i^{x_2}\}_{i=1,2,3}$ are the eigenvalues relative to M_{x_1} and M_{x_2} respectively. Theoretically the conditions (3.10) are suitable in the case of an hyperbolic system with constant coefficients.
Nonetheless, in the numerical simulations involving systems with variable coefficients, we have fixed Δt recovering inequalities like (3.10). In particular, by estimating a constant

Σ that bounds both $\max_i |\sigma_i^{x_1}|$ and $\max_i |\sigma_i^{x_1}|$ for each t, stability condition becomes $\lambda < (2\sqrt{2}\Sigma)^{-1}$.
This choice of stability condition in the case of variable coefficients it is sufficient to overcome numerical instability in most of all the simulation considered. To be honest, the research of stability conditions[12] for our systems with variable coefficients has been left incomplete for lack of time.

We now discuss the stability of the Lax-Wendroff scheme when applied to the systems of equations (3.1) and (3.4). As we are going to see, in both cases we will have to deal with a system of partial differential equations with variable coefficients. Moreover, one has to remember that the components of the velocity vector are functions of the spatial and temporal coordinates. Furthermore, if one consider the case of an electromagnetic wave that propagates in a domain in which different media are present, also ε and μ become functions of the spatial coordinates. For our purposes, the latter generalization is not necessary, we avoid this further complication by placing ourselves in a uniform medium. Actually, in section 4.3, we investigate the case of a wave that cross a layer between a linear homogeneous medium (whose permittivity is ε_1) and the vacuum (whose permittivity is ε_0). Thus, only in that case, the matrices M_{x_1} and M_{x_2} have a coefficient ε that is a function of the space coordinates. In particular, $\varepsilon = \varepsilon_1$ in the points that belong to the region occupied by the medium, while $\varepsilon = \varepsilon_0$ in the remaining part of the domain.

Cartesian framework
By considering the system (3.1), it is convenient to rewrite its equations by substituting to ρ its formulation in cartesian coordinates:

$$\begin{aligned}
\frac{\partial E_x}{\partial t} &= \frac{1}{\varepsilon}\frac{\partial H_z}{\partial y} - V_x\frac{\partial E_x}{\partial x} - V_x\frac{\partial E_y}{\partial y} \\
\frac{\partial E_y}{\partial t} &= -\frac{1}{\varepsilon}\frac{\partial H_z}{\partial x} - V_y\frac{\partial E_x}{\partial x} - V_y\frac{\partial E_y}{\partial y} \\
\frac{\partial H_z}{\partial t} &= -\frac{1}{\mu}\frac{\partial E_y}{\partial x} + \frac{1}{\mu}\frac{\partial E_x}{\partial y}.
\end{aligned} \tag{3.11}$$

[12] In [21] the problem of establish conditions on h and Δt that guarantee numerical stability of discrete schemes is treated in the case of systems with variables coefficients. Specific stability conditions for the Lax-Wendroff scheme are given only for strictly or symmetric hyperbolic problems.

By using the notation introduced in (3.8), we obtain

$$\boldsymbol{F} = \begin{bmatrix} E_x(x,y,t) \\ E_y(x,y,t) \\ H_z(x,y,t) \end{bmatrix}, \qquad M_x = \begin{bmatrix} -V_x & 0 & 0 \\ -V_y & 0 & -\frac{1}{\varepsilon} \\ 0 & -\frac{1}{\mu} & 0 \end{bmatrix}, \qquad M_y = \begin{bmatrix} 0 & -V_x & \frac{1}{\varepsilon} \\ 0 & -V_y & 0 \\ \frac{1}{\mu} & 0 & 0 \end{bmatrix}.$$

The characteristic polynomials of M_x and M_y are

$$\det\Big(M_x - \kappa\ I_3\Big) = -\kappa^2\ (V_x + \kappa) + (V_x + \kappa)\tfrac{1}{\varepsilon\mu} = (V_x + \kappa)(c^2 - \kappa^2),$$

$$\det\Big(M_y - \kappa\ I_3\Big) = -\kappa^2\ (V_y + \kappa) + (V_y + \kappa)\tfrac{1}{\varepsilon\mu} = (V_y + \kappa)(c^2 - \kappa^2).$$

Thus, in both situations, two out of three eigenvalues of each matrix are equal to the real constants c and $-c$, each one having algebraic multiplicity 1. The third eigenvalue is $-V_x$ for M_x and $-V_y$ for M_y, which are functions of x, y and t.

We have the following results

Proposition. 3.1 *The system of equations* (3.11) *is weakly hyperbolic according to definition 3.1.*

Proof. To carry out the analysis required to apply definition 3.1, we actually need to compute the eigenvalues of the matrix

$$P(\boldsymbol{\omega}) = \omega_x M_x + \omega_y M_y, \qquad \boldsymbol{\omega} = (\omega_x, \omega_y) \in \mathbb{R}^2 \quad \text{s.t.} \quad \omega_x^2 + \omega_y^2 = 1.$$

$$P(\boldsymbol{\omega}) = \begin{bmatrix} -\omega_x V_x & -\omega_y V_x & \omega_y \frac{1}{\varepsilon} \\ -\omega_x V_y & -\omega_y V_y & -\omega_x \frac{1}{\varepsilon} \\ \omega_y \frac{1}{\mu} & -\omega_x \frac{1}{\mu} & 0 \end{bmatrix}, \tag{3.12}$$

$$\det\Big(P(\boldsymbol{\omega}) - \kappa\ I_3\Big) = (\omega_x V_x + \omega_y V_y + \kappa)(c^2 - \kappa^2).$$

Thus, the eigenvalues of $P(\boldsymbol{\omega})$ are c, $-c$ and $-(\omega_x V_x + \omega_y V_y)$ that are real numbers. This proves that system (3.11) is weakly hyperbolic.

□

As it stated at the beginning of this section, the weak hyperbolicity it is not enough to ensure well-posedness of our problem. The matrix $P(\boldsymbol{\omega})$ defined in (3.12) it is clearly non symmetric, neither has distinct eigenvalues for each values of ω and (x, y, t). It is impossible to achieve a stronger result without showing the existence of a smooth *symmetrizer*, but this go behind our purposes.

Proposition. 3.2 *The system of equations* (3.11) *is not strongly hyperbolic according to definition 3.1.*

Proof. Let us consider the constant coefficient case $V_x = c$ and $V_y = 0$.
Let us further assume that $\varepsilon = \mu = c = 1$.
Under this assumptions the matrix $P(\boldsymbol{\omega})$ reduces to

$$P(\boldsymbol{\omega}) = \begin{bmatrix} -\omega_x & -\omega_y & \omega_y \\ 0 & 0 & -\omega_x \\ \omega_y & -\omega_x & 0 \end{bmatrix}.$$

The eigenvalues of $P(\boldsymbol{\omega})$ are $1, -1, -\omega_x$. Thus, recalling that ω_x and ω_y are two real numbers such that $\omega_x^2 + \omega_y^2 = 1$, we can conclude that:

i) when $\omega_x \neq \pm 1$ the matrix $P(\boldsymbol{\omega})$ has three distinct real eigenvalues, thus it is diagonalizable;

ii) when $\omega_x = \pm 1$, and consequently $\omega_y = 0$, the matrix $P(\boldsymbol{\omega})$ is diagonalizable if $m_g(-\omega_x) = 2$, i.e. $\operatorname{rank}(P(\boldsymbol{\omega}) + \omega_x I_3) = 1$.

Considering the case i) and by solving the three systems of equations ($\kappa = 1, -1, -\omega_x$)

$$\Big(P(\boldsymbol{\omega}) - \kappa I_3\Big) \begin{pmatrix} x_1 \\ x_2 \\ x_3 \end{pmatrix} = \begin{pmatrix} 0 \\ 0 \\ 0 \end{pmatrix}$$

it is possible to compute the three columns of the matrix $T(\boldsymbol{\omega})$:

$$T(\boldsymbol{\omega}) = \begin{bmatrix} \omega_x & -\omega_y & 0 \\ -\omega_x & \omega_x & 1 \\ 1 & 1 & 1 \end{bmatrix}.$$

Since $\det(T(\boldsymbol{\omega})) = -2\omega_y$, and $\omega_y \neq 0$ as a consequence of $\omega_x \neq \pm 1$, the matrix $T(\boldsymbol{\omega})$ is invertible and

$$T^{-1}(\boldsymbol{\omega}) = \begin{bmatrix} \dfrac{1-\omega_x}{2\omega_y} & -\dfrac{1}{2} & \dfrac{1}{2} \\ -\dfrac{1+\omega_x}{2\omega_y} & -\dfrac{1}{2} & \dfrac{1}{2} \\ \dfrac{\omega_x}{\omega_y} & 1 & 0 \end{bmatrix}.$$

The norms of the matrices T and T^{-1} are defined as $||A|| = \max_{|\boldsymbol{\nu}|=1} |A\boldsymbol{\nu}|$. We have:

$$||T(\boldsymbol{\omega})|| = \sqrt{2 + \sqrt{\frac{1+\omega_x^2}{2}}},$$

$$||T^{-1}(\boldsymbol{\omega})|| \geq \frac{1+\omega_x^2}{3(1-\omega_x^2)}.$$

The last norm is not bounded since it can indiscriminately grow when ω_x tends to either 1 or -1. It is clear that, independently on the choice of $T((1,0))$ and $T((-1,0))$, we get

$$\sup_{\boldsymbol{\omega}} \Big(||T(\boldsymbol{\omega})|| + ||T^{-1}(\boldsymbol{\omega})|| \Big) > K \qquad \forall K \in \mathbf{N},$$

which means that the definition of *strongly hyperbolic* problem is not satisfied in our case.

□

We apply the Lax-Wendroff scheme to the set of weakly hyperbolic equations in cartesian coordinates (3.11) on a finite domain $[a_x, b_x] \times [a_y, b_y] \times [0, T]$. To this end, we introduce a grid $\mathcal{G}_{x,y,t}$.
According to (3.10), a sufficient condition for stability is $\lambda \leq (2\sqrt{2}\ \max\{V_x, V_y, c\})^{-1}$.

Cylindrical framework

By considering the system (3.4), it is convenient to rewrite its equations multiplying the first and the third equations by r and explicitly expressing the definition of ρ in cylindrical coordinates. We get

$$\begin{aligned}
\frac{\partial(rE_r)}{\partial t} &= \frac{1}{\varepsilon}\frac{\partial(rH_\varphi)}{\partial y} - V_r\frac{\partial(rE_r)}{\partial r} - r\,V_r\frac{\partial E_y}{\partial y} \\
\frac{\partial E_y}{\partial t} &= -\frac{1}{r\,\varepsilon}\frac{\partial(r\,H_\varphi)}{\partial r} - \frac{V_y}{r}\frac{\partial(rE_r)}{\partial r} - V_y\frac{\partial E_y}{\partial y} \\
\frac{\partial(rH_\varphi)}{\partial t} &= -\frac{1}{\mu}\frac{\partial(rE_r)}{\partial y} + \frac{r}{\mu}\frac{\partial E_y}{\partial r}
\end{aligned} \tag{3.13}$$

that, by using notation of (3.8), leads to

$$\boldsymbol{F} = \begin{bmatrix} rE_r(r,y,t) \\ rH_\varphi(r,y,t) \\ E_y(r,y,t) \end{bmatrix}, \qquad M_r = \begin{bmatrix} -V_r & 0 & 0 \\ 0 & 0 & \frac{r}{\mu} \\ -\frac{V_y}{r} & \frac{1}{r\varepsilon} & 0 \end{bmatrix}, \qquad M_y = \begin{bmatrix} 0 & -\frac{1}{\varepsilon} & -rV_r \\ -\frac{1}{\mu} & 0 & 0 \\ 0 & 0 & -V_y \end{bmatrix}.$$

Though the matrices M_r and M_y, that look a bit different from the ones involved in the cartesian case since they contain the extra variable r, the computation of the eigenvalues provides the same results

$$\det\Big(M_r - \kappa\, I_3\Big) = -\kappa^2\,(V_r+\kappa) + (V_r+\kappa)\tfrac{1}{\varepsilon\mu} = (V_r+\kappa)(c^2-\kappa^2),$$

$$\det\Big(M_y - \kappa\, I_3\Big) = -\kappa^2\,(V_y+\kappa) + (V_y+\kappa)\tfrac{1}{\varepsilon\mu} = (V_y+\kappa)(c^2-\kappa^2).$$

Thus, also in this case, two of the three eigenvalues of each matrix are equal to the real constants c and $-c$, with algebraic multiplicity 1. The third eigenvalue is $-V_r$ for M_r and $-V_y$ for M_y, which are functions of the coordinates r, y and t.

We have the following result:

Proposition. 3.3 *The system of equations* (3.13) *is weakly hyperbolic according to definition 3.1.*

Proof. To carry out the analysis required to apply definition 3.1 we need to compute

the eigenvalues of the matrix

$$P(\boldsymbol{\omega}) = \omega_r M_r + \omega_y M_y, \qquad \boldsymbol{\omega} = (\omega_r, \omega_y) \in \mathbb{R}^2 \quad \text{s.t.} \quad \omega_r^2 + \omega_y^2 = 1.$$

$$P(\boldsymbol{\omega}) = \begin{bmatrix} -\omega_r V_r & -\omega_y \frac{1}{\varepsilon} & \omega_y r V_r \\ -\omega_y \frac{1}{\mu} & 0 & \omega_r \frac{r}{\mu} \\ -\omega_y \frac{1}{r} V_y & \omega_r \frac{1}{r\varepsilon} & -\omega_y V_y \end{bmatrix},$$

$$\det\Big(P(\boldsymbol{\omega}) - \kappa\ I_3\Big) = (\omega_r V_r + \omega_y V_y + \kappa)(c^2 - \kappa^2).$$

Thus eigenvalues of $P(\boldsymbol{\omega})$ are c, $-c$ and $-(\omega_r V_r + \omega_y V_y)$ which are real numbers.

□

We apply the Lax-Wendroff scheme to the set of weakly hyperbolic equations in cylindrical coordinates (3.13) on a finite domain $[a_r, b_r] \times [a_y, b_y] \times [0, T]$. To this end, we introduce a grid $\mathcal{G}_{r,y,t}$. According to (3.10) stability condition turns out to be $\lambda \leq (2\sqrt{2}\max\{V_r, V_y, c\})^{-1}$.

3.2. Approximation of the divergence

To begin with, it is important to notice that the divergence of the electric field is computed implicitly by the Lax-Wendroff scheme. This is clear when we compare (3.1) with (3.11) and (3.4) with (3.13).
Nevertheless, since we are going to approximate equations (3.2), (3.3), (3.5) and (3.6) with the finite-differences schemes that will be defined in the following sections, there is the need to compute explicitly the divergence of the electric field ρ. In order to estimate ρ on the same grids $\mathcal{G}_{x,y,t}$ and $\mathcal{G}_{r,y,t}$ used for the Lax-Wendroff scheme, we approximate $\rho(ih, jh, k\Delta t) \sim \rho_{i,j}^k$ by centred finite-differences approach.
The explicit form of the scheme depends on the coordinate system considered, and, in the case of cylindrical coordinates the possible presence of the rotation axis in the domain may originate some problems. Thus, we prefer to discuss separately the cartesian and the cylindrical frameworks, as already done in the presentation of the Lax-Wendroff scheme.
The computation of the divergence at time $k\Delta t$ will involve only the values of the electric

field at the same time $k\Delta t$. At the borders of the computational domain, where central difference cannot be implemented, forward difference will be used instead.

Cartesian framework

At the interior of the computational domain defined by the grid $\mathcal{G}_{x,y,t}$, the discrete divergence of the electric field in cartesian coordinates is expressed as follows

$$\rho_{i,j}^{k} = \frac{E_{x}{}_{i+1,j}^{k} - E_{x}{}_{i-1,j}^{k}}{2h} + \frac{E_{y}{}_{i,j+1}^{k} - E_{y}{}_{i,j-1}^{k}}{2h} \qquad \begin{matrix} i = 1, \ldots, N_x - 1 \\ j = 1, \ldots, N_y - 1 \end{matrix} . \tag{3.14}$$

Near the boundaries we use the following scheme

$$\rho_{i,j}^{k} = \begin{cases} \dfrac{E_{x}{}_{0,j}^{k} - E_{x}{}_{1,j}^{k}}{-h} + \dfrac{E_{y}{}_{0,j+1}^{k} - E_{y}{}_{0,j-1}^{k}}{2h} & j = 1, \ldots, N_y - 1 \\ \dfrac{E_{x}{}_{N_x,j}^{k} - E_{x}{}_{N_x-1,j}^{k}}{h} + \dfrac{E_{y}{}_{N_x,j+1}^{k} - E_{y}{}_{N_x,j-1}^{k}}{2h} & j = 1, \ldots, N_y - 1 \\ \dfrac{E_{x}{}_{i+1,0}^{k} - E_{x}{}_{i-1,0}^{k}}{2h} + \dfrac{E_{y}{}_{i,0}^{k} - E_{y}{}_{i,1}^{k}}{-h} & i = 1, \ldots, N_x - 1 \\ \dfrac{E_{x}{}_{i+1,N_y}^{k} - E_{x}{}_{i-1,N_y}^{k}}{2h} + \dfrac{E_{y}{}_{i,N_y}^{k} - E_{y}{}_{i,N_y-1}^{k}}{h} & i = 1, \ldots, N_x - 1 \\ \dfrac{E_{x}{}_{0,0}^{k} - E_{x}{}_{1,0}^{k}}{-h} + \dfrac{E_{y}{}_{0,0}^{k} - E_{y}{}_{0,1}^{k}}{-h} & \\ \dfrac{E_{x}{}_{N_x,0}^{k} - E_{x}{}_{N_x-1,0}^{k}}{h} + \dfrac{E_{y}{}_{N_x,0}^{k} - E_{y}{}_{N_x,1}^{k}}{-h} & \\ \dfrac{E_{x}{}_{0,N_y}^{k} - E_{x}{}_{1,N_y}^{k}}{-h} + \dfrac{E_{y}{}_{0,N_y}^{k} - E_{y}{}_{0,N_y-1}^{k}}{h} & \\ \dfrac{E_{x}{}_{N_x,N_y}^{k} - E_{x}{}_{N_x-1,N_y}^{k}}{h} + \dfrac{E_{y}{}_{N_x,N_y}^{k} - E_{y}{}_{N_x,N_y-1}^{k}}{h} & \end{cases} \tag{3.15}$$

Cylindrical framework

Similar considerations are carried out in the case of the cylindrical coordinate system. At the interior of the computational domain defined by the grid $\mathcal{G}_{r,y,t}$ the discrete divergence of the electric field is written as

$$\rho_{i,j}^{k} = \frac{{E_r}_{i,j}^{k}}{a_r + ih} + \frac{{E_r}_{i+1,j}^{k} - {E_r}_{i-1,j}^{k}}{2h} + \frac{{E_y}_{i,j+1}^{k} - {E_y}_{i,j-1}^{k}}{2h} \qquad \begin{matrix} i = 1, \ldots, N_r - 1 \\ j = 1, \ldots, N_y - 1 \end{matrix} . \tag{3.16}$$

The evaluation of the divergence of electric field at the domain boundary[13] (Figure 3.2) could be obtained by applying forward difference. Nevertheless, it is important to distinguish between the case $a_r = 0$ or $a_r > 0$, or in other words we must treat in a different way computational domain that have the axis of rotation $r = 0$ as left side or not.

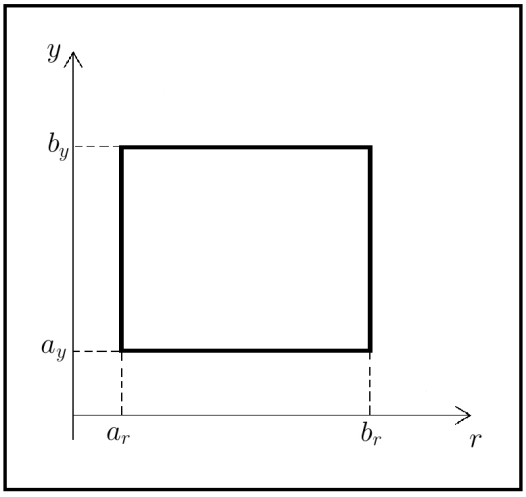

Figure 3.2: Representation of the computational domain $[a_r, b_r] \times [a_y, b_y]$.

[13]The nodes placed on the straight lines $r = a_r$, $r = b_r$, $y = a_y$, $y = b_y$ in the sense of definition 3.2.

When $a_r > 0$ a scheme similar to (3.15) is recovered as shown below

$$\rho^k_{i,j} = \begin{cases} \dfrac{E_r{}^k_{0,j}}{a_r} + \dfrac{E_r{}^k_{0,j} - E_r{}^k_{1,j}}{-h} + \dfrac{E_y{}^k_{0,j+1} - E_y{}^k_{0,j-1}}{2h} & j = 1, \dots, N_y - 1 \\ \dfrac{E_r{}^k_{N_r,j}}{a_r + N_r h} + \dfrac{E_r{}^k_{N_r,j} - E_r{}^k_{N_r-1,j}}{h} + \dfrac{E_y{}^k_{N_r,j+1} - E_y{}^k_{N_r,j-1}}{2h} & j = 1, \dots, N_y - 1 \\ \dfrac{E_r{}^k_{i,0}}{a_r + ih} + \dfrac{E_r{}^k_{i+1,0} - E_r{}^k_{i-1,0}}{2h} + \dfrac{E_y{}^k_{i,0} - E_y{}^k_{i,1}}{-h} & i = 1, \dots, N_r - 1 \\ \dfrac{E_r{}^k_{i,N_y}}{a_r + ih} + \dfrac{E_r{}^k_{i+1,N_y} - E_r{}^k_{i-1,N_y}}{2h} + \dfrac{E_y{}^k_{i,N_y} - E_y{}^k_{i,N_y-1}}{h} & i = 1, \dots, N_r - 1 \\ \dfrac{E_r{}^k_{0,0}}{a_r} + \dfrac{E_r{}^k_{0,0} - E_r{}^k_{1,0}}{-h} + \dfrac{E_y{}^k_{0,0} - E_y{}^k_{0,1}}{-h} & \\ \dfrac{E_r{}^k_{N_r,0}}{a_r + N_r h} + \dfrac{E_r{}^k_{N_r,0} - E_r{}^k_{N_r-1,0}}{h} + \dfrac{E_y{}^k_{N_r,0} - E_y{}^k_{N_r,-1}}{h} & \\ \dfrac{E_r{}^k_{0,N_y}}{a_r} + \dfrac{E_r{}^k_{0,N_y} - E_r{}^k_{1,N_y}}{h} + \dfrac{E_y{}^k_{0,N_y} - E_y{}^k_{0,N_y-1}}{h} & \\ \dfrac{E_r{}^k_{N_r,N_y}}{a_r + N_r h} + \dfrac{E_r{}^k_{N_r,N_y} - E_r{}^k_{N_r-1,N_y}}{h} + \dfrac{E_y{}^k_{N_r,N_y} - E_y{}^k_{N_r,N_y-1}}{h}. & \end{cases} \tag{3.17}$$

Unfortunately, when $a_r = 0$ the divergence becomes singular at $r = 0$, at which correspond the nodes with $i = 0$, thus it is impossible to define the scheme for that nodes placed on the left side of the computational domain, in such case boundary scheme (3.17) reduces

to the following one

$$\rho_{i,j}^k = \begin{cases} \dfrac{{E_r}_{N_r,j}^k}{N_r h} + \dfrac{{E_r}_{N_r,j}^k - {E_r}_{N_r-1,j}^k}{h} + \dfrac{{E_y}_{N_r,j+1}^k - {E_y}_{N_r,j-1}^k}{2h} & j = 1, \ldots, N_y - 1 \\ \dfrac{{E_r}_{i,0}^k}{ih} + \dfrac{{E_r}_{i+1,0}^k - {E_r}_{i-1,0}^k}{2h} + \dfrac{{E_y}_{i,0}^k - {E_y}_{i,1}^k}{-h} & i = 1, \ldots, N_r - 1 \\ \dfrac{{E_r}_{i,N_y}^k}{ih} + \dfrac{{E_r}_{i+1,N_y}^k - {E_r}_{i-1,N_y}^k}{2h} + \dfrac{{E_y}_{i,N_y}^k - {E_y}_{i,N_y-1}^k}{h} & i = 1, \ldots, N_r - 1 \\ \dfrac{{E_r}_{N_r,0}^k}{N_r h} + \dfrac{{E_r}_{N_r,0}^k - {E_r}_{N_r-1,0}^k}{h} + \dfrac{{E_y}_{N_r,0}^k - {E_y}_{N_r,1}^k}{-h} & \\ \dfrac{{E_r}_{N_r,N_y}^k}{N_r h} + \dfrac{{E_r}_{N_r,N_y}^k - {E_r}_{N_r-1,N_y}^k}{h} + \dfrac{{E_y}_{N_r,N_y}^k - {E_y}_{N_r,N_y-1}^k}{h} & \end{cases} \tag{3.18}$$

The problem of the attribution of a value to the divergence of the electric field at the rotation axis, i.e. $\rho_{0,j}^k$, will be discussed in section 3.6.

3.3. An explicit upwind scheme for the Euler like equations

In both systems of equations (3.2) and (3.5), there are the time derivatives of the components of the field $\boldsymbol{V}$. In a finite-differences framework those equations are suitable to compute the time evolution of the discrete approximation of $\boldsymbol{V}$. The cartesian version (3.2) differ from the cylindrical one (3.5) only for the use of the x coordinate instead of r coordinate and for a minus sign in the *Lorentz force term* $\boldsymbol{E} + \mu \boldsymbol{V} \times \boldsymbol{H}$.
In order to simplify as much as possible the discussion, in this section the distinction between cartesian and cylindrical frameworks is avoided by treating only the cartesian case. The numerical methods proposed and all the considerations carried out for this case trivially hold for the cylindrical framework too, by taking into account a few differences. Thus, hereafter in this section we will refer only to the equations (3.2) that are rewritten

below

$$\begin{cases} \rho \left[\dfrac{\partial V_x}{\partial t} + V_x \dfrac{\partial V_x}{\partial x} + V_y \dfrac{\partial V_x}{\partial y} \; + \; \theta \left(E_x \; + \; \mu \, V_y \, H_z \right) \right] \; = \; - \dfrac{\partial p}{\partial x} \\ \\ \rho \left[\dfrac{\partial V_y}{\partial t} + V_x \dfrac{\partial V_y}{\partial x} + V_y \dfrac{\partial V_y}{\partial y} \; + \; \theta \left(E_y \; - \; \mu \, V_x \, H_z \right) \right] \; = \; - \dfrac{\partial p}{\partial y}. \end{cases} \tag{3.19}$$

Before proceeding, and with the aim to emphasize the various contributions present in the last two equations, we introduce the following notation

$$\begin{aligned} L_x &= \theta \left(E_x \; + \; \mu \, V_y \, H_z \right) & L_y &= \theta \left(E_y \; - \; \mu \, V_x \, H_z \right) \\ D_x &= V_x \frac{\partial V_x}{\partial x} + V_y \frac{\partial V_x}{\partial y} & D_y &= V_x \frac{\partial V_y}{\partial x} + V_y \frac{\partial V_y}{\partial y} \\ G_x &= \frac{1}{\rho} \frac{\partial p}{\partial x} & G_y &= \frac{1}{\rho} \frac{\partial p}{\partial y}. \end{aligned} \tag{3.20}$$

Basically the variables of each equation are grouped in three blocks. The first ones, referred with L_x and L_y, will be called *Lorentz force terms*, the second ones, referred with D_x and D_y, will be called *convection terms*, whereas the third ones, referred with G_x and G_y, will be called *gradient terms*. With the help of the above setting the equations (3.19) can be rewritten as

$$\begin{cases} \dfrac{\partial V_x}{\partial t} = -(D_x + L_x + G_x) \\ \\ \dfrac{\partial V_y}{\partial t} = -(D_y + L_y + G_y). \end{cases} \tag{3.21}$$

With the exception of the *Lorentz force terms*, the approximation of (3.21) presents several drawbacks. In order to compute the *convection terms* one needs to evaluate the derivatives of the a component of the field $\boldsymbol{V}$ along the direction defined by $\boldsymbol{V}$ itself. One can recognize in this system the so called *inviscid Burger problem* in two dimensions, with notable forcing terms. The solutions of this problem can display shock-waves that are difficult to simulate in the numerical procedure.

By considering the *gradient terms* things get even worse, since, to compute it, it is necessary to divide the approximation of the components of ∇p by the approximation of ρ. Both discrete fields can assume the value zero, or a value very close to zero, in some

nodes of the discrete grid. Thus, one have to pay attention not to perform meaningless operations like to divide a number by zero or to divide zero by zero.

The existing finite difference methods for Navier-Stokes equations, have been found to be unsuitable for our problem. This happens because, most of those methods have been developed for the incompressible case[14], that does not match our needs since the divergence of the field $\boldsymbol{V}$ can be different from zero[15].
We have explored some numerical schemes designed specifically for the equations in (3.19). In truth, we have followed different strategies including implicit methods, or explicit methods with additional diffusive term regulated through viscosity coefficient.
After some analysis and numerical tests, in which those schemes have been compared, we decided

- to use an upwind-like scheme to treat the *convection terms*,
- to use finite-differences to compute the *gradient terms* at each node (i, j) in which $\rho^k_{i,j} \neq 0$.

This approach will be the one that we describe in this section.
The approximation of (3.21), on the grid $\mathcal{G}_{x,y,t}$ and in the framework of finite difference will then consist of the following discrete equations

$$\begin{cases} V_{x\,i,j}^{\,k+1} = V_{x\,i,j}^{\,k} - \Delta t(D_{x\,i,j}^{\,k} + L_{x\,i,j}^{\,k} + G_{x\,i,j}^{\,k}) \\ \\ V_{y\,i,j}^{\,k+1} = V_{y\,i,j}^{\,k} - \Delta t(D_{y\,i,j}^{\,k} + L_{y\,i,j}^{\,k} + G_{y\,i,j}^{\,k}) \end{cases} \tag{3.22}$$

In this way it is possible to compute the values of $\boldsymbol{V}$ at time $k\Delta t + \Delta t$, on the spacial sub-grid $\mathcal{G}^{\text{sub}}_{x,y}$, by knowing the values of $\boldsymbol{V}$, and the other involved fields, at time $k\Delta t$ on the same sub-grid. There are also some boundary conditions that will be discussed in section 3.6. To close this section, the numerical treatment of the three typologies of terms is given.

To compute the approximation of the *Lorentz force terms*, at each time-step $k\Delta t$, it

[14] As an example see [3].
[15] Two examples in which this occurs are exhibited is section 2.6 and section 2.7.

is sufficient to evaluate its analytical expression on the sub-grid $\mathcal{G}_{x,y}^{\text{sub}}$, i.e.

$$\begin{cases} {L_x}_{i,j}^{k} = {E_x}_{i,j}^{k} + \mu \; {V_y}_{i,j}^{k} \; {H_z}_{i,j}^{k} \\ \\ {L_y}_{i,j}^{k} = {E_y}_{i,j}^{k} - \mu \; {V_x}_{i,j}^{k} \; {H_z}_{i,j}^{k} \end{cases} \tag{3.23}$$

To compute the approximation of the *convection terms*, at each time-step $k\Delta t$, two one-dimensional upwind difference, one along the x-direction and the other along the y-direction, replace the directional derivatives $V_x \frac{\partial}{\partial x}$ and $V_y \frac{\partial}{\partial y}$ operators on the discrete sub-grid $\mathcal{G}_{x,y}^{\text{sub}}$. The resulting scheme is

$$\begin{cases} {D_x}_{i,j}^{k} = \left[\; \max({V_x}_{i,j}^{k}, 0) \dfrac{{V_x}_{i,j}^{k} - {V_x}_{i-1,j}^{k}}{h} + \min({V_x}_{i,j}^{k}, 0) \dfrac{{V_x}_{i+1,j}^{k} - {V_x}_{i,j}^{k}}{h} \; \right] \\ \qquad\qquad + \left[\; \max({V_y}_{i,j}^{k}, 0) \dfrac{{V_x}_{i,j}^{k} - {V_x}_{i,j-1}^{k}}{h} + \min({V_y}_{i,j}^{k}, 0) \dfrac{{V_x}_{i,j+1}^{k} - {V_x}_{i,j}^{k}}{h} \; \right] \\ {D_y}_{i,j}^{k} = \left[\; \max({V_x}_{i,j}^{k}, 0) \dfrac{{V_y}_{i,j}^{k} - {V_y}_{i-1,j}^{k}}{h} + \min({V_x}_{i,j}^{k}, 0) \dfrac{{V_y}_{i+1,j}^{k} - {V_y}_{i,j}^{k}}{h} \; \right] \\ \qquad\qquad + \left[\; \max({V_y}_{i,j}^{k}, 0) \dfrac{{V_y}_{i,j}^{k} - {V_y}_{i,j-1}^{k}}{h} + \min({V_y}_{i,j}^{k}, 0) \dfrac{{V_y}_{i,j+1}^{k} - {V_y}_{i,j}^{k}}{h} \; \right] \end{cases} \tag{3.24}$$

To discretize the *gradient terms*, at each time-step $k\Delta t$, we use the discrete divergence of the electric field, computed as described in section 3.2 and central finite difference on the sub-grid $\mathcal{G}_{x,y}^{\text{sub}}$, to approximate the partial derivatives of ∇p. Thus, we write

$$\begin{cases} {G_x}_{i,j}^{k} = \dfrac{p_{i+1,j}^{k} - p_{i-1,j}^{k}}{2h \; \rho_{i,j}^{k}} \\ \\ {G_x}_{i,j}^{k} = \dfrac{p_{i,j+1}^{k} - p_{i,j-1}^{k}}{2h \; \rho_{i,j}^{k}} \end{cases} \tag{3.25}$$

At the nodes of $\mathcal{G}_{x,y}^{\text{sub}}$ such that $\rho_{i,j}^{k}$ is equal to zero, instead of computing the velocity with (3.22), the value at the previous time step is retrieved, i.e. ${V_y}_{i,j}^{k+1} = {V_y}_{i,j}^{k}$ and ${V_y}_{i,j}^{k+1} = {V_y}_{i,j}^{k}$.

3.4. An explicit scheme for the equation involving p

In the equation (3.3) explicitly appears only the time derivative of p, that can be approximated with forward difference. In the cartesian framework, by using the numerical divergence $\rho^k_{i,j}$, defined as in section 3.2, and the values of the fields E_x, E_y, V_x and V_y computed at time $k\Delta t$ on the spatial grid $\mathcal{G}^{\text{sub}}_{x,y}$, one can formulate the following discrete equation

$$\frac{p^{k+1}_{i,j} - p^k_{i,j}}{\Delta t} = \theta\ \rho^k_{i,j}\big(E_x{}^k_{i,j} V_x{}^k_{i,j} + E_y{}^k_{i,j} V_y{}^k_{i,j}\big).$$

An explicit scheme for p is than derived by isolating $p^{k+1}_{i,j}$ on the left-hand side of the last equation, i.e.

$$p^{k+1}_{i,j} = p^k_{i,j} + \Delta t\ \theta\ \rho^k_{i,j}\big(E_x{}^k_{i,j} V_x{}^k_{i,j} + E_y{}^k_{i,j} V_y{}^k_{i,j}\big). \tag{3.26}$$

3.5. Boundary conditions on conductive guides

According to what has been stated in section 2.8, we are going to discuss here how the conductive wave guides, present the computational domain, have been numerically treated. Note that the electric and magnetic fields at the nodes that belong to the conducting guides cannot be computed through the Lax-Wendroff scheme used for the other nodes. In the next chapter, we will numerically simulate electromagnetic fields related to computational domains where a couple of straight wave guides are present. The wave guides are placed in such a way that the approximated fields will be constrained to move between them. Two examples are displayed in figure 3.3. Thus, it is possible to distinguish between an *internal region*, as the part of the domain delimited by the guides, and an *external region*. Furthermore, at each point of a guide, an outward normal is defined by taking a unit vector orthogonal to the guide itself and directed from the *internal region* to the *external region*.

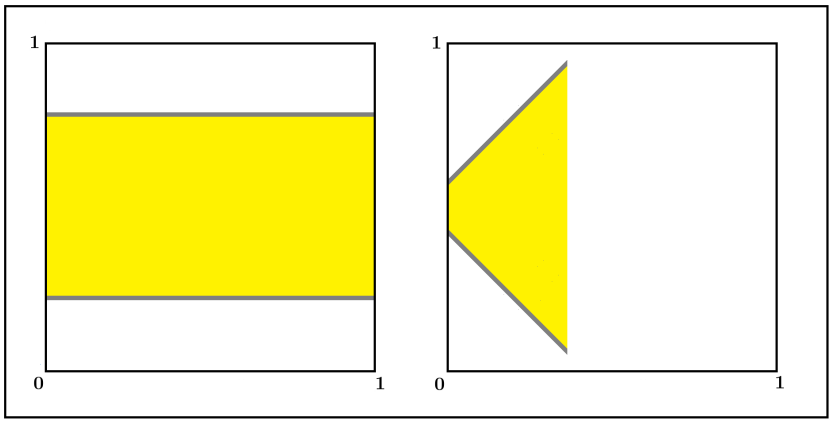

Figure 3.3: Two examples of wave guides (in gray) placed into the computational domain. In yellow is highlighted the *internal region*, while the *external region* is left blank.

The procedure used to attribute the values of the electric and magnetic fields at a node of the wave guide, say it (i^*, j^*), at time $k\Delta t$, is described below. Since it will be used in both cylindrical and cartesian frameworks, we will refer to the approximated magnetic field, that in both cases has only a scalar component, using the symbol $H^k_{i^*,j^*}$. Furthermore, with $E^{\ k}_{n\,i^*,j^*}$ and $E^{\ k}_{t\,i^*,j^*}$ we denote the components of the electric field in the directions of the outward normal (n) and along the guide itself (t), respectively.
At each node of the boundaries, the magnetic field and the tangential component of the electric field are computed through the equations[16]

$$\begin{aligned} H^k_{i^*,j^*} &= 2H^k_{i',j'} - H^k_{i'',j''}, \\ E^{\ k}_{t\,i^*,j^*} &= 0. \end{aligned} \tag{3.27}$$

The nodes (i', j') and (i'', j''), belonging to the spacial sub-grid $\mathcal{G}^{sub}_{i,j}$, are the first one and the second one, respectively encountered when moving from (i^*, j^*) towards the outward normal direction.
The normal component of the electric field is computed with the following equation, inspired by the transport equation (2.32),

$$E^{\ k}_{n\,i^*,j^*} = 2E^{\ k}_{n\,i',j'} - E^{\ k}_{n\,i'',j''} + \lambda(1 - v_g)\big(E^{\ k}_{n\,i',j'} - E^{\ k}_{n\,i''',j'''}\big). \tag{3.28}$$

[16]The magnetic field is computed through the application of Neumann boundary conditions in the direction of the outward normal to the guide. Neumann boundary conditions will be the object of the following section.

Here the node (i''', j''') is taken in such a way the difference $E^{k}_{ni',j'} - E^{k}_{ni''',j'''}$ is forward in the direction of the boundary at which $(i*, j*)$ belongs, according to the fact that the electromagnetic wave moves from the left-hand side to the right-hand side. The disposition of the nodes involved in equations (3.27) and (3.28), in the cases of figure 3.3, is shown in figure 3.4.

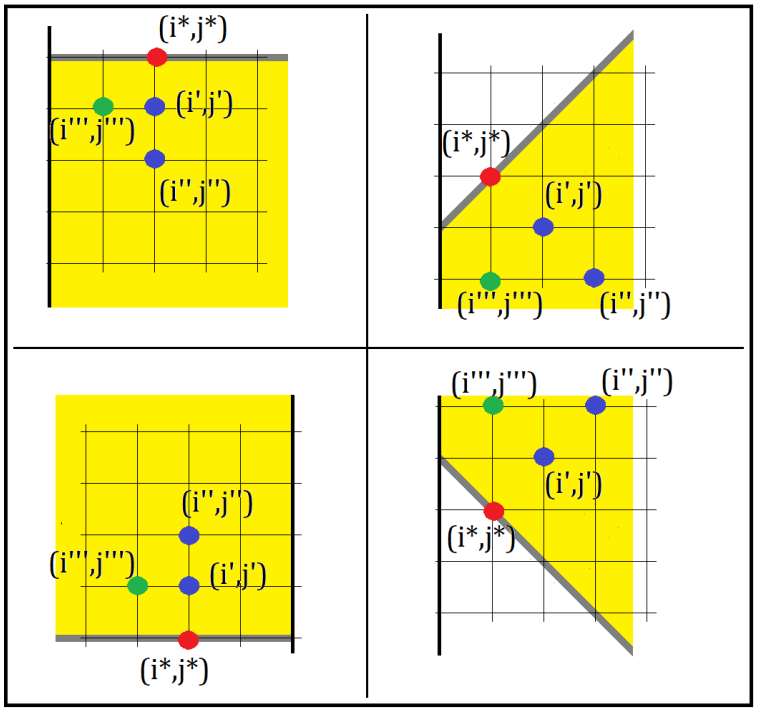

Figure 3.4: Positions of the nodes (i', j'), (i'', j'') and (i''', j'''), involved in the computation of boundary conditions (3.27) and (3.28), at a node $(i*, j*)$ belonging to the wave guides displayed the figures 3.3. We suppose that the electromagnetic wave is moving from left-hand side to the right-hand side. The wave guides (in gray) slit the domain into an *internal region* (in yellow) and an *external region* (in white).

In the last equation the parameter v_g, that can be fixed to be in $[0, 1]$, weights the transport of the normal component of the electric field at the boundaries. The choice $v_g = 1$ brings back to the case of PEC boundary conditions, and $E^{k}_{ni*,j*}$ is computed with the same discrete equation used for $H^{k}_{i^*,j^*}$.

3.6. Free exit condition from the computational domain boundaries

All the numerical experiments discussed in the following chapter have been performed in the bounded domain $[0,1] \times [0,1]$. As we have seen through this chapter, finite difference techniques are used to discretize a system of partial differential equations. Thus, some boundary conditions are required, at each time step, at the nodes that lie on the boundaries. According to definition 3.2, these nodes have one of the two indices i, j equal to 1, N_x or N_y for the cartesian framework or to 1, N_r or N_y for the cylindrical framework. Since the choice of a limited domain comes form computational needs, when it is possible, it comes natural to handle the boundaries as they are not existing. To this end, we decided to impose vanishing conditions on the outward flux, in such a way to avoid undesired reflections. These kind of conditions, of Neumann type, are realised by imposing that some first derivative vanishes in correspondence to the domain boundaries. Several types of conditions have been considered, depending on the way with the field approaches to the boundary.

For example, if one considers the case of a soliton in cartesian coordiantes[17] moving along the x-direction, it is possible to determine the values of the component $E_y(1, y, t)$ at the right side of the the squared domain $[0,1] \times [0,1]$ by imposing that $\frac{\partial E_y}{\partial x} = 0$ in all points having $x = 1$ and $y \in [0,1]$. Indeed, by fixing $\bar{j} \in \{0, \ldots, N_y\}$ and subtracting the Taylor expansions of E_y at the nodes $(N_x - 2, \bar{j})$ from the Taylor expansion of E_y at the node $(N_x - 1, \bar{j})$ multiplied by 2, one gets

$$2{E_y}^k_{N_x-1,\bar{j}} - {E_y}^k_{N_x-2,\bar{j}} = 2{E_y}^k_{N_x,\bar{j}} - {E_y}^k_{N_x,\bar{j}} + h\frac{\partial E_y}{\partial x}(1, \bar{y}h) + o(h),$$

which, thanks to the constraint on the derivative, gives the following finite difference approximation

$${E_y}^k_{N_x,\bar{j}} = 2{E_y}^k_{N_x-1,\bar{j}} - {E_y}^k_{N_x-2,\bar{j}}. \tag{3.29}$$

The above condition ensures that the soliton exits without reflections through the left side of the domain. This happens because such a soliton travels along the normal direction to the boundary.

The Neumann conditions described in the above example, in the case of a generic field f

[17] For instance the soliton defined in section 2.6.

and extended to cover each side of the discrete grid $\mathcal{G}_{x,y}^{\text{sub}}$ at time $k\Delta t$, are:

$$\begin{cases} f_{1,j}^k = 2f_{2,j}^k - f_{3,j}^k & j = 2, \dots, N_y - 1 \\ f_{N_x,j}^k = 2f_{N_x-1,j}^k - f_{N_x-2,j}^k & j = 2, \dots, N_y - 1 \\ f_{i,1}^k = 2f_{i,2}^k - f_{i,3}^k & i = 2, \dots, N_x - 1 \\ f_{i,N_y}^k = 2f_{i,N_y-1}^k - f_{i,N_y-2}^k & i = 2, \dots, N_x - 1 \\ f_{1,1}^k = 2f_{2,2}^k - f_{3,3}^k \\ f_{N_x,1}^k = 2f_{N_x-1,2}^k - f_{N_x-2,3}^k \\ f_{1,N_y}^k = 2f_{2,N_y-1}^k - f_{3,N_y-2}^k \\ f_{N_x,N_y}^k = 2f_{N_x-1,N_y-1}^k - f_{N_x-2,N_y-2}^k. \end{cases} \tag{3.30}$$

Actually, avoiding reflections is a difficult task to reach in general, as this feature occurs with no major troubles only for particular configurations. Boundary conditions of this kind have been applied to all the fields of our numerical simulations, except for the case of cylindrical coordinates at $i = 1$, where the right side of the domain is the rotation axis. In such a case imposing Neumann boundary conditions has no meaning, since the rotation axis is a symmetry axis for all the fields. In addition, the equations of system (2.21) are not defined in $r = 0$. This exception has been solved by imposing the electric and magnetic fields to vanish on the rotation axis. This choice is suitable for the fields H_φ and E_r. The vector field $\boldsymbol{H}$ has to rotate around the y axis and in the case $H_\varphi(0, y, t) \neq 0$, for some y and t, then in each plane $\varphi = \bar{\varphi}$ (where $\bar{\varphi}$ is fixed in $[0, 2\pi]$) a radial component of $\boldsymbol{H}$ appears. This is in contrast whit our hypothesis of $\boldsymbol{H}$ directed only along the φ direction. By considering the divergence of the electric field in cylindrical coordinates, i.e.

$$\nabla \cdot \boldsymbol{E} = \frac{E_r}{r} + \frac{\partial E_r}{\partial r} + \frac{\partial E_y}{\partial y}.$$

Thus, we expect that $E_r = \alpha r + o(r)$ when $r \to 0$ (here α is a real constant), otherwise the first term in the divergence will diverge at $r = 0$.

The determination of E_y in such a way to impose consistently boundary conditions at $r = 0$ it is non trivial. As it will be remarked in the conclusion, due to lack of time this problem cannot be adequately treated during this work.

Numerical Simulations

This chapter is dedicated to the presentation of some numerical simulations obtained by applying the schemes described in chapter 3. These numerical methods belong to the family of finite-differences schemes.

We will mainly choose as computational domain the parallelepiped $[0,1] \times [0,1] \times [0,T]$. This means that space variables belong to the square $[0,1] \times [0,1]$, while time variable takes values in $[0,T]$, where T will be specified in each numerical experiment.
Inside the computational domain, according to definition 3.2 and relatively to the cartesian case, a discrete grid $\mathcal{G}_{x,y,t}$ is constructed by fixing a positive integer N and considering $h := 1/N$, so that $\Delta x = \Delta y = h$, and $\Delta t = \lambda h$. In the cylindrical case the same procedure is replicated by reminding that the grid will be named $\mathcal{G}_{r,y,t}$ and the step-length Δr is used instead of Δx. Notice that, by choosing equal step-lengths in both spatial dimensions, on each side of the spatial domain $[0,1] \times [0,1]$ are placed $N+1$ nodes, for a total of $(N+1)^2$ nodes.

The constant λ is related to the stability condition of the Lax-Wendroff scheme, and it will be always chosen in such a way conditions (3.10) are satisfied.
The speed of light in vacuum is normalized to 1. Similarly, also the vacuum permittivity and permeability coefficients have been both set to 1. The constant θ has been fixed to 0.1. Though other values may be taken, this choice comes from heuristic considerations[1] concerning the balance of the terms in equations (3.22).

Summarizing, the general setting for all the numerical simulations reported in this chapter is the following one

[1]This choice is also suggested by some preliminary tests whose aim was to ensure numerical stability in the case of the numerical experiments proposed in this chapter. Those rudimentary tests will not be discussed here. Nevertheless, due to lack of time, the research of a constant which has a more significant connection with the theoretical value of θ is left to further works.

- the computational domain for the spatial variables is the square $[0,1] \times [0,1]$,
- the time variable takes values in $[0,T]$,
- N is a positive integer,
- $h = 1/N$ is the space-step length in both spacial direction,
- $\Delta t = \lambda h$ is the time-step length,
- N_t is the number of part in which the time interval $[0,T]$ is divided, i.e. $N_t = \lfloor \frac{T}{\Delta t} \rfloor$,
- the speed of light c in vacuum is normalized to 1,
- both the constants ε and μ take the value 1,
- the mass-charge coupling constant is set to $\theta = 0.1$.

4.1. Numeric approximations of free-solitons in vacuum

The first series of experiments is aimed to checked if the numerical approximations of the fields defined in (2.22) and (2.24) are actually close to their analytical counterparts. This comparison is necessary in view of the approximation of the extended equations.
In truth, only the Lax-Wendroff scheme will be fully operative in the numerical simulations discussed in this section, since the solutions considered have the fields $\boldsymbol{V}$ and p constant with respect to time. As stated in section 2.6, in the case of travelling solitons it is convenient to choose $\frac{D\boldsymbol{V}}{Dt} = 0$ and $p = 0$. We want this feature to be preserved during the approximation. The discrete equations (3.22) and (3.26) will be also implemented, in order to investigate their consistency.
Some numerical simulations of a solitonic solution of equations (2.20) and (2.21) have been carried out for example in [36] and [11]. In those cases the velocity field $\boldsymbol{V}$ was fixed and the pressure does not appear.

In order to compare exact solutions with their numerical approximations, we follow the strategy described below. Suppose that F is one of the scalar fields (or a component of a vector field) that solves exactly the system (2.20). Let $k\Delta t$ a discrete time value. We will name F^k_{an} the matrix whose entries are obtained through the evaluation of F at time $k\Delta t$, at the nodes of the discrete sub-grid $\mathcal{G}^{sub}_{i,j}$. We will indicate with F^k_{num} the numerical

approximation of F on the same sub-grid obtained after k steps of the schemes described in the previous chapter, starting from the initial condition F^0_{an}. It is clear that F^k_{num} is a matrix of the same size as F^k_{an} and that, in addition, $F^0_{an} = F^0_{num}$.
According to the above introduced notation, we can examine the behaviour of the two following errors:

$$\epsilon(F) := \frac{1}{N_t}\sum_{k=1}^{N_t} \mathrm{err}^k(F), \qquad \epsilon_\Gamma(F) := \frac{1}{N_t}\sum_{k=1}^{N_t} \mathrm{err}^k_\Gamma(F),$$

where

$$\mathrm{err}^k(F) := \frac{1}{(N+1)^2}\sum_{i=1}^{N_x}\sum_{j=1}^{N_y} |F^k_{an}(i,j) - F^k_{num}(i,j)|,$$
$$\mathrm{err}^k_\Gamma(F) := \frac{1}{N^k_\Gamma}\sum_{i,j\in\Gamma^k} |F^k_{an}(i,j) - F^k_{num}(i,j)|.$$

Here in the definition of $\mathrm{err}^k(F)$ and $\mathrm{err}^k_\Gamma(F)$ the matrix indices i, j are written as function variables to avoid confusion with the other subscripts. The vertical bar has the meaning of absolute value[2]. Finally, the set of matrix indices named Γ^k, that compares in the definition of $\mathrm{err}^k_\Gamma(F)$, contains the indices of each node belonging to the support of the soliton at time $k\Delta t$, while N^k_Γ is the cardinality of Γ^k.
It turns out that, at fixed time $k\Delta t$, the real number $err^k(F)$ is the L^1 norm between the exact solution and the approximated one evaluated at each node of the spatial sub-grid $\mathcal{G}^{sub}_{i,j}$. Moreover, $err^k_\Gamma(F)$ is the restriction of $err^k(F)$ to the nodes belonging to the support of the soliton at time $k\Delta t$. The error $\epsilon(F)$ is the norm defined over the Bochner space $L^1(\{0, \Delta t, \ldots, N_t\Delta t\}; L^1(\mathcal{G}^{sub}_{i,j}))$, while similarly $\epsilon_\Gamma(F)$ is the norm related to $L^1(\{0, \Delta t, \ldots, N_t\Delta t\}; L^1(\Gamma^k))$.
The same notation will hold in the case of equations (2.21).

Cartesian framework: a comparison between exact and numerical solution
We now consider the numerical approximations in cartesian coordiantes of the fields associated to the soliton in (2.22). To investigate how the choice of N and λ influence such approximations, we evaluate the errors ϵ and ϵ_Γ for the fields $|E|$, H_z, ρ and V_x, for different values of those two parameters. The results pertaining to this series of numerical experiments are reported in table 4.1. The following choice of parameters has been made:

[2]Let $M = \{m_{i,j}\}_{i,j}$ be a $(n_1 \times n_2)$-matrix, then $|M| := \{|m_{i,j}|\}_{i,j}$.

- the center C of the soliton at initial time $t = 0$ is $(0.25, 0.5)$,
- the half-side of the support is $\tau = 0.1$,
- $T = 0.65$.

This choice $T = 0.65$ ensures that the support of soliton remains entirely contained in $[0, 1] \times [0, 1]$ for the whole duration of the simulation. The other parameters not mentioned here have been set according to what was stated in the introduction of this chapter.

N	λ	$\epsilon(\lvert\boldsymbol{E}\rvert)$	$\epsilon_\Gamma(\lvert\boldsymbol{E}\rvert)$	$\epsilon(H_z)$	$\epsilon_\Gamma(H_z)$	$\epsilon(\rho)$	$\epsilon_\Gamma(\rho)$	$\epsilon(V_x)$	$\epsilon_\Gamma(V_x)$
50	1/3	0.0039098	0.061627	0.0039098	0.061627	0.086405	1.4524	0	0
100	1/3	0.0012306	0.021853	0.0012322	0.021893	0.027133	0.49985	0	0
200	1/3	0.00033087	0.0063341	0.00034473	0.0063706	0.0076031	0.14493	0	0
400	1/3	0.000092747	0.0017528	0.00009333	0.0017672	0.0020471	0.039825	0	0
50	1/4	0.0043803	0.065118	0.0043803	0.065118	0.095066	1.5128	0	0
100	1/4	0.0013127	0.023029	0.0013142	0.023065	0.028696	0.52175	0	0
200	1/4	0.00036411	0.0066551	0.00036573	0.0066949	0.0080152	0.15125	0	0
400	1/4	0.000098445	0.001846	0.000099063	0.0018613	0.0021601	0.041667	0	0
50	1/6	0.0049558	0.067772	0.0049562	0.067781	0,10588	1.561	0	0
100	1/6	0.0013929	0.023901	0.0013947	0.023946	0.030236	0.53802	0	0
200	1/6	0.00038098	0.0068868	0.0003827	0.0069292	0.0083485	0.15581	0	0
400	1/6	0.00010296	0.001913	0.00010361	0.0019292	0.0022497	0.042993	0	0
50	1/8	0.0052815	0.068905	0.0052819	0.068915	0.11202	1.5814	0	0
100	1/8	0.0014465	0.024232	0.0014483	0.024277	0.031272	0.54402	0	0
200	1/8	0.0003884	0.0069694	0.00039017	0.007013	0.0084954	0.15744	0	0
400	1/8	0.00010482	0.0019369	0.00010548	0.0019534	0.0022866	0.043465	0	0

Table 4.1: Numerical result relative to the numerical simulation of the same cartesian soliton for different values of N and λ. The duration of each simulation is $T = 0.65$.

As expected, from table 4.1 it turns out that the error committed in the approximation of the support decrease as N increases. This behaviour is independent of λ. This is true for all the fields here considered. The reason why error committed in the approximation of the divergence of the electric field is higher with respect to the other ones is explained in appendix III. The approximation error of the non zero component of the velocity field, i.e. V_x, goes below machine precision, so we can conclude that in the case

of the cartesian soliton discrete equations (3.22) work as expected.
From results of table 4.1, we can estimate that the global finite-difference scheme is only of the first order in space. Moreover, by observing table 4.2, we can conclude that the numerical method provides a first order approximation in time.

N	λ	$\frac{1}{N_t}\mathrm{err}^{N_t}(\lvert\boldsymbol{E}\rvert)$	$\frac{1}{N_t}\mathrm{err}^{N_t}(H_z)$	$\frac{1}{N_t}\mathrm{err}^{N_t}(\rho)$
50	1/4	$6.0173 \cdot 10^{-5}$	$6.0173 \cdot 10^{-5}$	0.0012249
50	1/8	$3.8761 \cdot 10^{-5}$	$3.8761 \cdot 10^{-5}$	0.00077796
50	1/16	$2.0728 \cdot 10^{-5}$	$2.0728 \cdot 10^{-5}$	0.00041465
50	1/32	$9.9856 \cdot 10^{-6}$	$9.9856 \cdot 10^{-6}$	0.0002001
50	1/64	$4.7258 \cdot 10^{-6}$	$4.7258 \cdot 10^{-6}$	$9.4954 \cdot 10^{-5}$
50	1/128	$2.2872 \cdot 10^{-6}$	$2.2872 \cdot 10^{-6}$	$4.6031 \cdot 10^{-5}$
100	1/4	$9.307 \cdot 10^{-6}$	$9.307 \cdot 10^{-6}$	0.00019321
100	1/8	$5.2593 \cdot 10^{-6}$	$5.2593 \cdot 10^{-6}$	0.0001084
100	1/16	$2.9949 \cdot 10^{-6}$	$2.9949 \cdot 10^{-6}$	$6.1341 \cdot 10^{-5}$
100	1/32	$1.5834 \cdot 10^{-6}$	$1.5834 \cdot 10^{-6}$	$3.2345 \cdot 10^{-5}$
100	1/64	$7.7955 \cdot 10^{-7}$	$7.7955 \cdot 10^{-7}$	$1.5928 \cdot 10^{-5}$
100	1/128	$3.7694 \cdot 10^{-7}$	$3.7694 \cdot 10^{-7}$	$7.7105 \cdot 10^{-6}$
200	1/4	$1.2883 \cdot 10^{-6}$	$1.2985 \cdot 10^{-6}$	$2.7167 \cdot 10^{-5}$
200	1/8	$6.8607 \cdot 10^{-7}$	$6.919 \cdot 10^{-7}$	$1.4425 \cdot 10^{-5}$
200	1/16	$3.6469 \cdot 10^{-7}$	$3.676 \cdot 10^{-7}$	$7.6449 \cdot 10^{-6}$
200	1/32	$2.0137 \cdot 10^{-7}$	$2.0283 \cdot 10^{-7}$	$4.2023 \cdot 10^{-6}$
200	1/64	$1.0572 \cdot 10^{-7}$	$1.0645 \cdot 10^{-7}$	$2.2017 \cdot 10^{-6}$
200	1/128	$5.2222 \cdot 10^{-8}$	$5.2587 \cdot 10^{-8}$	$1.0882 \cdot 10^{-6}$

Table 4.2: Numerical result relative to the simulation of the same cartesian soliton for different values of N and λ. The duration of each simulation is $T = 0.65$. The error is estimated by evaluating the L^1-norm at each node of the spatial subgrid $\mathcal{G}_{i,j}^{sub}$ only at $t = N_t$.

In figure 4.2 different approximated fields are plotted for different values of k, i.e. for different time values. We observe that the Nuemann boundary conditions imposed at the right-hand side of the domain allow for a correct exit of the soliton. Another feature that one can clearly see from figure 4.2 and figure 4.1 is that the Lax-Wendroff scheme adds some non-physical wiggles to the tail of the soliton. This is a question of numerical

inaccuracy[3].

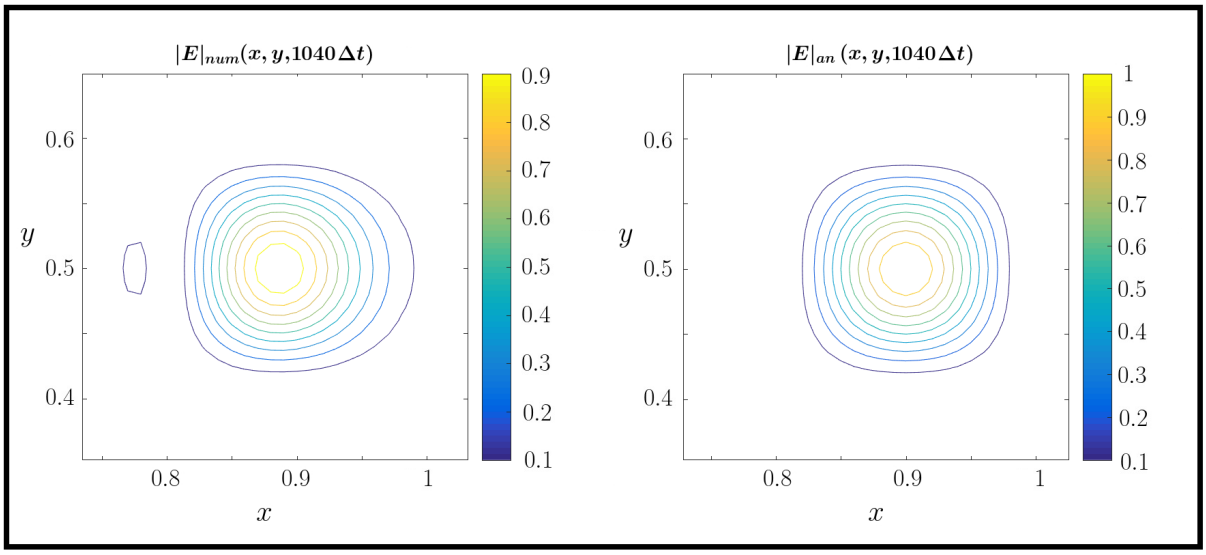

Figure 4.1: Contour lines representation of the matrices $|\boldsymbol{E}|_{num}^{N_t}$ and $|\boldsymbol{E}|_{an}^{N_t}$ relative to the choice of $N = 400$, $\lambda = 1/4$ and $T = 0.65$. The soliton travels from the left-hand side to the right-hand one.

[3]The question of little numerical inaccuracy in the approximation of travelling solitons is discussed also in [36].

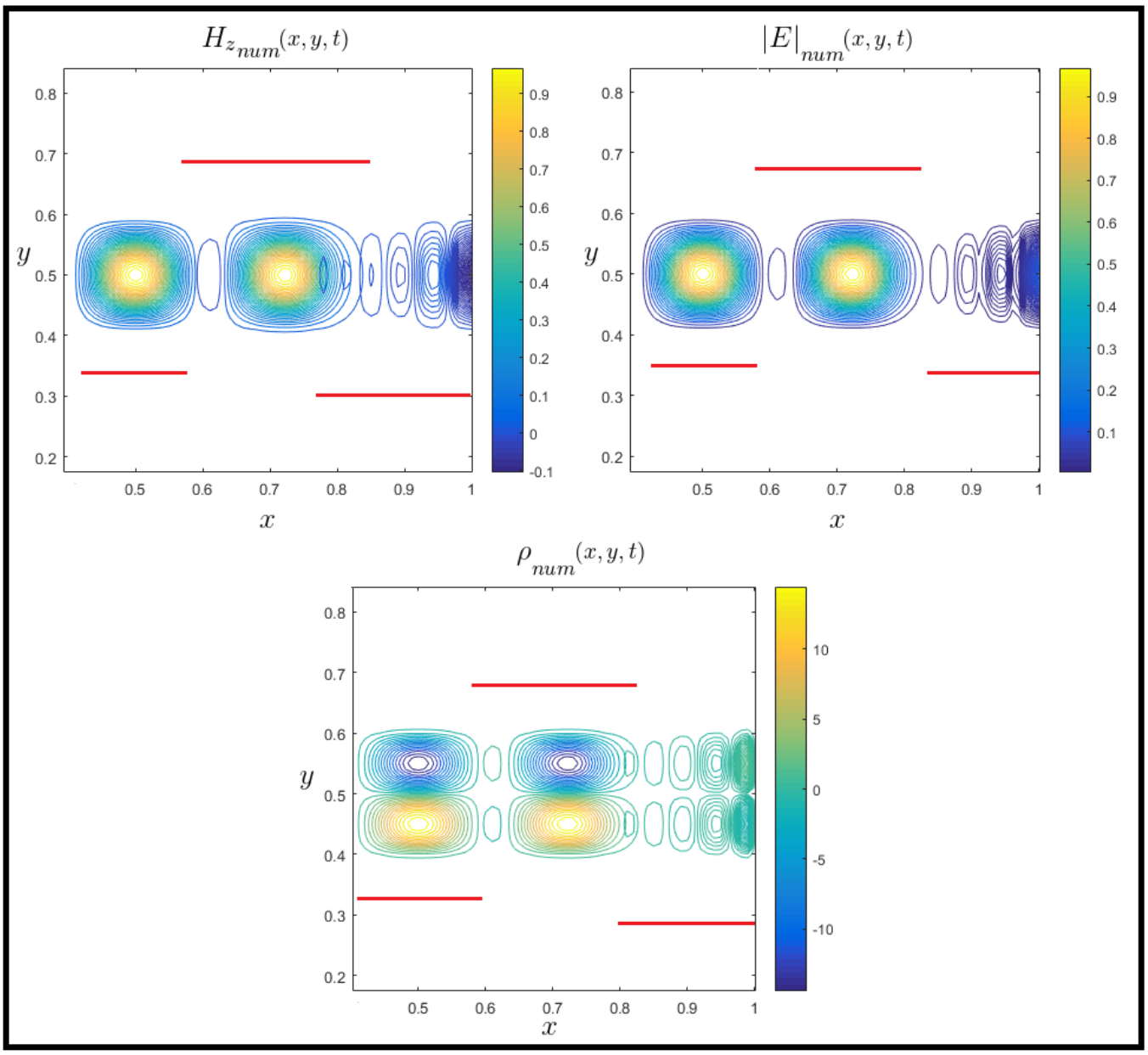

Figure 4.2: Contour lines representation of the matrices $H_{z_{num}}^k$ (top-left), $|\boldsymbol{E}|_{num}^k$ (top-right) and ρ_{num}^k (bottom) relative to the choice of $N = 200$ and $\lambda = 1/4$ for $k = 0, 90, 250$ ($t = k\Delta t$). In each picture the three matrices relative to one of the field are over-plotted. The supports of the soliton at the considered times are completely disjoint, but the tails due to numerical inaccuracy of the Lax-Wendroff scheme sometimes overlap with the previous fields. For this reason are displayed the red segments that may help to distinguish between them. The solitons travels from the left side to the right side of the domain in each picture. At $k = 0$ the center of the support is $(0.5, 0.5)$.

Cylindrical framework: a comparison between exact and numerical solution
We will consider the numerical approximations of the fields that define a cylindrical soliton according to (2.24). To investigate how the choice of N and λ influence such approximations we will evaluate the errors ϵ and ϵ_Γ concerning with the fields $|E|$, H_z, ρ, V_r, V_y and p, for different values of the two parameters. The results relative to this series of numerical experiments are reported in table 4.3. The following choice of the parameters has been performed:

- the center C of the soliton at initial time $t = 0$ is $(0.25, 0.5)$,
- the constants related to the shape of the soliton have been fixed at $\tau = 0.1$ $K_\tau = 2\pi$,
- $T = 0.65$.

The choice $T = 0.65$ ensures that the support of soliton remains entirely contained in $[0, 1] \times [0, 1]$ for the whole duration of the simulation. All the other parameters not mentioned above have been set according to what stated in the introduction of this chapter.

Unfortunately, one finds out that the schemes are not numerically stable. By this we mean that the approximated fields have an indiscriminate growth. This drawback occurs for each choice of N and λ that we tried. We observed that the node from which the instability is generated never belongs to the support of the soliton. An example is shown in figure 4.3. By analysing in detail the behaviour of several numerical simulations, it is possible to conclude that the instability arises from the discrete Euler equation (3.22), because some entries of the matrices $V_{x_{num}}^k$ and $V_{y_{num}}^k$ become greater than 1. As a consequence of this fact, the eigenvalues of the matrices M_r and M_y, that define the Lax-Wendroff scheme (see section 3.1) increase, compromising the stability of the whole set of discrete equations.
Again, we stress that at the discrete time instant in which the instability arises (let us say $k^*\Delta t$) the grid node (i^*, j^*) where the computation of the discrete velocity produces unsuitable results, does not belong to the support of the soliton. We also recall that the electromagnetic field, the divergence of $\boldsymbol{E}$ and the scalar field p, theoretically, should be zero at the node (i^*, j^*, k^*) of $\mathcal{G}_{r,y,t}$. Nevertheless, as it happens also in the cartesian case previously analysed, the Lax-Wendroff scheme allow for the creation of tails in the

approximated electric and magnetic fields[4]. Those tails are due to numerical inaccuracy of the scheme and this latter may cause the instability affecting our experiments. Another element that supports these conclusions is that the numerical simulation relative to figure 4.3, where $N = 100$ and $\lambda = 1/4$, blows up at $k^* = 77$, whereas by choosing $N = 100$, $\lambda = 1/10$ it blows up at $k^* = 1729$. In the first case, the soliton is inside the computational domain, while in the second case the soliton has enough time to exit through the right-hand side. The instability is generated at two different nodes of the sub-grid $\mathcal{G}_{r,y}^{sun}$ depending if we are in the case $\lambda = 1/4$ or $\lambda = 1/10$.

We guess that stability can be recovered by choosing λ suitably small, but this may result in extremely expensive simulations in terms of computational costs. To avoid those drawbacks a more practical strategy has been adopted, as described below.

We decided to impose the following constraint on the entries of the matrices $V_{r_{i,j}}^{k+1}$ and $V_{y_{i,j}}^{k+1}$ after that they have been computed with the discrete equations (3.22)

$$V_{r_{i,j}}^{k+1} = \begin{cases} V_{r_{i,j}}^{k+1} & \text{if } \left(V_{r_{i,j}}^{k+1} - V_{r_{i,j}}^{k}\right)^2 + \left(V_{y_{i,j}}^{k+1} - V_{y_{i,j}}^{k}\right)^2 \leq (R_V \Delta t)^2 \\ V_{r_{i,j}}^{k} & \text{otherwise} \end{cases}$$

$$V_{y_{i,j}}^{k+1} = \begin{cases} V_{y_{i,j}}^{k+1} & \text{if } \left(V_{r_{i,j}}^{k+1} - V_{r_{i,j}}^{k}\right)^2 + \left(V_{y_{i,j}}^{k+1} - V_{y_{i,j}}^{k}\right)^2 \leq (R_V \Delta t)^2 \\ V_{y_{i,j}}^{k} & \text{otherwise} \end{cases} \tag{4.1}$$

here R_V is a real positive number that, in the simulation concerning the results of table 4.3, has been set to 1. The conditions (4.1) are checked for $V_{r_{i,j}}^{k+1}$ and $V_{y_{i,j}}^{k+1}$ each time they are computed with (3.22). In each node (i, j) in which the L^2 norm of the difference between $\left(V_{r_{i,j}}^{k+1} V_{y_{i,j}}^{k+1}\right)$ and $\left(V_{r_{i,j}}^{k} V_{y_{i,j}}^{k}\right)$ is grater than $R_V \Delta t$, the the discrete velocity vector is not adjourned.

[4]See figure 4.2 and 4.6.

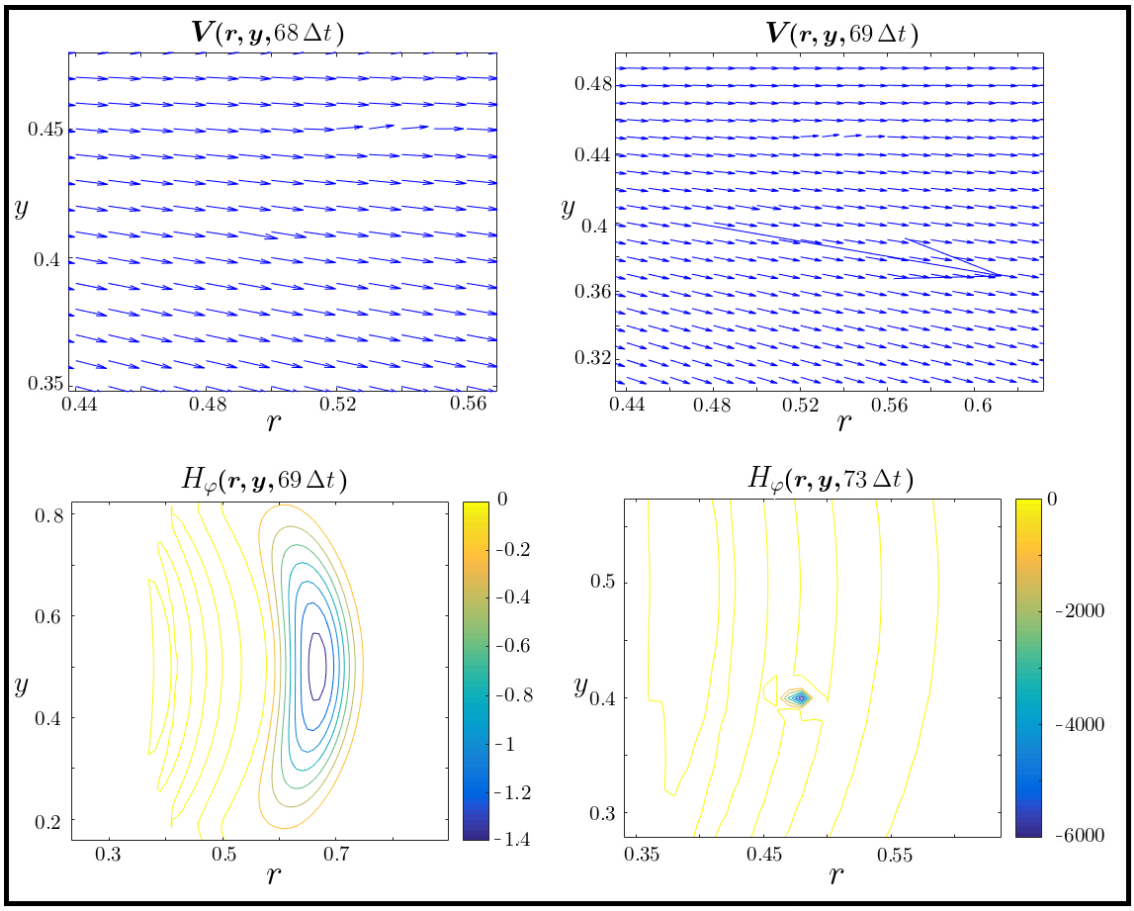

Figure 4.3: Instability in the numerical simulations of a cylindrical soliton. In the case relative to this figure $N = 100$ and $\lambda = 1/4$. At $k = 77\Delta t$ the matrix p^{77}_{num} has some entries that are no more representable as floating point numbers. The instability is generated by the discrete equations (3.22), as it is clear by comparing the two top picture relative to $\boldsymbol{V}^k_{num}$ for $k = 68$ and $k = 69$. Then the instability affects all the other fields. For example consider the pictures of the approximated magnetic field for $k = 69$ and $k = 74$ at the bottom. Note that the grid node in which the instability arises it is outside of the support of the soliton. The constraints (4.1) on the discrete velocity field are not imposed in this simulation.

N	λ	$\epsilon(\|\boldsymbol{E}\|)$	$\epsilon_{supp}(\|\boldsymbol{E}\|)$	$\epsilon(H_\varphi)$	$\epsilon_{supp}(H_\varphi)$	$\epsilon(\rho)$	$\epsilon_{supp}(\rho)$
50	1/3	0.027869	0.11368	0.026887	0.11212	0.12518	0.49963
100	1/3	0.008963	0.03592	0.0085947	0.035668	0.038423	0.15556
200	1/3	0.002784	0.010322	0.0026447	0.010482	0.015231	0.068609
400	1/3	0.00097079	0.0032021	0.00090034	0.0032816	0.007568	0.037818
50	1/4	0.029336	0.12021	0.028586	0.11865	0.14071	0.58354
100	1/4	0.0091224	0.03788	0.0088695	0.037625	0.041561	0.17175
200	1/4	0.0026881	0.010632	0.0025912	0.010694	0.013952	0.058945
400	1/4	0.00086331	0.0030908	0.00081794	0.0031412	0.0060992	0.028287
50	1/6	0.03085	0.12573	0.030259	0.12413	0.15876	0.67158
100	1/6	0.0093042	0.039611	0.0091377	0.039348	0.046363	0.20049
200	1/6	0.0026286	0.011023	0.0025658	0.011007	0.014243	0.060822
400	1/6	0.00077878	0.0030587	0.00075105	0.0030681	0.0052137	0.022727
50	1/8	0.031686	0.12821	0.031135	0.12657	0.16861	0.71553
100	1/8	0.0094174	0.040372	0.0092789	0.04009	0.049269	0.21758
200	1/8	0.002621	0.011255	0.0025694	0.011216	0.014938	0.065921
400	1/8	0.0007521	0.0030911	0.0007283	0.0030777	0.0050892	0.022289

N	λ	$\epsilon(V_r)$	$\epsilon_{supp}(V_r)$	$\epsilon(V_y)$	$\epsilon_{supp}(V_y)$	$\epsilon(p)$	$\epsilon_{supp}(p)$
50	1/3	0.024341	0.0099555	0.052034	0.0027867	0.0003828	0.00067948
100	1/3	0.021276	0.0043145	0.048336	0.001344	0.00016564	0.00032969
200	1/3	0.018982	0.0020715	0.040371	0.0007973	0.000079117	0.0001646
400	1/3	0.0232854	0.0011347	0.0410601	0.00056652	0.000038657	0.00008153
50	1/4	0.027142	0.010164	0.056244	0.0027928	0.00028134	0.00049736
100	1/4	0.022191	0.0044155	0.047467	0.001312	0.00012179	0.00024317
200	1/4	0.019627	0.0021085	0.04155	0.00067202	0.000058196	0.00012116
400	1/4	0.020326	0.0010567	0.039092	0.00042861	0.000028391	0.000059963
50	1/6	0.026466	0.010497	0.054699	0.0028098	0.00018358	0.00032303
100	1/6	0.023231	0.0044817	0.049367	0.0012742	0.000079146	0.00015786
200	1/6	0.021314	0.0021334	0.04481	0.00064484	0.000037615	0.000078091
400	1/6	0.018496	0.0010556	0.038349	0.00032951	0.00001831	0.000038502
50	1/8	0.029425	0.010629	0.063043	0.002871	0.00013704	0.00024054
100	1/8	0.025489	0.0045197	0.053667	0.0013109	0.000058484	0.00011621
200	1/8	0.022112	0.0021526	0.044401	0.00060352	0.000027534	0.000056951
400	1/8	0.020008	0.0010469	0.039321	0.00030279	0.000013347	0.000027961

Table 4.3: Numerical result relative to the numerical simulation of the same cylindrical soliton for different values of N and λ. The duration of each simulation is $T = 0.65$.

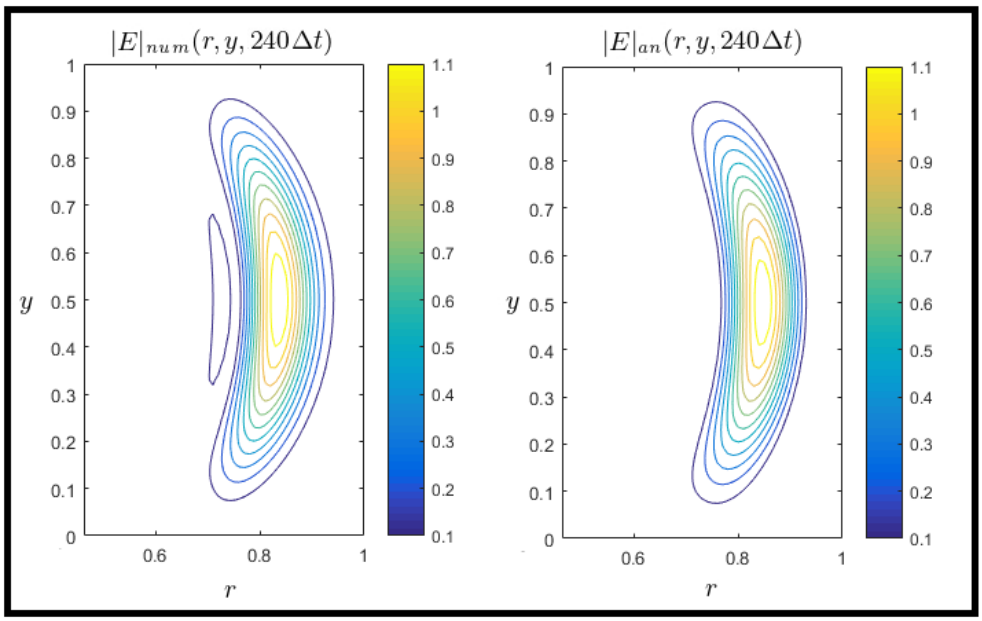

Figure 4.4: Contour lines representation of the matrices $|\boldsymbol{E}|^{240}_{num}$ and $|\boldsymbol{E}|^{240}_{an}$ relative to the choice of $N = 100$ and $\lambda = 1/4$. $T = 0.65 = 260\Delta t$.

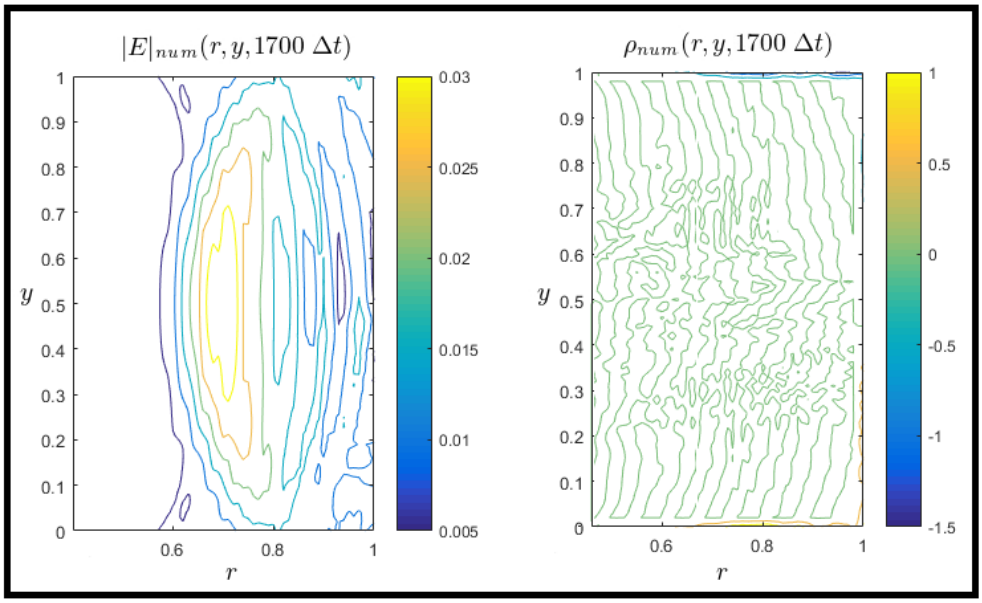

Figure 4.5: Contour lines representation of the matrices $|\boldsymbol{E}|^{k}_{num}$ (left) and ρ^{k}_{num} (right) relative to the choice of $N = 100$ and $\lambda = 1/10$ for $k = 1700$. The soliton reach the right side of the domain after 820 time iterations. Than it goes out thank to the imposition of Neuman boundary conditions. The figure shows that a reflected wave is generated for the electric field (also for the magnetic field). The reflect wave is divergence free.

From table 4.3 one can notice that the error committed in the approximation decrease as N increase for all the considered values of λ. This is true for all the fields here examined. Considerations similar to those carried out for the cartesian case, explain why the error committed at the approximation of ρ, in the nodes belonging to the support of the soliton, is high with respect to the other ones.

By comparing the values of the errors ϵ and ϵ_{supp}, it is possible to observe that the behaviour of each considered field outside the support of the soliton is not perfectly approximated. Together with the problems related to the numerical implementation of the Lax-Wendroff scheme discussed before[5], there are some other features that can contribute to explain this fact.

To begin with, the Neumann conditions imposed at the domain boundary do not guarantee the soliton to exit without reflections, as we can see for example in figure 4.5.

Moreover, the scalar field p, defined up to a constant factor, has been set identically zero at $t = 0$ in accordance to what stated in section 2.6. Nevertheless, in a relatively small number of time steps, through the discrete equation (3.26) a discrete *pressure* p^k_{num} emerges as a consequence of the lack of orthogonality between the approximated electric and velocity fields $\boldsymbol{E}^k_{num}$ and $\boldsymbol{V}^k_{num}$. When the discrete pressure appears has the same shape of the numeric divergence of the electric field, as show in figure 4.7. This figure exhibit another annoying property: while ρ^k_{num} moves together with the support of the soliton, the discrete *pressure* p^k_{num}, once created, does not "travels", but remains practically constant. This fact is explained by considering the structure of equation (3.26): the discrete divergence ρ^k_{num} is not zero only in the travelling support of the soliton. The creation of new discrete pressure at time $k\Delta t$, sum up the one existing at time $(k-1)\Delta t$. This takes place only in the set of nodes belonging to the support. At each nodes $(i, j) \in \mathcal{G}^{sub}_{r,y}$ that do not belong to the support of the soliton, ρ^k_{num} is zero and the equation (3.26) reduces to $p^{k+1}_{i,j} = p^k_{i,j}$, which means that the discrete pressure is conserved. This behaviour is an artefact due to how the numerical scheme works. It has no counterpart in the analytical solution. It would be interesting to find a way to modify the discrete equations in order to remove this drawback.

[5] See figure 4.4.

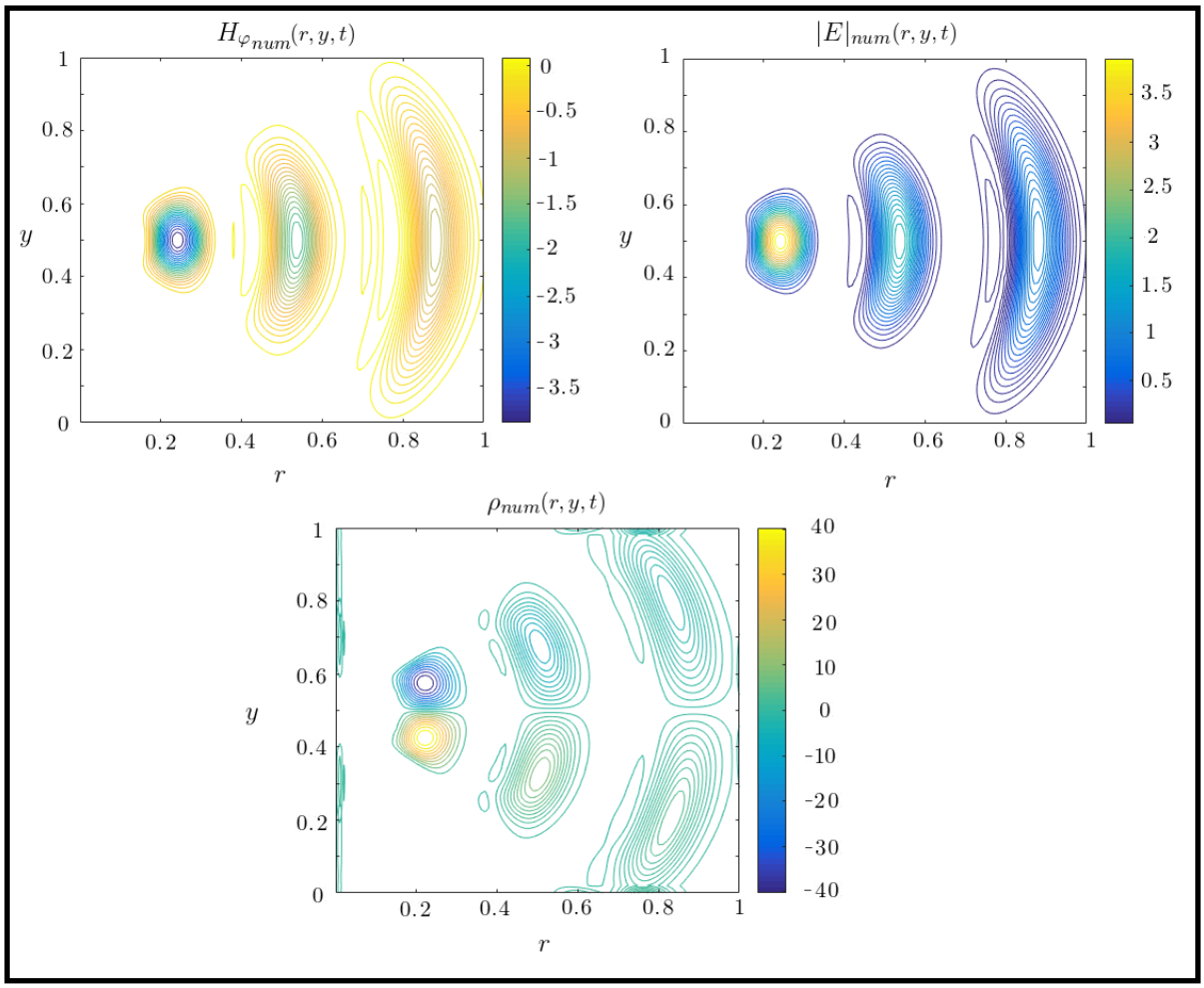

Figure 4.6: Contour lines representation of the matrices $H_{\varphi_{num}}^{\ k}$ (top-left), $|\boldsymbol{E}|_{num}^{k}$ (top-right) and ρ_{an}^{k} (bottom) relative to the choice of $N = 100$ and $\lambda = 1/4$ for $k = 0, 120, 260$ ($t = k\Delta t$). In each picture the three matrices relative to one of the field are over-plotted. The supports are completely disjoint. The soliton travels from the left side to the right side of the domain in each picture.

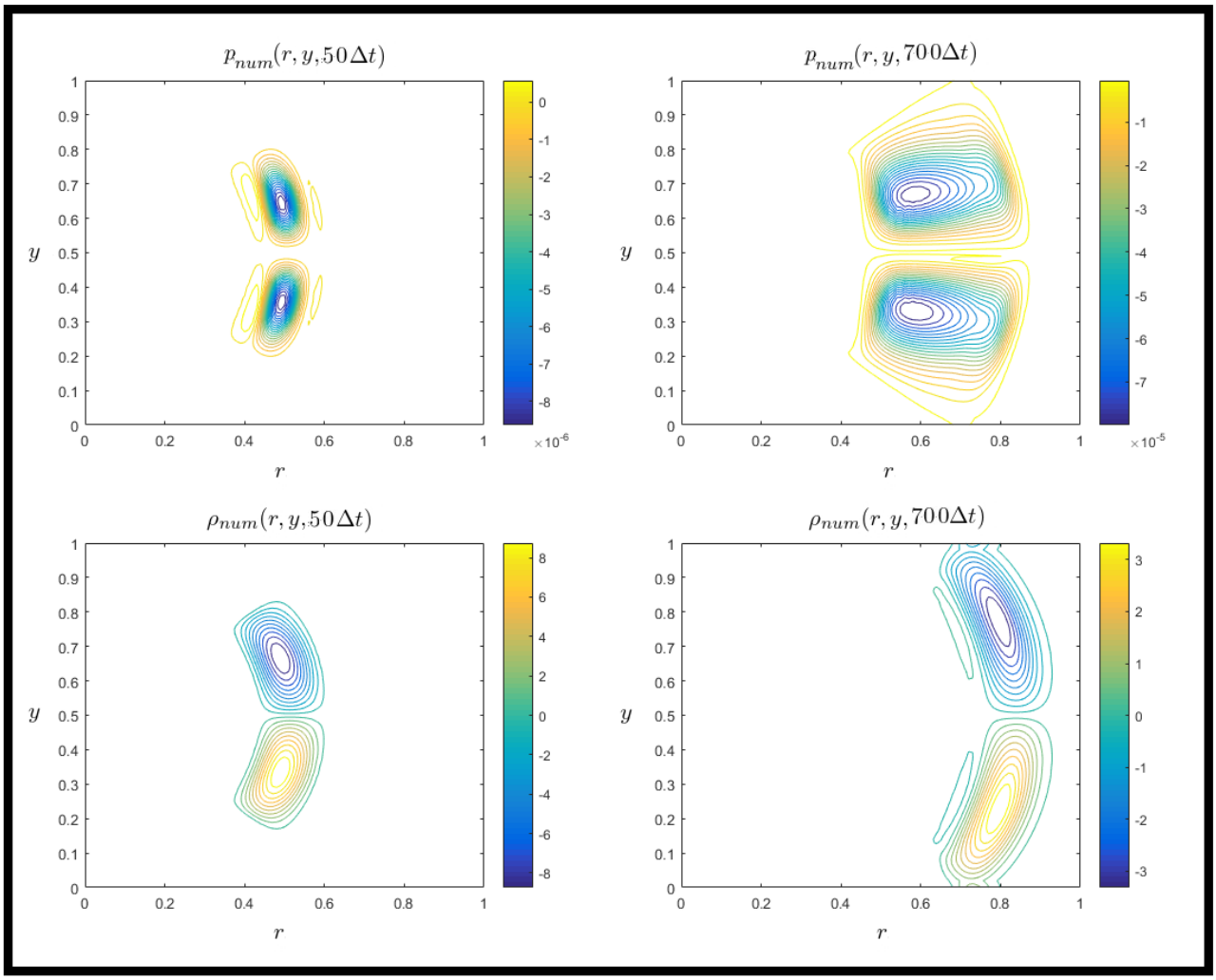

Figure 4.7: Contour lines representation of the matrices $p_{\varphi_{num}}^{50}$ (top-left), $p_{\varphi_{num}}^{700}$ (top-right), ρ_{num}^{50} (bottom-left) and ρ_{num}^{700} (bottom-right) relative to the choice of $N = 100$ and $\lambda = 1/10$.

We have introduced the constraints (4.1) in order to avoid the numerical instability that arises by performing the simulations here considered. It would be likely not to use (4.1) in general. We have explored two strategies in order to increase the duration of the simulations, even though this does not remove the instabilities for arbitrarily long numerical experiments. We expect that reducing λ, for fixed N and T, will have a positive impact on the stability of the simulation. Moreover, since another possible drawback is connected to the spurious modes that can arise by computing the divergence using central differences, we have considered the following upwind approximation (along the direction of $\boldsymbol{V}$) of ρ in place of (3.16)

$$\rho^k_{i,j} = \frac{E^k_{r\,i,j}}{a_r + ih} + \frac{E^k_{r\,i+1,j} - E^k_{r\,i-1,j}}{2h} U_{r\,i,j} + \frac{E^k_{y\,i,j+1} - E^k_{y\,i,j-1}}{2h} U_{y\,i,j} \qquad \begin{matrix} i = 1, \ldots, N_r - 1 \\ j = 1, \ldots, N_y - 1 \end{matrix} . \tag{4.2}$$

Our choice of the computational domain implies $a_r = 0$. Furthermore, according to (2.24) we have

$$U_{r\,i,j} = \frac{ih}{\sqrt{(ih)^2 + (jh - 1/2)^2}}, \qquad U_{y\,i,j} = \frac{jh - 1/2}{\sqrt{(ih)^2 + (jh - 1/2)^2}} \qquad \begin{matrix} i = 1, \ldots, N_r - 1 \\ j = 1, \ldots, N_y - 1 \end{matrix} . \tag{4.3}$$

The results of a series of numerical experiments confirm that the more λ is small the longer the simulation is stable. The use of (4.2) in place of (3.16) in some cases enforce the stability of the numerical scheme, but this is not a general feature. For example, simulating a soliton on a discrete grid defined by taking $N = 200$, $\lambda = 1/16$ and $T = 0.65$, the numerical scheme with (3.16) does not produce instability, while the one with (4.2) do it.

4.2. Guided Waves

In this section we take in to account some numerical simulations where suitable fixed wave guides are placed into the computational domain.
For the sake of simplicity, we consider straight wave guides intersecting the nodes of the sub-grids $\mathcal{G}^{sub}_{x,y}$ and $\mathcal{G}^{sub}_{r,y}$ in the cartesian and cylindrical frameworks, respectively. The configurations of the wave guides used in the numerical experiments of this section are displayed in figure 3.4 and figure 4.15. This way of placing the wave guides allow us to define a subset of nodes, that, at each time $k\Delta t$, belongs to the sub-grids $\mathcal{G}^{sub}_{x,y}$ and $\mathcal{G}^{sub}_{r,y}$ identifying the guides.
According to what was stated in section 2.8, the boundary conditions defining the behaviour of the fields on the wave guides, will be imposed in order to take into account the mutual interaction between the guides themselves and the electromagnetic field existing in the nearby free-space. The procedure followed to impose the boundary conditions is described is section 3.5.

Cartesian framework: wave propagation between two parallel guides
Here, we consider the computational domain $[a_x, b_x] \times [0, 1] \times [0, T]$, with $a_x, b_x \in \mathbb{R}^+$. In the space domain $[a_x, b_x] \times [0, 1]$ the usual sub-grid $\mathcal{G}^{sub}_{x,y}$ is fixed and two parallel wave guides are placed at $y = 0$ and $y = 1$. We will refer to two different Maxwellian solutions that are reported below:

$$\boldsymbol{E} = \Big(\ 0 \ , \ c \ \cos(x - ct) \ , \ 0 \ \Big), \qquad \boldsymbol{H} = \Big(\ 0 \ , \ 0 \ , \ \frac{1}{\mu_0} \ \cos(x - ct) \ \Big) \tag{4.4}$$

$$\boldsymbol{E} = \Big(\ 0 \ , \ c \ \sin x \ \sin(ct) \ , \ 0 \ \Big), \qquad \boldsymbol{H} = \Big(\ 0 \ , \ 0 \ , \ \frac{1}{\mu_0} \ \cos x \ \cos(ct) \ \Big). \tag{4.5}$$

The exact solution (4.4) is a travelling plane wave such that the oscillating electric and magnetic fields have the same phase. On the contrary, the fields of the exact solution (4.5) produce a standing wave, since they have a difference of phase equal to $\pi/2$.
The aim of the simulations discussed here is to investigate the possibility that a standing wave can be transformed into a travelling one through the influence of the guides. This transition is observed when the parameter v_g (defined in section 2.8 and section 3.6) is different from 1, i.e. when a transport of the normal component of the electric field at the guide is activated.

In a first series of numerical experiments, the fields (4.4) and (4.5), evaluated at $t = 0$ are set as initial condition on the domain defined by choosing[6] $a_x = -\pi$ and $b_x = \pi$. Periodic boundary conditions, that identify $x = -\pi$ with $x = \pi$, are imposed. The following choice of the parameters has been performed

- $N = 20$,
- $\lambda = 1/10$,
- $T = 5$.

Initial condition	v_g	Related Figures	Comments
Tr.	1	Figure 4.8	The electric and magnetic fields travel unperturbed. The wave guides act as in the PEC case.
Tr.	0	Figure 4.9	The electric and magnetic fields start travelling with the same phase. After some time iterations, a little phase shift arises. The reached configuration seems stable.
St.	0	Figure 4.10	The electric and magnetic fields start travelling out-of-phase of a factor $\pi/2$ in both space and time dimensions. During the simulation the phase shift decreases. The configuration that emerges resembles the stable one described above.
St.	1	Figure 4.11	The electric and magnetic fields start travelling out-of-phase of a factor $\pi/2$ in both space and time dimensions. The phase shift is conserved during the simulation.

Table 4.4: In this table are compared the behaviours of a series of experiments in which an electromagnetic wave may evolve between two conductive parallel guides. Conductive guides can produce a delay in the propagation of the wave in its neighbourhood, this feature is trimmed by the coefficient v_g. In the column headed "Initial condition", the label "Tr." refers to solution (4.4) evaluated for $t = 0$, while the label "St." refers to solution 4.5 evaluated at $t = 0$. The discretization parameters are defined by setting $N = 20$ and $\lambda = 1/10$.

[6] In general it is only required that $b_x - a_x$ is a multiple of the wave length.

The outcomes of the corresponding simulations are summarized in table 4.4. The case that we are interested in is the one related to the third row of the table. A standing initial condition, where the electric and the magnetic are $\pi/2$ out-of-phase, slowly turns into something very close to a travelling wave by the action of the boundary conditions. By comparing this case with the one relative to the fourth row, it turns out that without introducing the transport term in the boundary conditions (by setting $v_g = 0$), the wave do not diminish the phase shift between the electric and magnetic fields.
The cases relative to the second and third rows have different initial conditions but, after a transient period, they settle down on similar travelling configurations, different from the one of the first row, where the wave is a typical Maxwellian plane wave ($v_g = 0$). In both cases, when $v_b = 1$, by observing figure 4.9 and figure 4.10, we note that the intensity of the electric and the magnetic fields increases during the simulation. This trouble, due to the choice of the explicit time advancing method, is corrected by reducing the time step, as documented in table 4.5.

λ	$\max \left\lvert {E_y}_{num}^{N_t} \right\rvert$	$\max \left\lvert {H_z}_{num}^{N_t} \right\rvert$
1/16	6.9495	6.4062
1/32	3.1171	3.3702
1/64	1.5022	1.9736
1/128	0.7345	1.3780

Table 4.5: This table is relative to the numerical settings described in the third row of table 4.4. Thus, a stationary electromagnetic field at $t = 0$ evolves between two wave guides such that $v_g = 0$. The duration of the simulations here considered is $T = 5$. We recall that $T = N_t \Delta t$ and $\lambda = \Delta t/h$, with $h = 1/N$. Four simulations relative to the choice $N = 20$ have been performed for decreasing values of λ. Here are reported the values $\max_{(x,y)\in\mathcal{G}_{x,y}^{sub}} \left\lvert {E_y}_{num}^{N_t} \right\rvert$ and $\max_{(x,y)\in\mathcal{G}_{x,y}^{sub}} \left\lvert {H_z}_{num}^{N_t} \right\rvert$ to show that those numbers decrease with λ. Theoretically, those norms should be around 1.

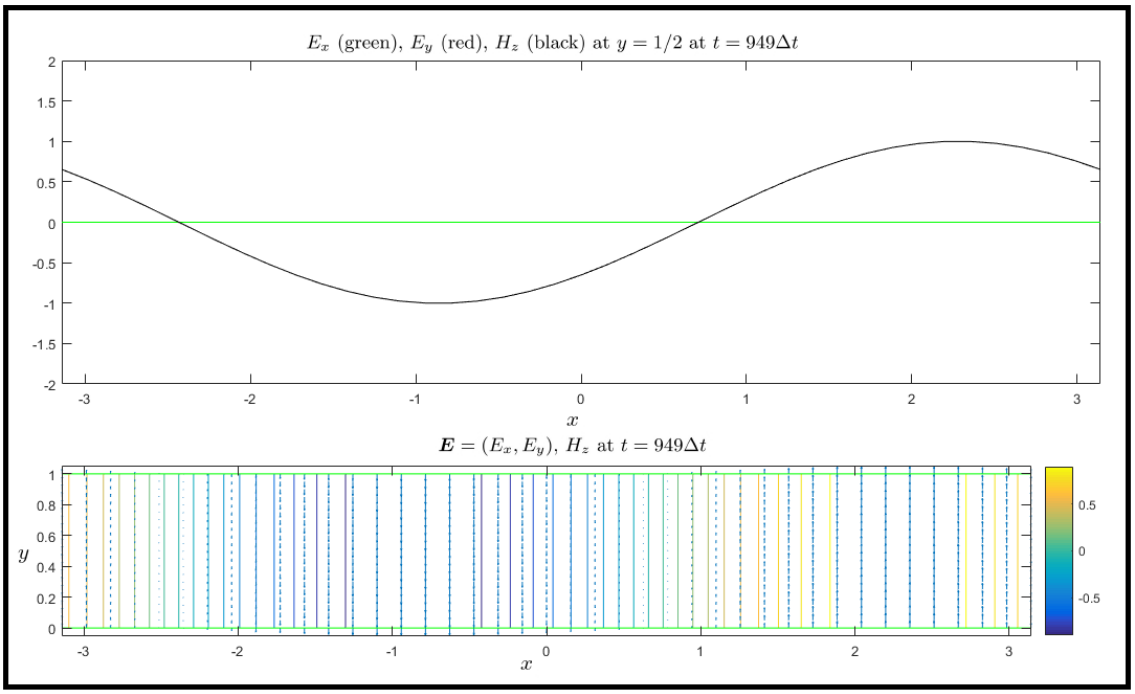

Figure 4.8: Relative to first row of table 4.4.

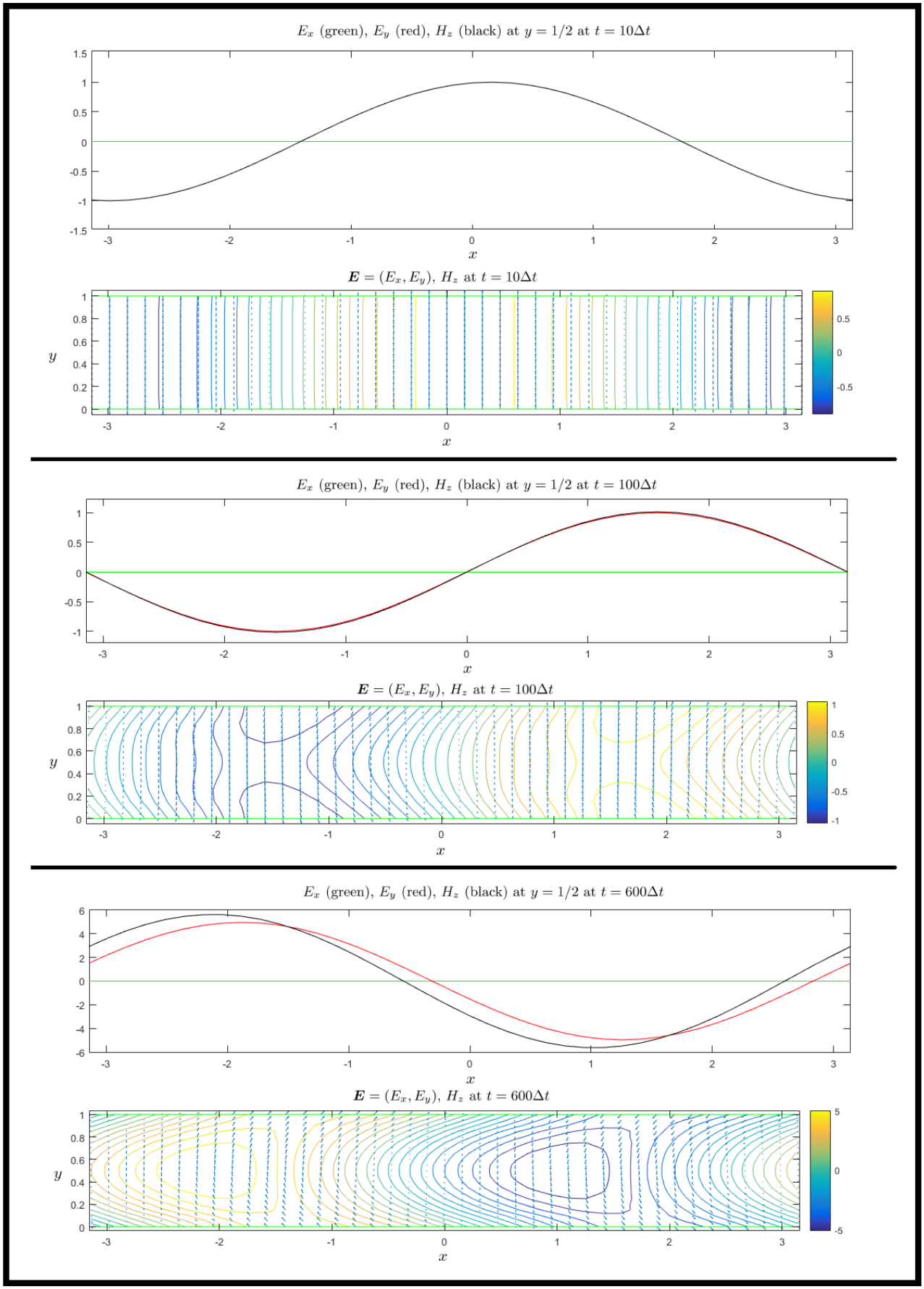

Figure 4.9: Relative to second row of table 4.4.

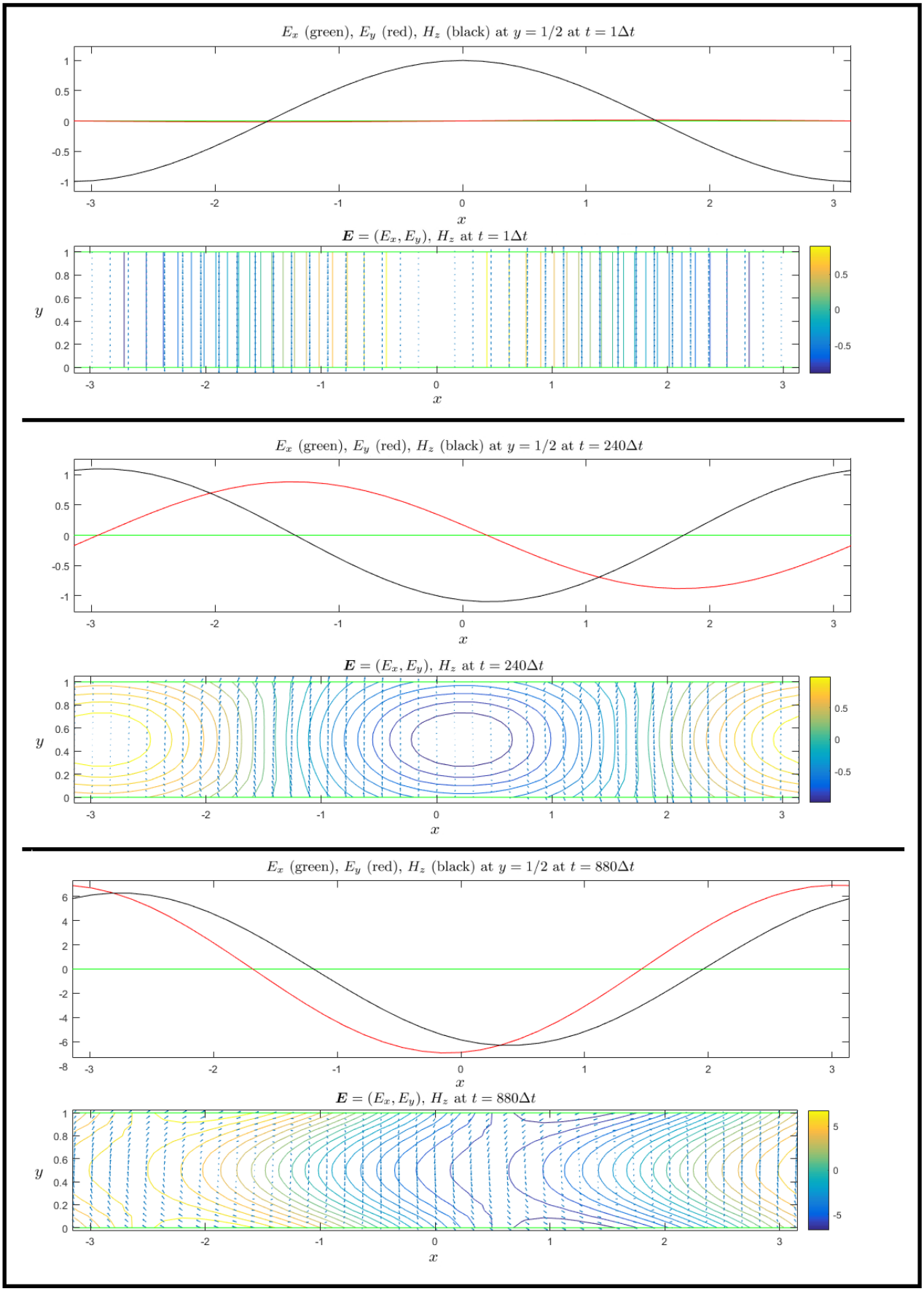

Figure 4.10: Relative to third row of table 4.4.

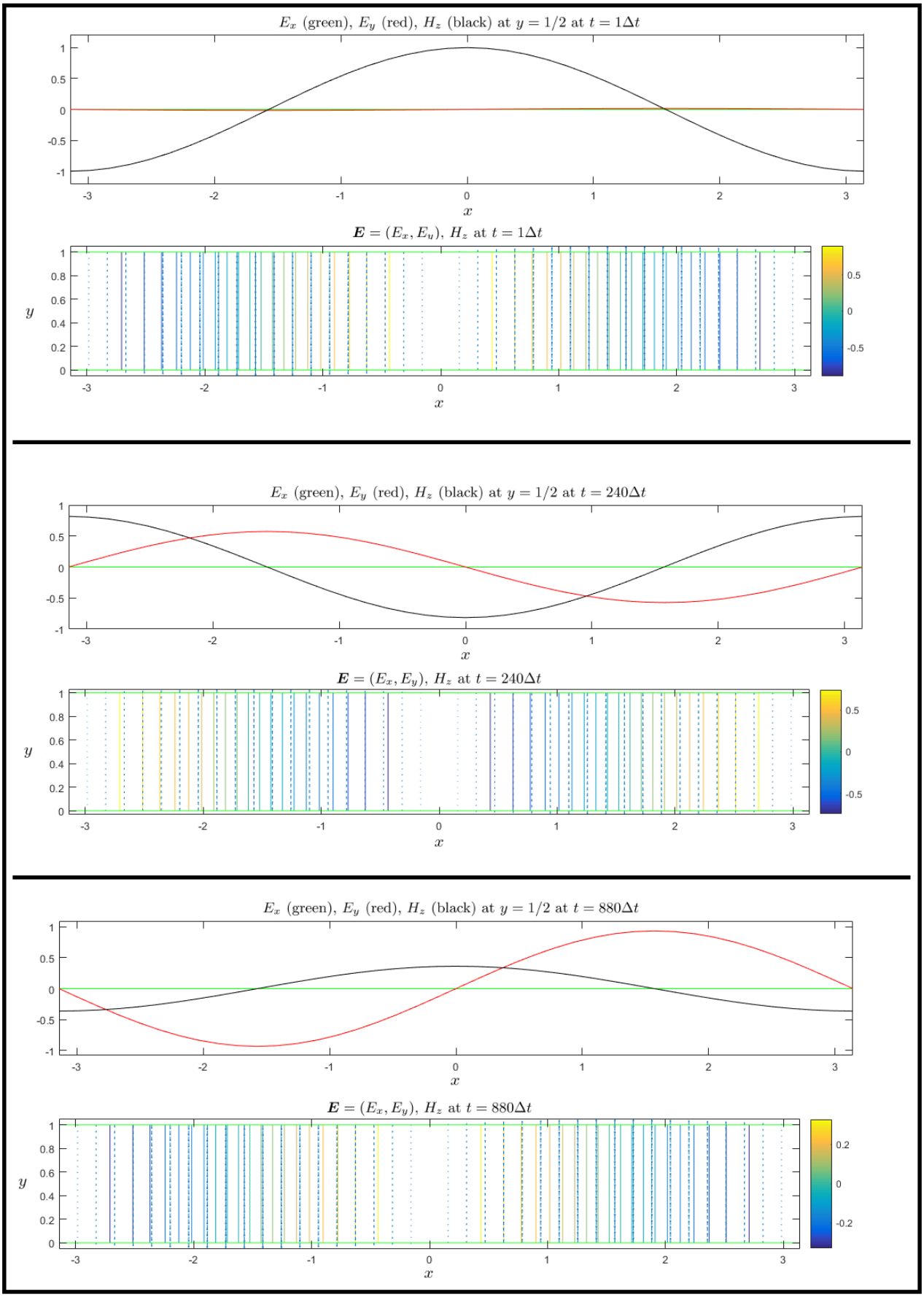

Figure 4.11: Relative to fourth row of table 4.4.

The periodic boundary conditions imposed at $x = -\pi$ and $x = \pi$, allow us to simulate the case in which the electromagnetic wave propagates indefinitely between the guides. By imposing periodicity one neither has to care about how the wave is generated at the entrance of the "tube"(the region of the domain delimited by the guides), nor how the wave exits at the end of the "tube". When a domain of finite extension along the x-direction is considered, the periodic boundary conditions have to be substituted by suitable inflow and outflow boundary conditions, to be imposed at $x = a_x$ and at $x = b_x$ respectively.
From the above example (in particular we refer to third row of table 4.4) we see that a standing wave turns into a travelling one after a considerably long transient. We expect that, in order to reproduce this behaviour without periodic boundary conditions, the length of the "tube" $b_x - a_x$ and the duration T of the simulation have to be sufficiently large.
The natural inflow boundary condition at $x = a_x$ is given by imposing, at each time-step, the exact solution (4.5) evaluated at $x = a_x$ and $y \in [0, 1]$. Nevertheless, the action of the conductive wave guides produces a reduction of the phase difference between the electric and the magnetic field. As in the case of periodic boundary conditions, the standing initial condition changes into a travelling wave after a certain number of time iterations. During this process unsuitable oscillations arise, for both fields, in the neighborhood of the points that have $x = a_x$. Such a behaviour is displayed in figre 4.12.
Imposing Neaumann boundary conditions at $x = x_b$ does not help to cure this behaviour. This occurrence is shown in figure 4.13, where Neumann boundary conditions are imposed both in the cases of travelling and standing solutions, for a wave guide of the type $v_b = 1$. When the electric and magnetic fields are out of phase, i.e for the standing wave, the boundary conditions at the right-hand side of the domain do not allow the wave to "exit", on the contrary when the electric and magnetic fields have the same phase, i.e for the travelling wave, the boundary conditions become of the outflow type and work as expected.
Imposing Neumann conditions at $x = b_x$ for a standing wave that evolves between guides of the type $v_b = 0$ produces a growth of the electric and magnetic fields at $x = b_x$, as one can observe in figure 4.12.
Thus, to replicate the behaviour of the fields as in the third row of table 4.4, on a spacial sub-grid with 20 nodes per unit length, it has been necessary to consider $T = 10$ and $b_x - a_x = 12\pi$.

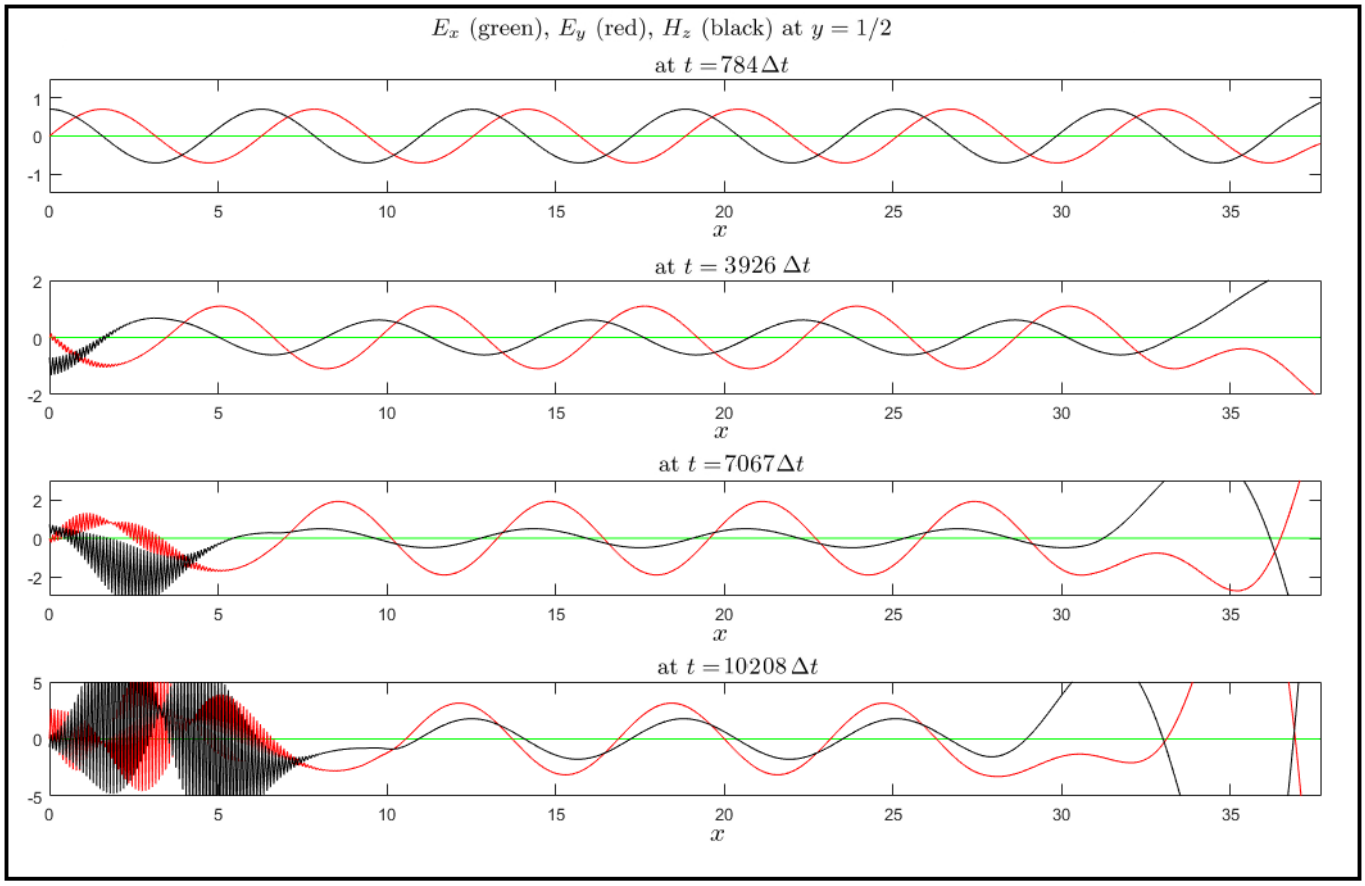

Figure 4.12: Approximated electric and magnetic fields at the center $y = 1/2$ of two conductive guides placed at $y = 1$ and $y = 0$. The guides have an extension of 12π along the x direction. In this numerical simulation 20 nodes for unit length are placed. $\lambda = 1/64$.

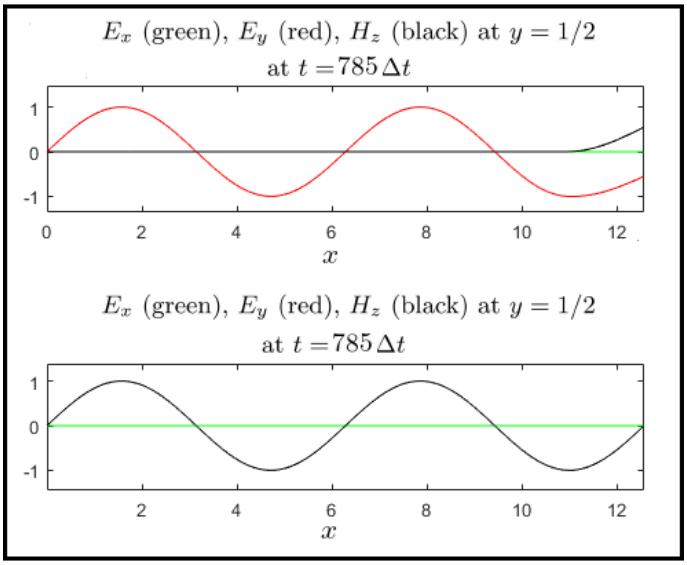

Figure 4.13: At the top the electric and magnetic fields are out of phase and the outward flux boundary conditions at the right-hand side of the domain do not preserve the behaviour of the initial condition. On the contrary, at the bottom, the electric and magnetic fields have the same phase (overlie each other) and the boundary conditions work as expected.

Cylindrical framework: guided soliton

A three dimensional biconic antenna, schematized in figure 4.14, has a radial symmetry. As anticipated in section 2.5, by assuming that the electric and magnetic fields solve the equations in cylindrical framework (no dependence on the φ coordinate), the problem involving this device can be studied in a two dimensional environment. In particular, as shown in figure 4.14, in the (r, y)-plane the antenna consists of a couple of straight wave guides of the same length, the first one with angular coefficient $\gamma_g > 0$ named *upper guide*, and the second one with angular coefficient $-\gamma_g$ named *lower guide*.

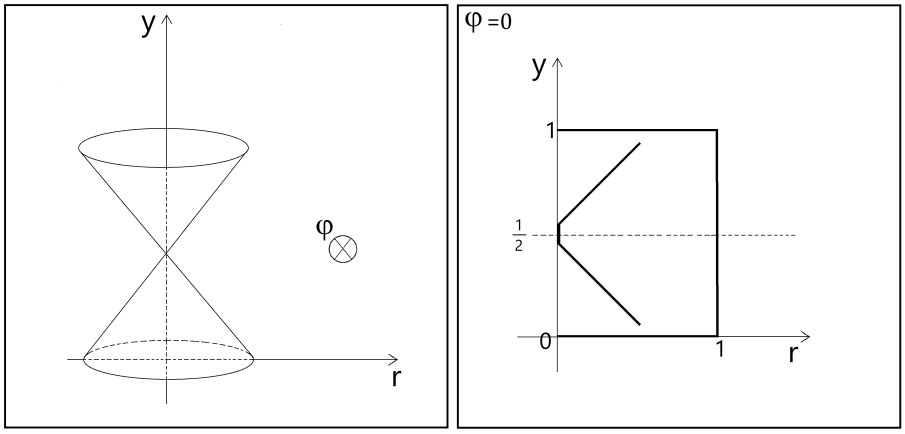

Figure 4.14: Schematic diagram of biconic antenna. At the left-hand side it is displayed in a three-dimensional cylindrical reference frame, at the right hand side it is displayed its intersection with the half-plane $\varphi = 0$.

Since the sub-grid $\mathcal{G}_{r,y}^{sub}$ is equispaced in the r and y directions, a suitable choice for the insertion of the wave guides is of at angle $\pm\pi/4$ ($\gamma_g = 1$) with respect to the distribution of the nodes of the grid.

For practical reasons the intersection between the upper and the lower guides, i.e. the center of the biconic antenna, will be placed outside the computational domain $[0, 1] \times [0, 1]$. Let us denote by $P_g = (r_g, y_g)$ this point. We will take $y_g = 1/2$ and $r_g < 0$. Actually, this is only a virtual point, since in the adopted cylindrical coordinate system the r coordinate cannot be negative. Nonetheless, the use of P_g helps us in the geometric definition of the two wave guides.

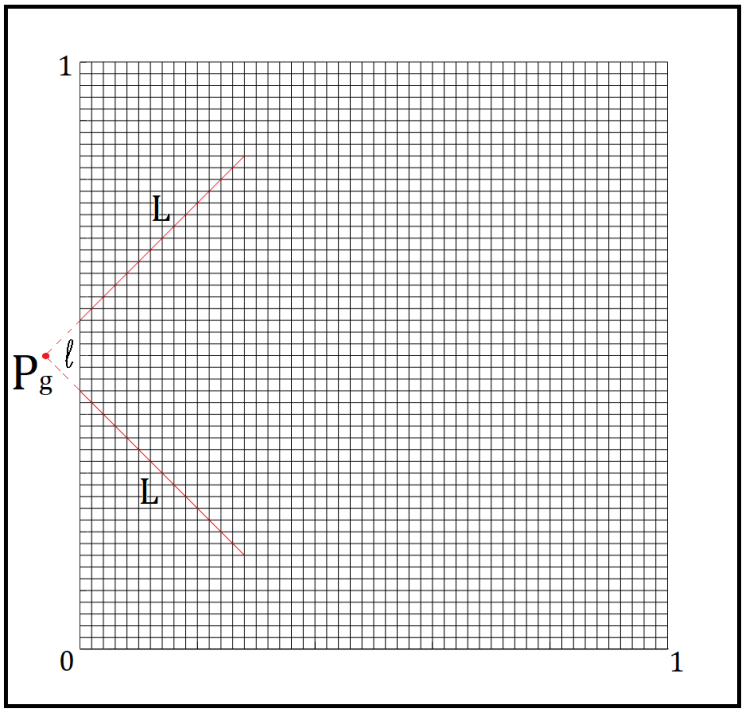

Figure 4.15: Two conductive guides (red) placed on a squared grid.

Together with $y_g = 1/2$ and $\gamma_g = 1$, the two wave guides can be identified by fixing the hollowing parameters

- ℓ, the minimum distance between the upper and the lower guide inside the computational domain,
- L, the length of both guides.

Note that $r_g = -\ell/2$, whereas the upper and lower guides are described by the following equations

$$y = \quad r + \frac{1+\ell}{2} \qquad \text{with} \quad r \in \left[0, \frac{L}{\sqrt{2}}\right],$$

$$y = -r + \frac{1-\ell}{2} \qquad \text{with} \quad r \in \left[0, \frac{L}{\sqrt{2}}\right].$$

In particular the wave guides will be fully contained into the computational domain if

the condition $2\ell + \sqrt{2}L < 1$ is satisfied.

It is convenient to fix ℓ as a multiple of $2h$, L as a multiple of $h\sqrt{2}$ and take N to be an even number. In such a way, on each column of the discrete spacial grid are placed $N+1$ nodes (the central node corresponds to $y = 1/2$). The wave guides intersect the grid $\mathcal{G}_{r,y}^{sub}$ at the following nodes:

$$\begin{aligned} \mathcal{G}_{r,y}^{up} &= \left\{ (ih, jh) \,\middle|\, j = i + \frac{1+\ell}{2h}, \quad \text{with } i = 0, \ldots, \frac{L}{h\sqrt{2}} \right\}, \\ \mathcal{G}_{r,y}^{low} &= \left\{ (ih, jh) \,\middle|\, j = -i + \frac{1-\ell}{2h}, \quad \text{with } i = 0, \ldots, \frac{L}{h\sqrt{2}} \right\}. \end{aligned} \tag{4.6}$$

An example illustrating the position of the wave guides in the discrete domain is given in figure 4.15.

On the discrete guides $\mathcal{G}_{r,y}^{up}$ and $\mathcal{G}_{r,y}^{low}$, boundary conditions are imposed by fixing the value of v_g and following the strategy described in section 3.5. The nodes involved in the computation of the boundary conditions are displayed on the right-hand side of figure 3.4.

It is important to notice that the Lax-Wndroff stencil centered at a node (i, j), such that $(i, j+1)$ belongs to $\mathcal{G}_{r,y}^{up}$ (or, similarly, such that $(i, j-1) \in \mathcal{G}_{r,y}^{low}$), has just one of the diagonal edges laying in a node outside of the boundary as show in figure 4.16. To ensure that the boundary conditions are effective in the whole region delimited by the guides, we decided to apply the discrete equations (3.27) and (3.28) also at the following sets of nodes

$$\mathcal{G}_{r,y}^{up-ext} = \left\{ (ih, jh) \,\middle|\, i = i^*,\ j = j^* + 1, \quad \text{with } (i^*, j^*) \in \mathcal{G}_{r,y}^{up} \right\},$$

$$\mathcal{G}_{r,y}^{low-ext} = \left\{ (ih, jh) \,\middle|\, i = i^*,\ j = j^* - 1, \quad \text{with } (i^*, j^*) \in \mathcal{G}_{r,y}^{up} \right\}.$$

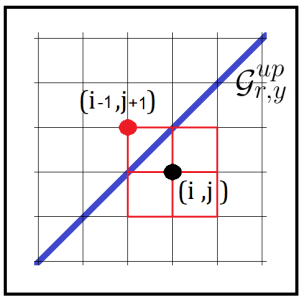

Figure 4.16: The Lax-Wndroff stencil (red) centered at a node (i, j), that is placed in the region between the guides (blue), has its diagonal edge $(i-1, j+1)$ laying in a node outside of the boundary.

Finally, the electric and magnetic fields are set to zero in the external region by imposing, at each time-step $k\Delta t$, that the values of the approximated fields ${E_r}_{i,j}^k$, ${E_y}_{i,j}^k$ and ${H_\varphi}_{i,j}^k$ are zero on the following subset of nodes

$$\mathcal{G}_{r,y}^{up-zero} = \Big\{ (ih, jh) \,\Big|\, i = i^*,\ j = j^* + 2, \quad \text{with } (i^*, j^*) \in \mathcal{G}_{r,y}^{up} \Big\},$$

$$\mathcal{G}_{r,y}^{low-zero} = \Big\{ (ih, jh) \,\Big|\, i = i^*,\ j = j^* - 2, \quad \text{with } (i^*, j^*) \in \mathcal{G}_{r,y}^{up} \Big\}.$$

At this point we have all the elements to numerically simulate the evolution of a soliton having its support between the wave guides. To this purpose we fixed the following parameters.

- The center C of the soliton at initial time $t = 0$ is $(0.1, 0.5)$,
- the constants relative to the shape of the soliton are $\tau = 0.05$, $K_\tau = 9\pi$,
- the duration of the simulation is $T = 0.5$,
- $N = 200$,
- $\lambda = 0.1$,
- $\ell = 14h$,
- $L = 70h\sqrt{2}$,
- $v_g = 0$.

Some plots of the numerical solution have been collected in figure 4.17. It is possible to observe that the soliton continues unperturbed along its path after the interruption of the guides.

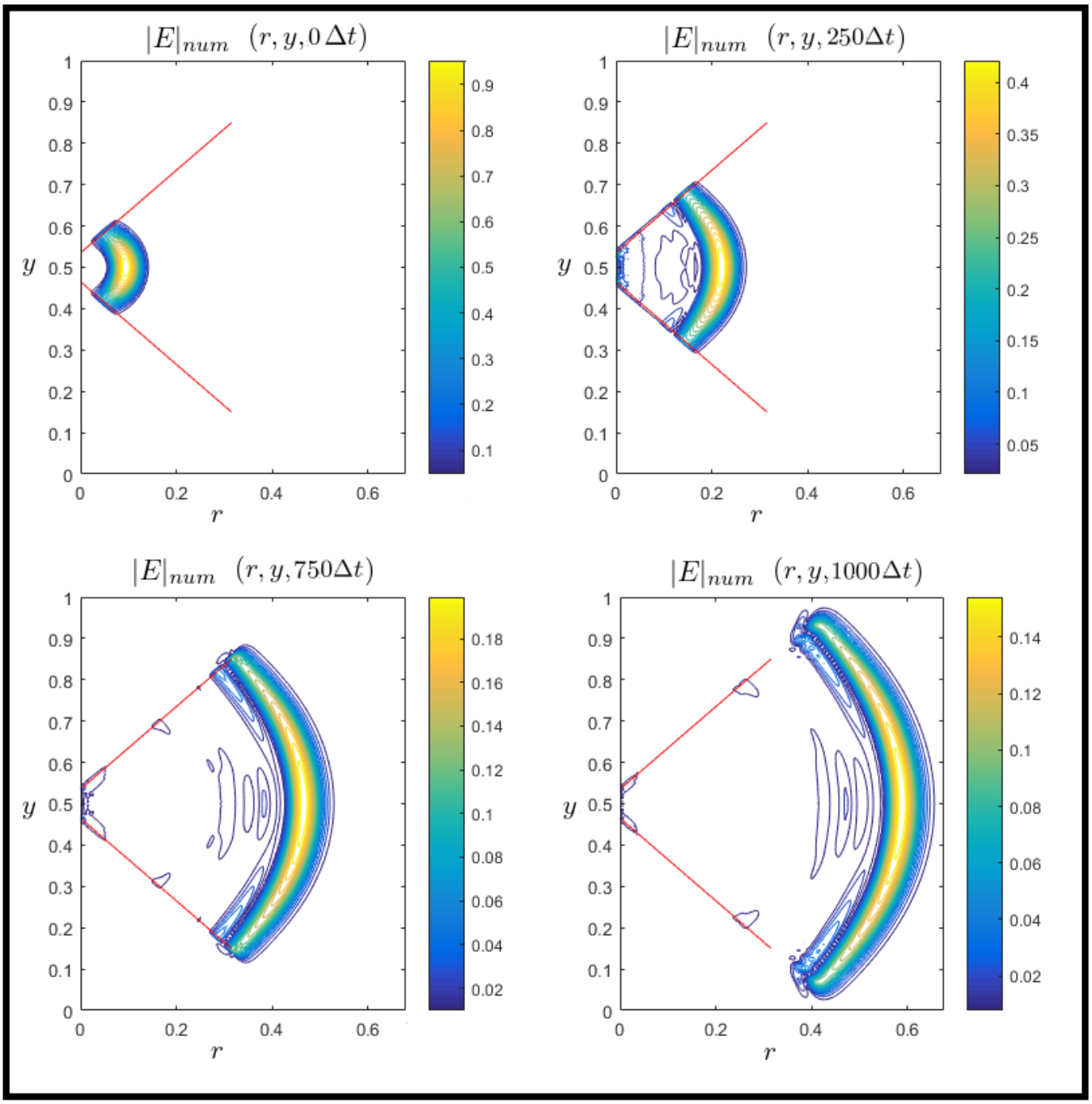

Figure 4.17: Contour representations of the norm of the approximated electric field relative to the numerical simulation of a solion between two conductive guides (red).

4.3. Optical Lens

In this section we will consider the case in which a region of the computational domain is occupied by a linear homogeneous medium, such that the phase velocity of the electromagnetic radiation through that medium is lower than c. In particular, in the numerical experiment presented below, the medium is defined by giving a permittivity coefficient $\varepsilon_1 > \varepsilon_0$, while the permeability coefficient is μ_0.

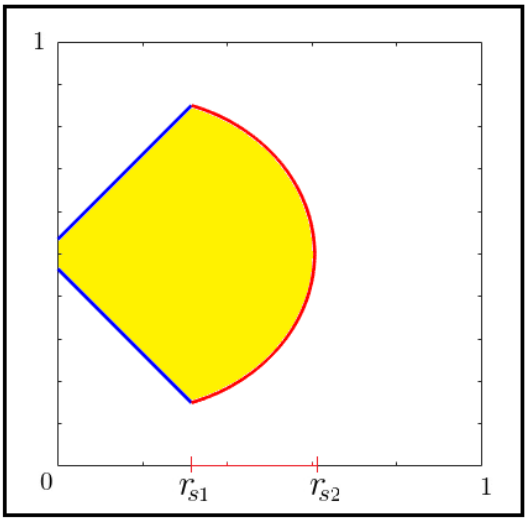

Figure 4.18: Representation of a computational domain where the region between two conductive guides (blue) is occupied by a medium (yellow). In red is highlighted the layer between the medium and the empty space.

Suppose that the medium is located at the right-hand side of the computational domain, and in such a way that the interface, between it and the empty space, is symmetric with respect to the straight line $y = 1/2$, as shown in figure 4.18. The interface can be defined on the interval $[r_{s1}, r_{s2}]$, where $r_{s1} = L/\sqrt{2}$, through the functions

$$y = s(r), \qquad y = 1 - s(r). \tag{4.7}$$

The following propertis are assumed to be satisfied

- $s(r)$ is monotonically decreasing,
- $s(r_{s1}) = \dfrac{1 + \ell + L\sqrt{2}}{2}$,

- $s(r_{s2}) = \dfrac{1}{2}$,
- $\lim\limits_{r \to r_{s2}} \dfrac{1}{s'(r)} = 0.$

At any point $(r, s(r))$, where r belongs to the interval $]r_{s1}, r_{s2}[$, the outward normal (directed from the region occupied by the medium to the empty part of the domain) forms an angle of $\beta = -\arctan\left(1/s'(r)\right)$ with the r-axis.

The velocity field $\boldsymbol{V}$, that exists in the region filled with the medium, is radially distributed with respect to the center P_g of the biconic antenna. Thus, at the point $(r, s(r))$ of the interface, the angle α_1, between the outward normal and the vector $\boldsymbol{V}$, is equal to $\beta - \arctan(V_y/V_r)$.
Reminding that the refractive indices can be express as $\eta = \sqrt{\varepsilon\mu}$, we can apply the Snell's law[7] that relates the above defined angle α_1 with the angle α_0, formed by the outward normal and the vector $\boldsymbol{V}$ at the right-hand side of the point $(r, s(r))$ (in the empty region), through the following equation

$$\sqrt{\varepsilon_1}\ \sin\alpha_1\ =\ \sqrt{\varepsilon_0}\ \sin\alpha_0. \tag{4.8}$$

A picture of the situation just described is given in figure 4.19.

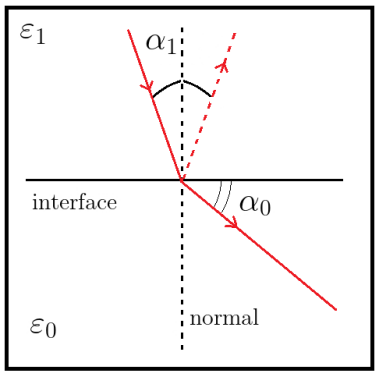

Figure 4.19: Diagram of refraction and reflection of an incoming electromagnetic wave directed to the interface between two media with an incident angle α_1. The medium at the upper part has an higher refraction index than the one of the medium in the lower part. In the medium under the interface the refracted radiation is directed as the solid line (α_0 is determined according to the Snell's law), while the reflected radiation is directed as the dotted line and forms an angle of α_1 with the normal.

[7] See [5].

Our purpose is to choose the function $s(r)$ in order to obtain a velocity field directed along the r-axis in the region at the right-hand side of the layer. To this end two constraint have to be satisfied at each point $(r, s(r))$:

i) $\arctan(V_y/V_r) < \beta$, that ensure that the vector $\boldsymbol{V}$ approaches the point $(r, s(r))$ in the half plane over the normal direction to the layer, and consequently that leaves the point in the complementary plane;

ii) $\alpha_1 < \alpha_{crit}$, where $\alpha_{crit} = \arcsin(\sqrt{\varepsilon_0}/\sqrt{\varepsilon_1})$ is the *critic angle*, when this condition is violated the phenomenon of the *total internal reflection* occurs, i.e. the wave is completely reflected by the layer between the media, so that it remains trapped in the medium at the left-hand side of he domain.

By noting that $\alpha_0 = \beta$ at every point $(r, s(r))$ and recalling the definition of α_1, the equation (4.8) can be rewritten as

$$\sqrt{\varepsilon_1}\ \sin\left(\ \beta - \arctan\left(\frac{V_y}{V_r}\right)\right) = \sqrt{\varepsilon_0}\ \sin(\beta).$$

From the last equation it is possible to isolate β obtaining the following expression for $s'(t)$

$$s'(r) = \frac{\sqrt{\frac{\varepsilon_0}{\varepsilon_1}}\sqrt{(r-r_g)^2 + (s(r)-y_g)^2} - (r-r_g)}{s(r)-y_g}. \tag{4.9}$$

Through the nonlinear relation (4.9) it is possible to approximate $s(t)$ with the following iterative procedure.

1) Fix a step-length $\bar{h}$ and set $(r_{s1}, s(r_{s1}))$ as the *current point* (r_c, y_c) of the layer.

2) Evaluate the slope $s'(r_c)$ of the tangent to the layer at *current point* (r_c, y_c) through the equation (4.9).

3) Find the *new point* (r_{c+1}, y_{c+1}) by computing $r_{c+1} = r_c + \bar{h}$ and $y_{c+1} = y_c + s'(r_c)\bar{h}$.

4) If $y_{c+1} > y_g$ set (r_{c+1}, y_{c+1}) as the *current point* (r_c, y_c) and repeat the operations 2) and 3); otherwise continue to 5).

5) Complete the sequence of $\bar{N}$ points, obtained with the above process, by adding the last point $(r_{\bar{N}+1}, y_{\bar{N}+1})$ such that $r_{\bar{N}+1} = s(r_{s2})$ and $y_{\bar{N}+1} = y_g$.

6) The sequence of points $\{(r_c, y_c)\}_{c=1,\dots,\bar{N}+1}$ obtained with this procedure is the approximation of the layer.

By choosing $\bar{h} << h$ it is possible to distinguish between the nearest nodes, of the discrete grid, placed at the left-hand side of $s(r)$ and the ones placed at the right-hand side. Let us name this two sets of nodes $\mathcal{G}_{r,y}^{left-s}$ and $\mathcal{G}_{r,y}^{right-s}$. We can then impose at the layer some boundary conditions for the approximated field $\boldsymbol{V}_{i,j}^k$, in order that the Snell's law holds. In particular, at any discrete time $k\Delta t$, the new discrete velocity $\boldsymbol{V}_{i,j}^{k+1}$ is computed according to (3.22), and successively at each node $(i,j) \in \mathcal{G}_{r,y}^{right-s}$ the following conditions are imposed

$$V_{r\,i,j}^{k+1} = c, \qquad V_{y\,i,j}^{k+1} = 0.$$

We can now perform a numerical simulation similar to the one discussed in the previous section, a soliton that moves between the guides of a biconic antenna, but this time place a medium in the region delimited by the guides and the curve $s(t)$. The computational domain is the one illustrated in figure 4.18. At time $t = 0$ the velocity field is everywhere radial, with respect to the center of the antenna, except at the nodes (ih, jh) at the right-hand side of $s(r)$ and such that $jh \in [s(r_{s1}), 1 - s(r_{s1})]$. At this last group of nodes the velocity field is directed as the r-axis. It must be precised that in the region occupied by the medium[8] the norm of the velocity field is $(\sqrt{\varepsilon_1\mu_0})^{-1}$, while in the rest of the domain it is c.
The following choice of the parameters has been performed.

- The center C of the soliton at initial time $t = 0$ is $(0.25, 0.5)$,
- the constants relative to the shape of the soliton are $\tau = 0.05$, $K_\tau = 9\pi$,
- the duration of the simulation is $T = 0.75$,
- $N = 200$, $\lambda = 0.1$,
- $\ell = 14h$, $L = 70h\sqrt{2}$,
- $v_g = 0$,
- $\varepsilon_1 = 4$.

[8]The presence of the medium influences also the ratio between the norms of the electric and the magnetic field througth the relation $\sqrt{\varepsilon_1}|\boldsymbol{E}| = \sqrt{\mu_0}|\boldsymbol{H}|$.

Some plots of the numerical solution have been collected in figure 4.20. By comparing it with figure 4.17, it is possible to observe that the presence of the medium straighten the soliton when it cross the layer. A reflected waves appears at the left-hand side of the layer while the soliton pass through it. The presence of the noise at the ends of the guides can be caused by the discontinuities of the velocity field, that in those regions change its distribution from a radial one to a uniform one.

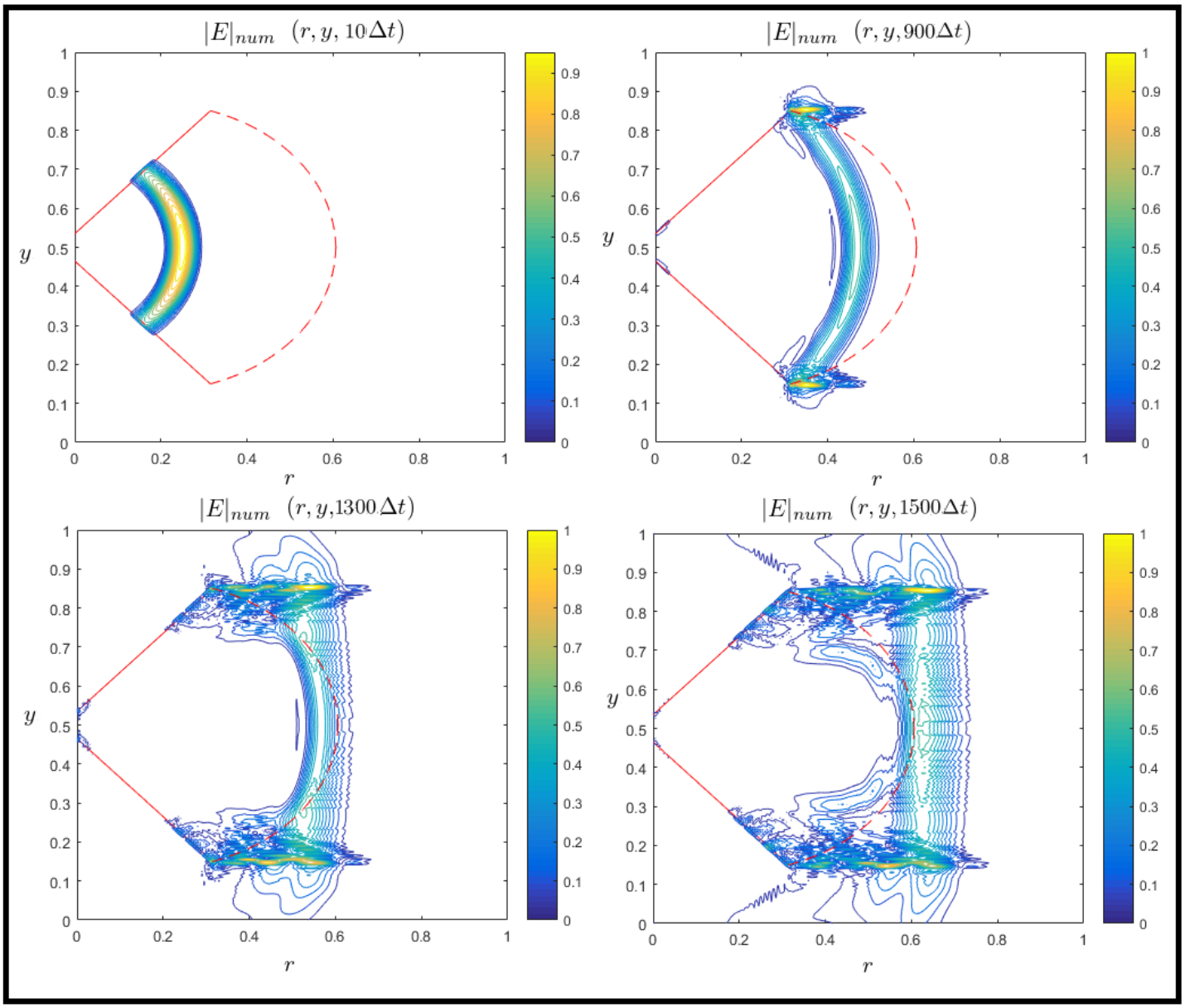

Figure 4.20: Contour representations of the norm of the approximated electric field relative to the numerical simulation of a soliton between two conductive guides (solid red lines). The region delimited by the guides and the dotted red line is occupied by a medium whose permittivity is higher than the vacuum one.

4.4. Antenna

We have already described the structure of a biconic antenna at the beginning of the second part of section 4.2. In that section some numerical experiments for a guided soliton where taken in to account.
Here we consider the case in which the electromagnetic field is emitted by a source. Once emitted the field is subjected, during its evolution, to the presence of conductive guides, as it happened for the soliton of section 4.2.
The source is modeled by giving time-dependent inflow boundary conditions, at a certain set of nodes. Since we expect that the emitted radiation advances according to the radial direction outward from the center of the antenna, these nodes are placed in the gap existing between the two wave guides at the left-hand side of the computational domain.
We are going to consider below two numerical experiments that differ from the set of nodes where inflow boundary conditions are imposed (see figure 4.21). In the first one the source is located at the nodes belonging to the part of the rotation axis included between the wave guides, i.e.

$$\mathcal{G}_{r,y}^{in1} = \Big\{ (ih, jh) \;\Big|\; i = 0,\ |jh - \frac{1}{2}| < \frac{\ell}{2} \Big\}.$$

In the second experiment the nodes of the source are contained at the interior of the circle centered in $P_g = (r_g, y_g)$ and with radius given by the distance between the center of the antenna and the nodes where the guides intersect the rotation axis, i.e.

$$\mathcal{G}_{r,y}^{in2} = \Big\{ (ih, jh) \;\Big|\; (ih - r_g)^2 + (jh - \frac{1}{2})^2 < \frac{\ell^2}{2} \Big\}.$$

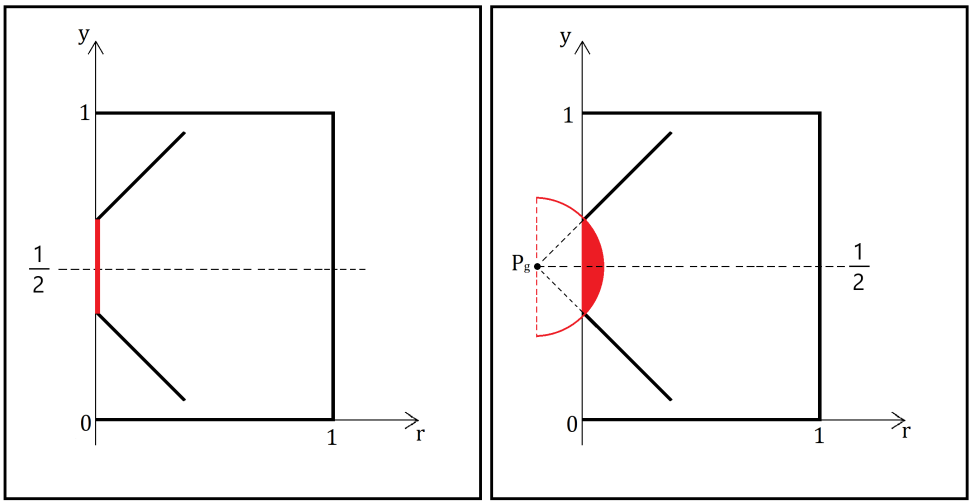

Figure 4.21: Representation of the set of nodes (in red) $\mathcal{G}_{r,y}^{in1}$, at the left-hand side, and $\mathcal{G}_{r,y}^{in2}$, at the right-hand side, where inflow boundary conditions are imposed, as defined in section 4.4.

Similarly to what have been done in section 4.2 in the case of the "tube", an electromagnetic field is present at $t = 0$. This initial condition is defined by the following vector fields

$$\boldsymbol{E} = \Big(\; -\frac{c}{r} \; \sin R \; \cos\vartheta \; \sin(ct) \; , \; 0 \; , \; \frac{c}{r} \; \sin R \; \sin\vartheta \; \sin(ct) \; \Big),$$

$$\boldsymbol{H} = \Big(\; 0, \; -\frac{1}{\mu_0 \; r} \; \cos R \; \cos(ct) \; , \; 0 \; \Big), \tag{4.10}$$

$$\boldsymbol{V} = \Big(\; c\cos\big(\frac{\pi}{2} - \vartheta\big), \; 0, \; c\sin\big(\frac{\pi}{2} - \vartheta\big) \; \Big).$$

Here $R = \sqrt{(r - r_g)^2 + (y - y_g)^2}$ and $\vartheta \in [0, \pi]$ is the angle measured clockwise from the straight line passing through the point P_g and parallel to the y-axis. The inflow boundary conditions are imposed evaluating the fields in (4.10) at the nodes of $\mathcal{G}_{r,y}^{in1}$ or $\mathcal{G}_{r,y}^{in2}$, for each $t = k\Delta t$.

In both of the numerical simulations considered, numerical errors arise in the neighbourhood of the inflow region, after a relatively small number of time iterations. This undesired behaviour compromises the entire evolution of the emitted radiation. It occurs

near the entrance of the guides in such a strong way that the information present at the source is no more effective.
It is also interesting to compare the orientation of the vectors of the electric field at the nodes in proximity of the source in the cases relative to the biconic antenna, with the ones relative to the cases of the guided soliton and the "tube" without periodic boundary conditions. To this purpose some pictures are collected in figure 4.22. The behaviour at the origin of the instability looks the same for all the considered cases.

To close this section, we want to remark that a number of changes and different choices of inflow boundary conditions have been tried. These are not reported here, also because we were not able to overcome our troubles. Thus, for lack of time, we were not able to find the right combination between the information at the inflow and the boundary conditions at the conductive guides in order to perform a complete simulation of the radiation from a biconic antenna. We are however confident that with some more effort, soon or later, this work can be completed.

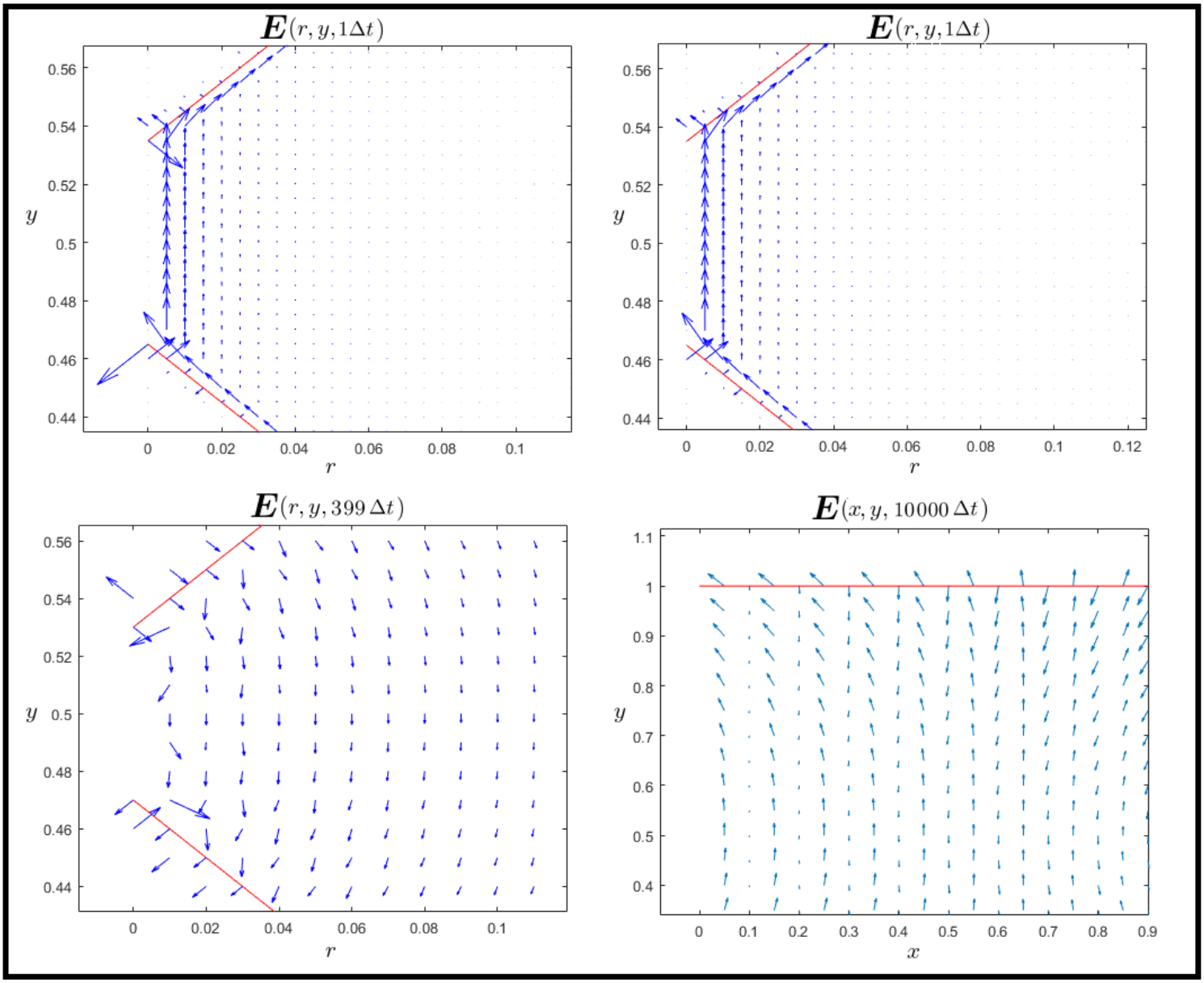

Figure 4.22: The approximated electric field in four different cases related to the arising of undesired growth of the numerical solution. At the top-left the case of a biconic antenna where the inflow conditions are given at the gap between the guides. At the top-right the case of a biconic antenna where the inflow conditions are given at the nodes of the circular sector $\mathcal{G}_{r,y}^{in2}$ (defined in section 4.4). At the bottom-right the case of the "tube" with inflow boundary conditions (see figure 4.12). At the bottom-left the case of the guided solton. Actually, the last one does not show an unstable behaviour, nevertheless the displayed field is a numerical artefact (it is present in both simulation of figure 4.17 and figure 4.20) that resemble the unnatural distribution of the other three cases.

Conclusion

5.1. Overview on the results

Our purposes were to better understand the physical process related to the emission of an electromagnetic field by a biconic antenna. We have decided to describe the process by adopting an extension of the Maxwell's equations and then carry out the related numerical simulations by applying finite-differences methods.
The biconic antenna emission begins with a dynamical source that produces an electromagnetic field, that successively evolves between two wave guides. During this transient the interactions between the fields and the guides act on the electromagnetic field itself in such a way that, at the end of the guides, the field will continue to propagate as a free-wave.
A certain number of features related to the above process have been experimented. To this end, the set of the extended equations (2.9) has been discretized through techniques based on finite-differences. The set of discrete equations has been tested in the case of solitonic solutions, and then applied in different situations. We used different coordinates systems in order to deal with kinds of electromagnetic radiations, such as free waves, guided waves and, finally, the case in which a change of medium occurs. We mainly applied low-order numerical schemes, since we were not actually interested in accurate solutions. Of curse high-order techniques could be implemented as well.

The main difficulties encountered were due to the imposition of boundary conditions. Although suitable "conductive" conditions and outward flow conditions have been successfully implemented, for a lack of time, we were not able to extend our investigation on inflow boundary conditions. Indeed, in the antenna simulations, some troubles arise in the region of the computational domain where the inflow conditions are strongly affected by the evolution of the wave itself, through a backward mechanism that still need further

investigation. A discussion about possible developments is carried out in the following section.

5.2. Possible improvements

To complete the model for the biconic antenna, a necessary step forward is to find the way to impose inflow boundary conditions matching those relative to the nearly wave guides. Boundary conditions (that may be chosen according to what stated in section 2.8) must be imposed at each time step without producing a numerical undesired growth of the solution in proximity of the source.
In addition, as we mentioned in section 3.6, an in-depth investigation of the boundary conditions to be imposed to the electric field at the rotation axis of the cylindrical reference frame, is needed.

Another theoretical question comes from the study of the well-posedness of the hyperbolic systems of partial differential equations (3.1) and (3.4) introduced in section 3.1. For instance, the search of smooth symmetrizers for these systems has been left behind due to lack of time. Also the problem of finding inequalities (like (3.10)) that set an upper bound for the ratio between the time and space discretization parameters should be considered. These studies involve the eigenvalues of the matrices M_{x_i} that define the Lax-Wendroff method.

Another subject concerns with the study of the constant θ in (2.9), related to charge-mass coupling. In the numerical simulations, where the speed of light has been normalized at 1, the value attributed to θ was 0.1. This choice was motivated by empirical considerations, related to stability issues.
Nevertheless, it would be convenient to attribute other values to θ. We recall that, in equation (2.11), such a constant multiplies the term $\boldsymbol{E} + \boldsymbol{V} \times \boldsymbol{B}$ (that emerges in the cases in which $\boldsymbol{E}, \boldsymbol{V}, \boldsymbol{B}$ are not mutually orthogonal) regulating the balance with the other terms present in the equation. Furthermore, θ is involved also in the determination of the time variation of the scalar field p, influencing its magnitude. Exploring the variation of θ, and its impact on the behaviour of the fields involved in the antenna simulation, could better explain the role of the wave guides in the emission process.

Other improvements concern with the use of higher order numerical methods.

It will be possible to simulate the electromagnetic field emitted by a biconic antenna filled with suitable media of different dielectric constant in order to focus the signal. The radiation generated by a source propagates between the antenna arms in a medium where the speed of light is lower than c. During such a guided evolution, the action of the conductive cones modifies the phase shift between the electric and magnetic fields. The electromagnetic radiation than assumes a toroid shape. By filling the space delimited by the antenna with a medium ending in correspondence with the cones, and such that the layer between the medium and the outside vacuum has a suitable curvature, the velocity field can pass from the radial distribution to another one. In this way, the emitted radiation can. be focused and forced to travel transversely to the direction of the rotation axis. Numerical simulations can then be used to collect useful information in order to project and improve such a device.

Appendix

I. On the wave equation related to the extended set of equations

A nonlinear wave equation (2.14) can be obtained from the extended set of equation with the procedure shown in section 2.3, i.e.

$$\frac{\partial^2 \boldsymbol{E}}{\partial t^2} = c^2 \Delta \boldsymbol{E} - c^2 \nabla \rho + \big(\nabla \rho \cdot \boldsymbol{V}\big)\boldsymbol{V} + \rho \boldsymbol{V}\ \nabla \cdot \boldsymbol{V} - \rho \frac{\partial \boldsymbol{V}}{\partial t}.$$

Assuming the hypothesis that $\boldsymbol{V}$ is a stationary and divergence-free field, it is possible to simplify the previous equation in order to get (2.17). Namely we have

$$\frac{\partial^2 \boldsymbol{E}}{\partial t^2} = c^2 \Delta \boldsymbol{E} - c^2 \nabla \rho + \big(\nabla \rho \cdot \boldsymbol{V}\big)\boldsymbol{V}.$$

According to the discussion carried out in section 2.4, regarding a free-wave, we have two characterizing properties that hold for the fields $\boldsymbol{E}$, $\boldsymbol{B}$ and $\boldsymbol{V}$:

i) $\boldsymbol{E} + \boldsymbol{V} \times \boldsymbol{B} = 0$ (which also implies $\boldsymbol{E} \perp \boldsymbol{B}$ and $\boldsymbol{E} \perp \boldsymbol{V}$),

ii) $\boldsymbol{E}$, $\boldsymbol{B}$, $\boldsymbol{V}$ mutually orthogonal at each point.

In section 2.4 we have stated that *the operator at the right-hand side (of equation* (2.17)*) contains only second partial derivatives in the direction of* $\boldsymbol{V}$ *and this may explain why solitons may be generated with this model.* Here we want to make clear what we mean with this last sentence.

First of all, note that considering the Maxwellian case, where $\rho = 0$, equation (2.17) reduces to the classical linear wave equation in three dimension, i.e.

$$\frac{\partial^2 \boldsymbol{E}}{\partial t^2} = c^2 \Delta \boldsymbol{E}.$$

This equation does not admit solitonic solutions. The diffusive Laplace operator Δ acts in each spatial direction, not allowing the possibility of solutions travelling at constant speed on a straight line and maintaining their shape. On the other hand, the wave equation in one space dimension (suppose that the space variable is x)

$$\frac{\partial^2 E}{\partial t^2} = c^2 \frac{\partial^2 E}{\partial x^2} \tag{.1}$$

admits travelling solution of the type $E(x - ct)$, where c is the shifting velocity. For example, the travelling solution with compact support

$$E(x,t) = \begin{cases} \cos(x - ct) + 1 & x \in [-\pi + ct, \pi + ct] \\ 0 & \text{otherwise} \end{cases}$$

is a weak solitonic solution of (.1). As stated above, this is not true anymore in higher dimensions.

Thus, by requiring that the operator at the right-hand side operator of equation (2.17), i.e. $c^2\Delta\boldsymbol{E} - c^2\nabla\rho + \big(\nabla\rho\cdot\boldsymbol{V}\big)\boldsymbol{V}$, contains second partial derivatives only in the direction of $\boldsymbol{V}$, a constraint is imposed at the diffusive term, that can act only in the direction of $\boldsymbol{V}$. This recreate in the case of the three dimensional wave equation (2.17), the feature of the classical wave equation in one dimension that allow solitonic solutions.

Going back to the standard space-time variables in $\mathbb{R}^3 \times \mathbb{R}_0^+$, we show that the operator $c^2\Delta\boldsymbol{E} - c^2\nabla\rho + \big(\nabla\rho\cdot\boldsymbol{V}\big)\boldsymbol{V}$ contains second partial derivatives only in the direction of $\boldsymbol{V}$, in the special case in which $\boldsymbol{V}$ is a constant field with respect to both space and time variables.
To this end, without loss of generality, let us fix a cartesian coordinate system (x, y, z) such that $\boldsymbol{V} = (V_x, 0, 0)$, with $V_x = c$. According to the conditions i) and ii) we have $\boldsymbol{E} = (0, E_y, E_z)$ and $\boldsymbol{B} = (0, B_y, B_z)$. Now, we compute

$$\Delta\boldsymbol{E} = \left(0\,,\ \frac{\partial^2 E_y}{\partial x^2} + \frac{\partial^2 E_y}{\partial y^2} + \frac{\partial^2 E_y}{\partial z^2}\,,\ \frac{\partial^2 E_z}{\partial x^2} + \frac{\partial^2 E_z}{\partial y^2} + \frac{\partial^2 E_z}{\partial z^2}\right),$$

$$\rho = \frac{\partial E_y}{\partial y} + \frac{\partial E_z}{\partial z},$$

$$\nabla\rho = \left(\frac{\partial^2 E_y}{\partial x \partial y} + \frac{\partial^2 E_z}{\partial x \partial z} \, , \, \frac{\partial^2 E_y}{\partial y^2} + \frac{\partial^2 E_z}{\partial y \partial z} \, , \, \frac{\partial^2 E_y}{\partial y \partial z} + \frac{\partial^2 E_z}{\partial z^2} \right),$$

$$\Big(\nabla\rho \cdot \boldsymbol{V}\Big)\boldsymbol{V} = \left(c^2 \frac{\partial^2 E_y}{\partial x \partial y} + c^2 \frac{\partial^2 E_z}{\partial x \partial z} \, , \, 0 \, , \, 0 \right).$$

By summing up this four terms and multiplying for c^2 where needed, we can fully write down the operator

$$c^2 \Delta \boldsymbol{E} - c^2 \nabla\rho + (\nabla\rho \cdot \boldsymbol{V})\boldsymbol{V} = \left(0 \, , \, c^2 \frac{\partial^2 E_y}{\partial x^2} + c^2 \frac{\partial^2 E_y}{\partial z^2} - c^2 \frac{\partial^2 E_z}{\partial y \partial z} \, , \, c^2 \frac{\partial^2 E_z}{\partial x^2} + c^2 \frac{\partial^2 E_z}{\partial y^2} - c^2 \frac{\partial^2 E_y}{\partial y \partial z} \right).$$

To prove our assert we must show that $\dfrac{\partial E_y}{\partial z} = \dfrac{\partial E_z}{\partial y}$. This is given by the relation $\boldsymbol{E} = \boldsymbol{B} \times \boldsymbol{V}$, which implies $\big(0, E_y, E_z\big) = \big(0, B_z V_x, -B_y V_z\big)$. By considering the last vector equality and subtracting the derivative with respect to z of the the second component to the derivative with respect to y of the third component one obtains

$$\frac{\partial E_z}{\partial y} - \frac{\partial E_y}{\partial z} = -c \left(\frac{\partial B_y}{\partial y} + \frac{\partial B_z}{\partial z} \right).$$

The right-hand side of this last equation we find the divergence of $\boldsymbol{B}$, which must be zero. Finally, we can use this last equality to see that

$$c^2 \Delta \boldsymbol{E} - c^2 \nabla\rho + (\nabla\rho \cdot \boldsymbol{V})\boldsymbol{V} = \left(0 \, , \, c^2 \frac{\partial^2 E_y}{\partial x^2} \, , \, c^2 \frac{\partial^2 E_z}{\partial x^2} \right)$$

and conclude that this operator has only second order derivatives along x, which is the direction indicated by $\boldsymbol{V}$.

II. On some exact solutions of the extended set of the electromagnetic equations

The aim of this appendix is to check that some of the *given solutions* of the extended set of electrodynamics equations considered in the previous chapters, actually verifies system (2.19).

Solitonic electromagnetic wave in cartesian coordinates

In this first case we are going to consider, in the suitable cartesian coordinate frame (x, y, z), the fields defined in (2.22) and reported here below. The goal is to prove that they solve equations (2.20), with $p = 0$.

$$\boldsymbol{E} = \Big(\, 0 \, , \, c\,\phi \, , \, 0 \, \Big), \qquad \boldsymbol{V} = \Big(\, c \, , \, 0 \, , \, 0 \, \Big), \qquad \boldsymbol{H} = \Big(\, 0 \, , \, 0 \, , \, \frac{1}{\mu}\,\phi \, \Big)$$

where

$$\phi = \phi(x - ct, y) = \phi_x(x - ct)\phi_y(y),$$

that gives

$$\rho := \nabla \cdot \boldsymbol{E} \; = \; c\,\phi_x \, \frac{\partial \phi_y}{\partial y}.$$

Hereafter, each single equations of the system is taken in to account

i) $$\frac{\partial E_x}{\partial t} \, = \, \frac{1}{\varepsilon}\,\frac{\partial H_z}{\partial y} \, - \, \rho\, V_x \qquad \Rightarrow \qquad 0 \, = \, \frac{1}{\varepsilon\mu}\,\phi_x \, \frac{\partial \phi_y}{\partial y} \, - \, c^2\,\phi_x \, \frac{\partial \phi_y}{\partial y}$$

ii) $$\frac{\partial E_y}{\partial t} \, = \, -\frac{1}{\varepsilon}\,\frac{\partial H_z}{\partial x} \, - \, \rho\, V_y \qquad \Rightarrow \qquad -c^2 \, \frac{\partial \phi_x}{\partial x} \, \phi_y \, = \, -\frac{1}{\varepsilon\mu} \, \frac{\partial \phi_x}{\partial x} \, \phi_y$$

iii) $$\frac{\partial H_z}{\partial t} \, = \, -\frac{1}{\mu}\left(\frac{\partial E_y}{\partial x} \, - \, \frac{\partial E_x}{\partial y} \right) \qquad \Rightarrow \qquad -\frac{c}{\mu} \, \frac{\partial \phi_x}{\partial x} \, \phi_y \, = \, -\frac{c}{\mu} \, \frac{\partial \phi_x}{\partial x} \, \phi_y$$

iv) $$\frac{\partial p}{\partial t} \, = \, \theta\,\rho \Big(E_x\, V_x + E_y\, V_y \Big) \qquad \Rightarrow \qquad \frac{\partial p}{\partial t} \, = \, 0$$

$$\text{v)}\ \ \rho\left[\frac{\partial V_x}{\partial t}+V_x\frac{\partial V_x}{\partial x}+V_y\frac{\partial V_x}{\partial y}+\theta\left(E_x+\mu\,V_y\,H_z\right)\right]=-\frac{\partial p}{\partial x}\qquad\Rightarrow\qquad\frac{\partial p}{\partial x}=0$$

$$\text{vi)}\ \ \rho\left[\frac{\partial V_y}{\partial t}+V_x\frac{\partial V_y}{\partial x}+V_y\frac{\partial V_y}{\partial y}+\theta\left(E_y-\mu\,V_x\,H_z\right)\right]=-\frac{\partial p}{\partial y}\qquad\Rightarrow$$

$$c\,\phi_x\,\frac{\partial\phi_y}{\partial y}\left[\theta\left(\,c\,\phi_x\,\phi_y-c\,\phi_x\,\phi_y\right)\right]=-\frac{\partial p}{\partial y}\qquad\Rightarrow\qquad\frac{\partial p}{\partial y}=0.$$

Note that last three equations are satisfied for any choice of p constant.

Solitonic electromagnetic wave in cylindrical coordinates

Here is studied the case of the soliton in cylindrical coordinates (r,φ,y), which is an exact solution of the system (2.21). This is defined by the fields (2.24) that are reported here below

$$\boldsymbol{E}=\left(-\ \frac{c}{r}\,\zeta\,U_y\ ,\ 0\ ,\ \frac{c}{r}\,\zeta\,U_r\ \right)$$

$$\boldsymbol{V}=\left(\ c\,U_r\ ,\ 0\ ,\ c\,U_y\ \right)$$

$$\boldsymbol{H}=\left(\ 0\ ,\ -\frac{1}{\mu\,r}\,\zeta\ ,\ 0\ \right)$$

where

$$U_r(r,y):=\frac{r-r_0}{\sqrt{(r-r_0)^2+(y-y_0)^2}},\qquad U_y(r,y):=\frac{y-y_0}{\sqrt{(r-r_0)^2+(y-y_0)^2}}.$$

We are here considering the case in which r_0 is a real number. Later, we will show that r_0 must be zero as assumed in (2.24).

By construction, ζ depends on the variables r and y via the functions

$$r'(r,y)=r_0+\sqrt{(r-r_0)^2+(y-y_0)^2}\qquad\text{and}\qquad y'(r,y)=y_0+\frac{1}{K_\tau}\ \arctan\left(\frac{y-y_0}{r-r_0}\right).$$

Furthermore, ζ can be factorized as the product of two functions such that one depends only on r' and the other one depends only on y', i.e.

$\zeta = \zeta(r' - ct, y') = \phi_{r'}(r' - ct)\ \phi_{y'}(y')$.

From the above decomposition we deduce that, during its time evolution, the compact support of ζ moves along the radial directions centered at the point (r_0, y_0) with velocity c. Such a motion is the combination of a translation and a dilation in the plane defined by the axis $r = r_0$ and $y = y_0$.

The following identities will be useful later.

$$\frac{\partial \zeta}{\partial t} = -c\,\frac{\partial \zeta}{\partial r'}, \tag{.2}$$

$$\frac{\partial \zeta}{\partial r'} = \frac{\partial \zeta}{\partial y} U_y + \frac{\partial \zeta}{\partial r} U_r, \tag{.3}$$

The first one is immediate, the second one is derived as follows

$$\frac{\partial \phi_{r'}}{\partial r'}\phi_{y'} = \frac{\partial \phi_{r'}}{\partial r'}\frac{\partial r'}{\partial y}\phi_{y'}U_y + \phi_{r'}\frac{\partial \phi_{y'}}{\partial y'}\frac{\partial y'}{\partial y}U_y + \frac{\partial \phi_{r'}}{\partial r'}\frac{\partial r'}{\partial r}\phi_{y'}U_r + \phi_{r'}\frac{\partial \phi_{y'}}{\partial y'}\frac{\partial y'}{\partial r}U_r$$

$$\frac{\partial \phi_{r'}}{\partial r'}\phi_{y'} = \frac{\partial \phi_{r'}}{\partial r'}\phi_{y'}U_y^2 + \phi_{r'}\frac{\partial \phi_{y'}}{\partial y'}\frac{1}{K_\tau\sqrt{(r-r_0)^2+(y-y_0)^2}}U_rU_y +$$

$$\frac{\partial \phi_{r'}}{\partial r'}\phi_{y'}U_r^2 - \phi_{r'}\frac{\partial \phi_{y'}}{\partial y'}\frac{1}{K_\tau\sqrt{(r-r_0)^2+(y-y_0)^2}}U_rU_y$$

$$\frac{\partial \phi_{r'}}{\partial r'}\phi_{y'} = \frac{\partial \phi_{r'}}{\partial r'}\phi_{y'}U_y^2 + \frac{\partial \phi_{r'}}{\partial r'}\phi_{y'}U_r^2.$$

Finally, the divergence of $\boldsymbol{E}$ is given by

$$\rho := \frac{E_r}{r} + \frac{\partial E_r}{\partial r} + \frac{\partial E_y}{\partial y} =$$

$$-\frac{c}{r^2}\zeta U_y - \frac{c}{r}\frac{\partial \zeta}{\partial r}U_y + \frac{c}{r^2}\zeta U_y - \frac{c}{r}\zeta\frac{\partial U_y}{\partial r} + \frac{c}{r}\frac{\partial \zeta}{\partial y}U_r + \frac{c}{r}\zeta\frac{\partial U_r}{\partial y} = \qquad \left(\text{by using} \quad \frac{\partial U_r}{\partial y} = \frac{\partial U_y}{\partial r}\right)$$

$$-\frac{c}{r}\frac{\partial \zeta}{\partial r}U_y + \frac{c}{r}\frac{\partial \zeta}{\partial y}U_r.$$

We now have all the elements to verify that our fields are solutions of the equations of the electromagnetism in cylindrical coordinates.

i) $\dfrac{\partial E_r}{\partial t} = -\dfrac{1}{\varepsilon}\dfrac{\partial H_\varphi}{\partial y} - \rho\, V_r \qquad \Rightarrow$

$$\frac{c^2}{r}\frac{\partial\zeta}{\partial r'}U_y \;=\; \frac{c^2}{r}\frac{\partial\zeta}{\partial y} \;+\frac{c^2}{r}\frac{\partial\zeta}{\partial r}U_rU_y - \frac{c^2}{r}\frac{\partial\zeta}{\partial y}U_r^2$$

$$\frac{\partial\zeta}{\partial r'}U_y \;=\; \frac{\partial\zeta}{\partial y}U_y^2 \;+\; \frac{\partial\zeta}{\partial r}U_rU_y$$

$$\frac{\partial\zeta}{\partial r'} \;=\; \frac{\partial\zeta}{\partial y}U_y \;+\; \frac{\partial\zeta}{\partial r}U_r, \quad \text{that is true since (.3) holds.}$$

ii) $$\frac{\partial E_y}{\partial t} \;=\; \frac{1}{r\varepsilon}\frac{\partial(rH_\varphi)}{\partial r} \;-\; \rho\,V_y \qquad \Rightarrow$$

$$-\frac{c^2}{r}\frac{\partial\zeta}{\partial r'}U_r \;=\; -\frac{c^2}{r}\frac{\partial\zeta}{\partial r} \;+\frac{c^2}{r}\frac{\partial\zeta}{\partial r}U_y^2 - \frac{c^2}{r}\frac{\partial\zeta}{\partial y}U_rU_y$$

$$\frac{\partial\zeta}{\partial r'}U_r \;=\; \frac{\partial\zeta}{\partial r}U_r^2 \;+\; \frac{\partial\zeta}{\partial y}U_rU_y$$

$$\frac{\partial\zeta}{\partial r'} \;=\; \frac{\partial\zeta}{\partial r}U_r \;+\; \frac{\partial\zeta}{\partial y}U_y, \quad \text{that is true since (.3) holds.}$$

iii) $$\frac{\partial H_\varphi}{\partial t} \;=\; -\frac{1}{\mu}\left(\frac{\partial E_r}{\partial y} \;-\; \frac{\partial E_y}{\partial r}\right) \qquad \Rightarrow$$

$$\frac{c}{\mu r}\frac{\partial\zeta}{\partial r'} \;=\; \frac{c}{\mu r}\frac{\partial\zeta}{\partial y}U_y \;+\; \frac{c}{\mu r}\zeta\frac{\partial U_y}{\partial y} \;+\; \frac{c}{\mu r}\frac{\partial\zeta}{\partial r}U_r \;+\; \frac{c}{\mu r}\zeta\frac{\partial U_r}{\partial r} \;-\; \frac{c}{\mu r^2}\zeta U_r$$

$$\frac{\partial\zeta}{\partial r'} \;=\; \frac{\partial\zeta}{\partial y}U_y \;+\; \zeta\frac{\partial U_y}{\partial y} \;+\; \frac{\partial\zeta}{\partial r}U_r \;+\; \zeta\frac{\partial U_r}{\partial r} \;-\; \frac{1}{r}\zeta U_r$$

some terms cancel out by using (.3)

$$0 \;=\; \zeta\left(\frac{\partial U_y}{\partial y} \;+\; \frac{\partial U_r}{\partial r} \;-\; \frac{1}{r}U_r\right)$$

$$0 \;=\; \zeta\left(\frac{U_r^2}{\sqrt{(r-r_0)^2+(y-y_0)^2}} \;+\; \frac{U_y^2}{\sqrt{(r-r_0)^2+(y-y_0)^2}} \;-\; \frac{1}{r}U_r\right)$$

$$0 \;=\; \frac{\zeta}{\sqrt{(r-r_0)^2+(y-y_0)^2}}\left(1-\frac{r-r_0}{r}\right),$$

note that this equation is satisfied, independently of ζ, only if $r_0 = 0$.

iv) $$\frac{\partial p}{\partial t} \;=\; \theta\,\rho\left(E_r\,V_r + E_y\,V_y\right) \qquad \Rightarrow$$

$$\frac{\partial p}{\partial t} \;=\; \theta\,\rho\left(-\frac{c^2}{r}\zeta U_rU_y + \frac{c^2}{r}\zeta U_rU_y\right)$$

$$\frac{\partial p}{\partial t} \;=\; 0$$

v) $$\rho\left[\frac{\partial V_r}{\partial t}+V_r\frac{\partial V_r}{\partial r}+V_y\frac{\partial V_r}{\partial y}\;+\;\theta\left(E_r\;-\;\mu\,V_y\,H_\varphi\right)\right]\;=\;-\frac{\partial p}{\partial r}\qquad\Rightarrow$$

$$\rho\left[c^2U_r\frac{\partial U_r}{\partial r}+c^2U_y\frac{\partial U_r}{\partial y}\;+\;\theta\left(-\frac{c}{r}\zeta U_y\;+\;\frac{c}{r}\,\zeta U_y\right)\right]\;=\;-\frac{\partial p}{\partial r}$$

$$\rho\left[c^2U_r\frac{U_y^2}{\sqrt{(r-r_0)^2+(y-y_0)^2}}-c^2U_r\frac{U_rU_y}{\sqrt{(r-r_0)^2+(y-y_0)^2}}\right]\;=\;-\frac{\partial p}{\partial r}$$

$$\frac{\partial p}{\partial r}\;=\;0.$$

vi) $$\rho\left[\frac{\partial V_y}{\partial t}+V_r\frac{\partial V_y}{\partial r}+V_y\frac{\partial V_y}{\partial y}\;+\;\theta\left(E_y\;+\;\mu\,V_r\,H_\varphi\right)\right]\;=\;-\frac{\partial p}{\partial y}\qquad\Rightarrow$$

$$\rho\left[c^2U_r\frac{\partial U_y}{\partial r}+c^2U_y\frac{\partial U_y}{\partial y}\;+\;\theta\left(\frac{c}{r}\zeta U_r\;-\;\frac{c}{r}\,\zeta U_r\right)\right]\;=\;-\frac{\partial p}{\partial y}$$

$$\rho\left[-c^2U_r\frac{U_rU_y}{\sqrt{(r-r_0)^2+(y-y_0)^2}}+c^2U_y\frac{U_r^2}{\sqrt{(r-r_0)^2+(y-y_0)^2}}\right]\;=\;-\frac{\partial p}{\partial y}$$

$$\frac{\partial p}{\partial y}\;=\;0.$$

Summarizing we note that last three equations are satisfied by each choice of p constant. In addition we have found the constraint $r_0 = 0$.

Spherical electromagnetic wave in spherical coordinates

By using a spherical system of coordinates (R, ϑ, φ), with $\vartheta \in [0, \pi]$ and $\varphi \in [0, 2\pi)$, we check that the fields considered in (2.27), and reported below, are exact solutions of the extended equations (2.15).

$$\boldsymbol{E} = \Big(0,\;\frac{c}{R}\;g_1(\vartheta,\varphi)f(ct-R),\;\frac{c}{R}\;g_2(\vartheta,\varphi)f(ct-R)\;\Big)$$

$$\boldsymbol{H} = \Big(0,\;-\frac{1}{\mu R}\;g_2(\vartheta,\varphi)f(ct-R),\;\frac{1}{\mu R}\;g_1(\vartheta,\varphi)f(ct-R)\;\Big)$$

$$\boldsymbol{V} = \Big(\;c,\;0\;,\;0\;\Big).$$

Here f, g_1 and g_2 are assumed to be smooth functions that satisfy the following identity

$$\frac{\partial\big(g_2 \sin\vartheta\big)}{\partial\theta} = \frac{\partial g_1}{\partial\varphi} \tag{.4}$$

that correspond to require that the divergence of the field $\boldsymbol{H}$ is zero. Another important relation can be obtained by deriving f with respect to both R and t, i.e.

$$\frac{\partial f}{\partial t} = -c\frac{\partial f}{\partial R}. \tag{.5}$$

We recall the expressions for divergence and curl of a generic field $\boldsymbol{F}$, expressed in spherical coordinates

$$\begin{aligned}
\nabla\cdot\boldsymbol{F} &= \frac{1}{R^2}\frac{\partial}{\partial R}\big(R^2 F_R\big) + \frac{1}{R\sin\vartheta}\frac{\partial}{\partial\vartheta}\big(\sin\vartheta F_\vartheta\big) + \frac{1}{R\sin\vartheta}\frac{\partial F_\varphi}{\partial\varphi},\\
\nabla\times\boldsymbol{F} &= \left(\frac{1}{R\sin\vartheta}\left[\frac{\partial}{\partial\vartheta}\big(F_\varphi\sin\vartheta\big) - \frac{\partial F_\vartheta}{\partial\varphi}\right],\ \frac{1}{R}\left[\frac{1}{\sin\vartheta}\frac{\partial F_R}{\partial\varphi} - \frac{\partial}{\partial R}\big(RF_\varphi\big)\right],\ \frac{1}{R}\left[\frac{\partial}{\partial R}\big(RF_\vartheta\big) - \frac{\partial F_R}{\partial\vartheta}\right]\right).
\end{aligned}$$

In the case of the fields here considered we obtain

$$\begin{aligned}
\rho := \nabla\cdot\boldsymbol{E} &= \frac{1}{R\sin\vartheta}\frac{\partial}{\partial\vartheta}\big(\sin\vartheta E_\vartheta\big) + \frac{1}{R\sin\vartheta}\frac{\partial E_\varphi}{\partial\varphi} = \frac{c}{R^2\sin\vartheta} f\left[\frac{\partial}{\partial\vartheta}\big(g_1\sin\vartheta\big) + \frac{\partial g_2}{\partial\varphi}\right],\\
\nabla\times\boldsymbol{E} &= \left(\frac{1}{R\sin\vartheta}\left[\frac{\partial}{\partial\vartheta}\big(E_\varphi\sin\vartheta\big) - \frac{\partial E_\vartheta}{\partial\varphi}\right],\ -\frac{1}{R}\frac{\partial}{\partial R}\big(RE_\varphi\big),\ \frac{1}{R}\frac{\partial}{\partial R}\big(RE_\vartheta\big)\right)\\
&= \left(\frac{c}{R^2\sin\vartheta} f\left[\frac{\partial}{\partial\vartheta}\big(g_2\sin\vartheta\big) - \frac{\partial g_1}{\partial\varphi}\right],\ -\frac{c}{R}g_2\frac{\partial f}{\partial R},\ \frac{c}{R}g_1\frac{\partial f}{\partial R}\right)\\
&= \left(0,\ -\frac{c}{R}g_2\frac{\partial f}{\partial R},\ \frac{c}{R}g_1\frac{\partial f}{\partial R}\right).
\end{aligned}$$

$$\begin{aligned}
\nabla\cdot\boldsymbol{H} &= \frac{1}{R\sin\vartheta}\frac{\partial}{\partial\vartheta}\big(\sin\vartheta H_\vartheta\big) + \frac{1}{R\sin\vartheta}\frac{\partial H_\varphi}{\partial\varphi} = \frac{1}{\mu R^2\sin\vartheta} f\left[-\frac{\partial}{\partial\vartheta}\big(g_2\sin\vartheta\big) + \frac{\partial g_1}{\partial\varphi}\right] = 0,\\
\nabla\times\boldsymbol{H} &= \left(\frac{1}{R\sin\vartheta}\left[\frac{\partial}{\partial\vartheta}\big(H_\varphi\sin\vartheta\big) - \frac{\partial H_\vartheta}{\partial\varphi}\right],\ -\frac{1}{R}\frac{\partial}{\partial R}\big(RH_\varphi\big),\ \frac{1}{R}\frac{\partial}{\partial R}\big(RH_\vartheta\big)\right)
\end{aligned}$$

$$= \left(\frac{1}{\mu R^2 \sin\vartheta} f \left[\frac{\partial}{\partial\vartheta}\left(g_1 \sin\vartheta\right) + \frac{\partial g_2}{\partial\varphi} \right] , \; -\frac{1}{\mu R} g_1 \frac{\partial f}{\partial R} \; , \; -\frac{1}{\mu R} g_2 \frac{\partial f}{\partial R} \right).$$

$$= \left(\frac{1}{\mu c}\rho \; , \; -\frac{1}{\mu R} g_1 \frac{\partial f}{\partial R} \; , \; -\frac{1}{\mu R} g_2 \frac{\partial f}{\partial R} \right).$$

Note that $\nabla \cdot \boldsymbol{H}$ is zero since we have assumed the condition (.4). We can proceed by showing that the fields written above are solution of the extended equation of electromagnetism in the case of free wave (2.15). The equations are first reported in vector form, and then each component is individually verified.

i) $\dfrac{\partial \boldsymbol{E}}{\partial t} = c^2 \nabla \times \boldsymbol{B} - \rho \boldsymbol{V} \qquad \Rightarrow$

$$0 = \frac{1}{\varepsilon\mu c}\rho - c\rho$$

$$\frac{c}{R} g_1 \frac{\partial f}{\partial t} = -\frac{1}{\varepsilon\mu R} g_1 \frac{\partial f}{\partial R}$$

$$\frac{c}{R} g_2 \frac{\partial f}{\partial t} = -\frac{1}{\varepsilon\mu R} g_2 \frac{\partial f}{\partial R}.$$

The first one holds since $\varepsilon\mu = 1/c^2$, while to verify the second and the third ones, one has to use (.5).

ii) $\dfrac{\partial \boldsymbol{B}}{\partial t} = -\nabla \times \boldsymbol{E} \qquad \Rightarrow$

$$0 = 0$$

$$-\frac{1}{\mu R} g_2 \frac{\partial f}{\partial t} = \frac{c}{\mu R} g_2 \frac{\partial f}{\partial R}$$

$$\frac{1}{\mu R} g_1 \frac{\partial f}{\partial t} = -\frac{c}{\mu R} g_1 \frac{\partial f}{\partial R}.$$

The second and the third scalar equations hold as a consequence of (.5).

iii) $\nabla \cdot \boldsymbol{B} = 0$ it is ensured by condition (.4),

iv) $\rho\big(\boldsymbol{E} + \boldsymbol{V} \times \boldsymbol{B}\big) = 0 \qquad \Rightarrow$

$$0 = 0$$

$$\frac{c}{R} g_1 f - \frac{c\mu}{\mu R} g_1 f = 0$$

$$\frac{c}{R} g_2 f + \mu c \Big(- \frac{1}{\mu R} g_2 f \Big) = 0.$$

III. On the numerical error on the approximation of the divergence of a soliton

In the numerical experiments related to the cartesian soliton, discussed in section 4.1, it is involved the numerical computation of ρ, i.e. the divergence of the electric field. According to what is stated in chapter 3, at each time-step the Lax-Wendroff scheme computes the divergence implicitly, however a direct computation of such a quantity is also needed to proceed with the numerical schemes dedicated to the update of velocity and pressure. In this case, ρ is approximated through the finite-differences scheme described in section 3.2, that has been tested in the case of cartesian and cylindrical solitons producing the results summarized in table 4.1 and table 4.3.
Proceeding with the analysis of those results it turned out that the error committed in the approximation of ρ decrease as the number of nodes increase. Nevertheless, looking at the columns relative to $\epsilon(\rho)$, of both tables 4.1 and 4.3, one note that those values are one order of magnitude high when compared with the columns in which ϵ is evaluated for the electric and magnetic fields.
The aim of this appendix is to give an explanation of such a fact. We believe that the origin of this anomaly is in the approximation of the derivatives of the components of the electric field at the nodes near the boundary of the support. This conclusion is supported by the numerical experiment described below, the results of which are reported in table .1.

If, as we expect, the error in the approximation of ρ depends on how the functions that define electric and magnetic fields of the solitons go to zero in proximity of the boundary, then this feature must be highlighted by comparing the solitonic solutions (2.22) and (2.23). Both these solutions have squared support and travel at the speed of light along the x-axis. The main difference between them is that in the definition of the electric and magnetic fields of (2.22) appears the function ϕ, while in the definition of (2.23) appears ϕ^2.

We recall here that in both cases the electric field has only the y component, which is defined as $c\phi$ in the case of (2.22) and by $c\phi^2$ in the case of (2.23). In addition we have $\phi(x, y) := \phi_x(x)\phi_y(y)$. By computing the divergence of the electric fields in both cases (we use the subscripts ϕ and ϕ^2 to distinguish between them) at $t = 0$ one finds

$$\rho_\phi \;=\; c\;\phi_x\;\frac{\partial \phi_y}{\partial y},$$

N	h	N_Γ	$N_{\partial\Gamma}$	$\epsilon_\Gamma(\rho_\phi)$	$\epsilon_{\partial\Gamma}(\rho_\phi)$	$\epsilon_\Gamma(\rho_{\phi^2})$	$\epsilon_{\partial\Gamma}(\rho_{\phi^2})$
100	0.01	441	80	0.12911	0.3059	0.11584	0.0056144
200	0.005	1681	160	0.034155	0.1539	0.031047	0.00071052
300	0.0033	3721	240	0.015453	0.10271	0.014063	0.00021101
400	0.0025	6561	320	0.0087689	0.077067	0.0079793	0.00008908
500	0.002	10201	400	0.0056413	0.061665	0.0051323	0.00004563

Table .1: Numerical result relative to the evaluation of the error committed in the approximation of the divergence of the electric field, in the cases of two solitons defined through the function ϕ or ϕ^2. Different space-steps $h = 1/N$ are considered, while the time is fixed at $t = 0$.

$$\rho_{\phi^2} \;=\; 2c\;\phi_x^2\;\phi_y \frac{\partial \phi_y}{\partial y},$$

where

$$\frac{\partial \phi_y}{\partial y} = \begin{cases} -\dfrac{\pi}{\tau}\sin\left((y-y_C)\;\dfrac{\pi}{\tau}\right) & \text{if} \quad |y-y_C| \le \tau \\ & \text{and} \quad |x-x_C| \le \tau \\ 0 & \text{elsewhere} \end{cases}$$

By comparing the analytical expressions of ρ_ϕ and ρ_{ϕ^2} one note that, at the side of the support parallel to the x-axis, the first one goes to zero as a $\sin(y)$ as $y \to \pm\pi$, while the second one goes to zero as a $\big(1+\cos(y)\big)\sin(y)$ as $y \to \pm\pi$. By computing the numerical divergence of both the initial configurations of the electric and magnetic fields in (2.22) and (2.23) and then evaluating the errors $\epsilon_\Gamma(\rho_\phi)$ and $\epsilon_\Gamma(\rho_{\phi^2})$, defined in section 4.1, as well as their restrictions to the boundaries of the support $\epsilon_{\partial\Gamma}(\rho_\phi)$ and $\epsilon_{\partial\Gamma}(\rho_{\phi^2})$. We obtain the results of table .1. Different space grid refinements have been used. The setting of the parameters has been done according to what is decided in section 4.1.
From the table it is clear that, while the errors in the approximation of ρ_ϕ and ρ_{ϕ^2} are close one to each other when considered on the whole support, there is instead a big difference if one restricts this comparison the boundary of the support.

IV. On the Yee's scheme

In this appendix we briefly present the Yee's scheme introduced in [39]. After describing the main features of the method[1], we will highlight some drawbacks that discouraged us to apply it to the problems proposed in this thesis.

By using the notation of section 1.2 for the modern formulation of Maxwell's equations (1.1), we can write the equations of electromagnetism, relatively to a region of the void space in absence of electric or magnetic sources, as follow:

$$\begin{cases} \nabla \times \boldsymbol{H} - \dfrac{1}{c}\dfrac{\partial \boldsymbol{D}}{\partial t} = 0 \\ \nabla \times \boldsymbol{E} + \dfrac{\partial \boldsymbol{B}}{\partial t} = 0 \\ \nabla \cdot \boldsymbol{D} = 0 \\ \nabla \cdot \boldsymbol{B} = 0. \end{cases} \tag{.6}$$

Let us place ourselves in a cartesian reference frame (x, y, z).
The six scalar equations constituting the first two vector equations of the previous system, form the basis of the Yee's scheme, also referred as FD-TD (finite-difference time-domain). The algorithm does not need to explicitly implement the the third and the fourth vector equations in (.6). The space grid will be structured in such a way that the location of the electric and magnetic fields components and their numerical space derivatives, are well-suited to reproduce the action of the curl operator. As a consequence of this choice, the divergence-free conditions for the electric and magnetic fields will be implicitly satisfied. By assuming that neither the electromagnetic field nor the space geometry have any variation in the z direction, we can rewrite the components of the first two vector equations

[1] We will follow the guideline in [35], chapter 3.

in (.6) as

$$\begin{cases} \dfrac{\partial H_z}{\partial t} = \dfrac{1}{\mu}\Big(\dfrac{\partial E_x}{\partial y} - \dfrac{\partial E_y}{\partial x}\Big) \\ \dfrac{\partial E_x}{\partial t} = \dfrac{1}{\varepsilon}\dfrac{\partial H_z}{\partial y} \\ \dfrac{\partial E_y}{\partial t} = -\dfrac{1}{\varepsilon}\dfrac{\partial H_z}{\partial x} \\ \dfrac{\partial E_z}{\partial t} = \dfrac{1}{\varepsilon}\Big(\dfrac{\partial H_y}{\partial x} - \dfrac{\partial H_x}{\partial y}\Big) \\ \dfrac{\partial H_x}{\partial t} = -\dfrac{1}{\mu}\dfrac{\partial E_z}{\partial y} \\ \dfrac{\partial H_y}{\partial t} = \dfrac{1}{\mu}\dfrac{\partial E_z}{\partial x}. \end{cases} \tag{.7}$$

Note that the first three equations only depend on H_z, E_x and E_y, whereas the other three only depend on E_z, H_x and H_y. The first group defines the so called "transverse electric mode" of the electromagnetic wave, the second set defines the "transverse magnetic mode". These two modes are decoupled[2], so that they are completely independent in the vacuum space case (the one we are considering here).

As done in section 2.5, we consider the TM mode i.e.

$$\begin{cases} \dfrac{\partial H_z}{\partial t} = \dfrac{1}{\mu}\Big(\dfrac{\partial E_x}{\partial y} - \dfrac{\partial E_y}{\partial x}\Big) \\ \dfrac{\partial E_x}{\partial t} = \dfrac{1}{\varepsilon}\dfrac{\partial H_z}{\partial y} \\ \dfrac{\partial E_y}{\partial t} = -\dfrac{1}{\varepsilon}\dfrac{\partial H_z}{\partial x}. \end{cases} \tag{.8}$$

The Yee's scheme relative to (.8) uses a three-dimensional grid, spaced of half space-step $h/2$ in both spatial directions ($h = 1/N$, where N is a fixed integer) and of half time-step $\Delta t/2$ along the time axis ($\Delta t = T/N_t$, where N_t is a fixed integer). The electric and magnetic fields are approximated on such a grid, in order to ensure that every $\boldsymbol{E}$ component

[2]The coupling actually comes into play when boundary conditions are taken in to account.

is surrounded by four $\boldsymbol{H}$ components, and every $\boldsymbol{H}$ component is surrounded by four $\boldsymbol{E}$ components. This construction is shown in figure .1.

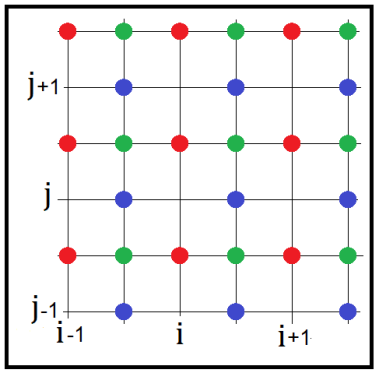

Figure .1: Disposition of the nodes at which H_z (green), E_x (blue) and E_y (red) are approximated o the grid relative to the Yee's scheme (.9).

According to what stated above and with the standard finite-difference notation, the Yee's scheme is written as follow:

$$\begin{cases} H_{z}{}^{k+\frac{1}{2}}_{i-\frac{1}{2},j+\frac{1}{2}} = H_{z}{}^{k-\frac{1}{2}}_{i-\frac{1}{2},j+\frac{1}{2}} + \dfrac{\Delta t}{h\mu}\Big(E_{x}{}^{k}_{i-\frac{1}{2},j+1} - E_{x}{}^{k}_{i-\frac{1}{2},j-1} - E_{y}{}^{k}_{i,j+\frac{1}{2}} + E_{y}{}^{k}_{i-1,j+\frac{1}{2}}\Big) \\ E_{x}{}^{k}_{i-\frac{1}{2},j} = E_{x}{}^{k-1}_{i-\frac{1}{2},j} + \dfrac{\Delta t}{h\varepsilon}\Big(H_{z}{}^{k-\frac{1}{2}}_{i-\frac{1}{2},j+\frac{1}{2}} - H_{z}{}^{k-\frac{1}{2}}_{i-\frac{1}{2},j-\frac{1}{2}}\Big) \\ E_{y}{}^{k}_{i,j+\frac{1}{2}} = E_{y}{}^{k-1}_{i,j+\frac{1}{2}} - \dfrac{\Delta t}{h\varepsilon}\Big(H_{z}{}^{k-\frac{1}{2}}_{i+\frac{1}{2},j+\frac{1}{2}} - H_{z}{}^{k-\frac{1}{2}}_{i-\frac{1}{2},j+\frac{1}{2}}\Big). \end{cases} \tag{.9}$$

Each derivative of the components of the electromagnetic field in (.9) is approximated with a central-difference. It is important to notice that such a discrete scheme leads to the knowledge of the approximated values of H_z, E_x and E_y only at a certain subset of the grid's nodes. Namely the components E_x are computed at the grid nodes with fractional x-coordinates and integer y-coordinates, the components E_y are computed at the grid nodes with fractional y-coordinates and integer x-coordinates, and finally the components H_z are computed at the grid nodes with both fractional x and y-coordinates. Thus, it comes natural to choose the nodes with both integer x and y coordinates in order

to compute the numeric divergence of the electric field:

$$\rho_{i,j}^{k} = \frac{1}{h}\Big({E_x}_{i+\frac{1}{2},j}^{\,k} - {E_x}_{i-\frac{1}{2},j}^{\,k} + {E_y}_{i,j+\frac{1}{2}}^{\,k} - {E_y}_{i,j-\frac{1}{2}}^{\,k} \Big). \tag{.10}$$

By substituting in (.10) the expressions of E_x and E_y given in (.9) it turns out that all the contributions relative to the magnetic field sum up to zero, as shown below

$$\begin{aligned}
\rho_{i,j}^{k} = \frac{1}{h}\Big[& {E_x}_{i+\frac{1}{2},j}^{\,k-1} + \frac{\Delta t}{h\varepsilon}\Big({H_z}_{i+\frac{1}{2},j+\frac{1}{2}}^{\,k-\frac{1}{2}} - {H_z}_{i+\frac{1}{2},j-\frac{1}{2}}^{\,k-\frac{1}{2}} \Big) \\
& - {E_x}_{i-\frac{1}{2},j}^{\,k-1} - \frac{\Delta t}{h\varepsilon}\Big({H_z}_{i-\frac{1}{2},j+\frac{1}{2}}^{\,k-\frac{1}{2}} - {H_z}_{i-\frac{1}{2},j-\frac{1}{2}}^{\,k-\frac{1}{2}} \Big) \\
& + {E_y}_{i,j+\frac{1}{2}}^{\,k-1} - \frac{\Delta t}{h\varepsilon}\Big({H_z}_{i+\frac{1}{2},j+\frac{1}{2}}^{\,k-\frac{1}{2}} - {H_z}_{i-\frac{1}{2},j+\frac{1}{2}}^{\,k-\frac{1}{2}} \Big) \\
& - {E_y}_{i,j-\frac{1}{2}}^{\,k-1} + \frac{\Delta t}{h\varepsilon}\Big({H_z}_{i+\frac{1}{2},j-\frac{1}{2}}^{\,k-\frac{1}{2}} - {H_z}_{i-\frac{1}{2},j-\frac{1}{2}}^{\,k-\frac{1}{2}} \Big) \Big] = \rho_{i,j}^{k-1}
\end{aligned} \tag{.11}$$

This last equations state that the divergence of the electric field is conserved during time iterations. This behaviour is comparable to the one relative to the Lax-Wendroff scheme when $V_x = V_y = 0$.

The troubles concerning the approximation of the extended equations (2.19) by the Yee's scheme arise when one tries to select the subset of the grid nodes where the approximated components of the velocity field have to be computed. All the different dispositions of the nodes in which V_x and V_y are approximated lead to difficulties in writing down a numerical approximation of the equations that involves the total derivative of V and the gradient of p. In order to obtain a scheme for the complete set of equations considered, it would be necessary to introduce the averages of some of the approximated quantities and this produces further complications of the equations and their implementation. On the contrary, by applying the Lax-Wendroff scheme all these troubles are overcome, since all the approximated fields are available at the nodes of the grid.
We would like also to point out that, by using the Yee's scheme, the imposition of the boundary conditions is complicated by the fact that at each node is impossible to express both conditions for the electric and magnetic fields. One can actually impose conditions only for one of the components E_x, E_y or H_z (See figure .1). On the contrary, the Lax-Wendroff method allows to express boundary conditions for all the components of the electromagnetic fields at each node belonging to the boundaries.

V. On the code implementing the Lax-Wendroff scheme

The $MATLAB^{®}$ code implementing the function relative to the Lax-Wendroff scheme in the case of cylindrical framework is given below.

```
% The function implements the Lax-Wendroff scheme for the p.d.e. sistem:
%       dQ/dt = Mr dQ/dr + My dQ/dy
% Q=(rU,rV,W) where U,V,W represent the components of the vector field
% depending on the variables r,y,t.
% Mr and My are the 3x3 matrices of the coefficients of the derivatives.
%
% INPUT:
% - Lambda the ratio between the spatial-step and the time-step.
% - r is a vector containing the coordinates of the nodes along the radial
%   direction.
% - U,V,W are the matrices of the components of the vector field (at
%   time t*Deltat) evaluated on a cartesian grid (i*Deltar,j*Deltay)
%   defined on a plane orthogonal to the polar plane (r,phi):
%       U is the component of the field in the r radial direction,
%       V is the component of the field in the phi angular direction,
%       W is the component of the field in the y direction, normal to the
%       polar plane defined by the other two components.
% - CV1, CV2 are two matrices of the same size of U,V and W
%   needed to construct Mr and My. The entries of these matrices are the
%   components of the velocity vector field (Vr,0,Vy).
% - CM1, CM2 are two matrices of the same size of U,V and W
%   needed to construct Mr and My. The entries of these matrices are the
%   values of the constants epsilon and mu at each node of the grid.
% - Stab, is a boolean: if is 1 stability analysis is activated, i.e. the
%   computation of RoMax.
% - ele_LW are the linear indices of the nodes in which the scheme is applied;
%   if they are not given they are automatically set as the internal
%   elements of the matrices (i=2:Nr-1, j=2:Ny-1).
```

```
%
% OUTPUT:
% - UNew,VNew,WNew are the matrices of the components of the vector
%   field (at time (t+1)*Deltat) evaluated on a cartesian grid
%   (i*Deltar,j*Deltay) of a plane orthogonal to the polar plane (r,phi):
%       UNew is the component of the field in the r radial direction,
%       VNew is the component of the field in the phi angular direction,
%       WNew is the component of the field in the y direction, normal to
%       the polar plane defined by the other two components.
% - RoMax is a vector whose kth-entry is equal to the maximum eigenvalue
%   between these of Mr and My at the iteration k.
%
% NUMERICAL SCHEME:
% (q is the numerical approximation of Q)
%
% q(iDr,jDy,(t+1)Dt) = [ Id - Lambda^2 (Mr^2 + My^2) ]  q(iDr,jDy,tDt)
%                     + 1/2 Lambda Mr (Id + Lambda Mr)  q((i+1)Dr,jDy,tDt)
%                     + 1/2 Lambda My (Id + Lambda My)  q(iDr,(j+1)Dy,tDt)
%                     - 1/2 Lambda Mr (Id - Lambda Mr)  q((i-1)Dr,jDy,tDt)
%                     - 1/2 Lambda My (Id - Lambda My)  q(iDr,(j-1)Dy,tDt)
%   + 1/8 Lambda^2 (Mr My + My Mr) (
%                        q((i+1)Dr,(j+1)Dy,tDt) + q((i-1)Dr,(j-1)Dy,tDt)
%                      - q((i-1)Dr,(j+1)Dy,tDt) - q((i+1)Dr,(j-1)Dy,tDt) )



function [UNew,VNew,WNew,RoMax] = LaxWendroffScheme_Cyl(Lambda,r,U,V,W,...
                                    CV1,CV2,CM1,CM2,Stab,ele_LW)

if nargin==10
    [Nj,Ni]=size(U);
    ele_LW=sub2ind([Nj,Ni],2:Nj-1,2:Ni-1);
end

I=diag(diag(ones(3)));
```

```
UNew=zeros(size(U));
VNew=zeros(size(V));
WNew=zeros(size(W));

RoMax=zeros(size(ele_LW));

[jLW,iLW]=ind2sub(size(U),ele_LW);

Id=ones(length(U),1);

R=Id*r;

U=R.*U;
V=R.*V;

for k=1:length(ele_LW)

    i=iLW(k);
    j=jLW(k);

    Mr=[     -CV1(j,i),                    0,                    0;
                     0,                    0,        r(i)/CM2(j,i);
        -CV2(j,i)/r(i),    1/(r(i)*CM1(j,i)),                    0       ];

    My=[          0,      -1/CM1(j,i),              -r(i)*CV1(j,i);
        -1/CM2(j,i),                0,                          0;
                  0,                0,                   -CV2(j,i)       ];

    if Stab
        RoMax(j,i)=max([abs(eig(Mr));abs(eig(My))]);
    end

    qc =  [ U(j,i),     V(j,i),     W(j,i)     ]';
    qn =  [ U(j+1,i),   V(j+1,i),   W(j+1,i)   ]';
```

```
    qs =  [ U(j-1,i),   V(j-1,i),   W(j-1,i)   ]';
    qw =  [ U(j,i-1),   V(j,i-1),   W(j,i-1)   ]';
    qe =  [ U(j,i+1),   V(j,i+1),   W(j,i+1)   ]';
    qne = [ U(j+1,i+1), V(j+1,i+1), W(j+1,i+1) ]';
    qse = [ U(j-1,i+1), V(j-1,i+1), W(j-1,i+1) ]';
    qsw = [ U(j-1,i-1), V(j-1,i-1), W(j-1,i-1) ]';
    qnw = [ U(j+1,i-1), V(j+1,i-1), W(j+1,i-1) ]';

    TC =       (I-Lambda^2*(Mr^2+My^2)) * qc;
    TN =    1/2*Lambda*My*(I+Lambda*My) * qn;
    TS =   -1/2*Lambda*My*(I-Lambda*My) * qs;
    TE =    1/2*Lambda*Mr*(I+Lambda*Mr) * qe;
    TW =   -1/2*Lambda*Mr*(I-Lambda*Mr) * qw;
    TDiag = 1/8*Lambda^2*(Mr*My+My*Mr)  * (qne+qsw-qse-qnw);

    LW=TC+TN+TS+TE+TW+TDiag;

    UNew(j,i)=LW(1)/R(j,i);
    VNew(j,i)=LW(2)/R(j,i);
    WNew(j,i)=LW(3);

end
```

Bibliography

[1] M. Abraham, A. Föppl, *Theorie der Elektrizität: Einführung in die Maxwellsche Theorie der Elektrizität*, Leipzig, Teubner, 1904.

[2] J.W. Arthur, *The evolution of Maxwell's equations from 1862 to the present day*, IEEE Antennas Propagat. Mag., Vol. 55, 61-81, Jun. 2013. doi:10.1109/MAP.2013.6586627

[3] M. K. Banda, A. Klar, L. Pareschi, M. Seaïd, *Lattice-Boltzmann type relaxation systems and higher order relaxation schemes for the incompressible Navier-Stokes equation*, Math.Comp. 2008. 77:943-965.
https://doi.org/10.1090/S0025-5718-07-02034-0 .

[4] M. Born, L. Infeld, *Foundations of the New Field Theory*, Proceedings of the Royal Society A: Mathematical, Physical and Engineering Sciences, 1934; 144 (852): 425-451.

[5] M. Born, E. Wolf, *Principles of Optics* (4th.ed), Pergamon Press, 1970.

[6] F. Calogero, A. Degasperis, *Spectral Transform And Solitons. Tools To Solve And Investigate Nonlinear Evolution Equations. Vol. 1*, Amsterdam, Netherlands, 1982.

[7] O. Darrigol, *Electrodynamics from Ampere to Einstein*, Oxford University Press, Oxford, 2002.

[8] L. Diazzi, *Studio Numerico delle Equazioni dell'Elettromagnetismo Mediante lo Schema Yee*, Thesis, Università di Modena e Reggio Emilia, 2016. https://morethesis.unimore.it/theses/available/etd-03232016-111843

[9] P.G. Drazin, *Solitons*, Cambridge University Press, New York, 1983.

[10] H. Friedberg, A. Insel, L. Spence, *Linear Algebra* (4th ed), Prentice Hall, 2003.

[11] D. Funaro, *Numerical Simulation of Electromagnetic Solitons and their Interaction with Matter*, J. Sci. Comput. 2010; 45: 259. https://doi.org/10.1007/s10915-009-9338-5.

[12] D. Funaro, *Electromagnetism and the Structure of Matter*, World Scientific, Singapore, 2008.

[13] D. Funaro, *From Photons to Atoms, The Electromagnetic Nature of Matter*, 2012; arXiv:1206.3110 [physics.gen-ph].

[14] D. Funaro, *A Full Review of the Theory of Electromagnetism*, arXiv:physics/0505068.

[15] D. Funaro, *Electromagnetic radiation as fluid flow*, arXiv:0911.4848v1.

[16] D. Funaro, *A Lagrangian for electromagnetic solitary waves in vacuum*, arXiv:1008.2103v1. arXiv:physics/0505068 [physics.gen-ph].

[17] D. Funaro, *High Frequency Electrical Oscillations in Cavities*, Mathematical Modelling and Analysis, 2018; 23(3), 345-358. https://doi.org/10.3846/mma.2018.021.

[18] D. Funaro, E. Kashdan, *Simulation of electromagnetic scattering with stationary or accelerating targets*, Int. J. Modern Phys. C, 2015; 26,7: 1-16. https://doi.org/10.1142/S0129183115500758.

[19] D. Graffi, *Teoria Matematica dell'Elettromagnetismo*, Pàtron, Bologna, 1972.

[20] N.A. Krall, A.W. Trivelpiece, *Principles of plasma physics*, McGraw-Hill, New York, 1973.

[21] B. Gustafsson, H.O. Kreiss, J. Oliger, *Time Dependent Problems and Difference Methods* Wiley, New York, 1995.

[22] H.R. Hertz, *Electric Waves*, Dover, New York, 1962.

[23] J.D. Jackson, *Classical Electrodynamics*, Wiley, New York, 2nd ed. , 1975.

[24] J.D. Jackson, *How an antenna launches its input power into radiation: The pattern of the Poynting vector at and near an antenna*, American Journal of Physics, 2006; 74, 280. https://doi.org/10.1119/1.2063069

[25] L.D. Landau & E.M. Lifshitz, *The Classical Theory of Fields (Volume 2 of A Course of Theoretical Physics)*, Pergamon Press, 1971.

[26] P.D. Lax, B. Wendroff *Systems of Conservation Laws*, Communications on Pure and Applied Mathematics, Vol.XIII, 217-237; 1960.

[27] H.A. Lorentz, *The Fundamental Equations for Electromagnetic Phenomena in Ponderable Bodies Deduced from the theory of Electrons*, Proceedings of the Royal Netherlands Academy of Science (KNAW), Amsterdam, 1902; 5, 254-266.

[28] J.C. Maxwell, *A Dynamical Theory of the Electromagnetic Field*, Phil. Trans. R. Soc. Lond. 1865; 155, 459-512.

[29] J.C. Maxwell, *A Treatise on Electricity and Magnetism*, Dover Publication, New York, 3rd ed. 1954.

[30] K.T. McDonald, *Radiation in the near zone of a center-fed linear antenna*, Preprint, Princeton University, 2004.

[31] W.J. Miloch, *Plasma Physics and Numerical Simulations*, University of Oslo, 2014. https://www.uio.no/studier/emner/matnat/math/MEK4470/h14/plasma.pdf

[32] A. Quateroni, *Modellistica Numerica per Problemi Differenziali*, Springer-Verlag Italia, Milano, 2000.

[33] D. Siegel, *Innovation in Maxwell's electromagnetic theory: Molecular vortices, displacement current, and light*, Cambridge, 1991.

[34] J.C. Strikwerda, *Finite Difference Schemes and Partial Differential Equations*, Wadsworth & Brooks/Cole Mathematics Series, California,1994.

[35] A. Taflove, *Computational Electrodynamics: the Finite-Difference Time-Domain Method*, Artech House, Norwood, MA, 1995.

[36] A. Ugolini, *Approssimazione di onde elettromagnetico-gravitazionali*, Thesis, Università di Modena e Reggio Emilia, 2007.

[37] A. Waser, *On the Notation of Maxwell's Field Equations*, http://www.andrewaser.ch/Publications/OnTheNotationOfFieldEquationsOfElectrodynamics.pdf, 2007.

[38] G.B. Whitham, *Linear and Nonlinear Waves*, Wiley, New York, 1974.

[39] K.S. Yee, *Numerical Solution of Initial Boundary Value Problems Involving Maxwell's Equations in Isotropic Media*, IEEE Trans. Antennas Propag. 1966; 14, 302.

[40] N.J. Zabusky, M.D. Kruskal, *Interactions of "soliton" in a collisionless plasma and the recurrence of initial states*, Phys. Reu. Lett. 15, 1965; 240-243.